

THIS IS A COPY

2

NAVAL POSTGRADUATE SCHOOL

Monterey, California

AD-A205 072



THESIS

EFFECT OF VAPOR VELOCITY DURING
CONDENSATION ON HORIZONTAL
FINNED TUBES

by

Charles Louis Hopkins III

December 1988

Thesis Co-advisors: P.J. Marto
A.S. Wanniarachchi

Approved for public release; distribution is unlimited

DTIC
ELECTE
MAR 13 1989
S H D

29 8 13 029

REPORT DOCUMENTATION PAGE

1a. REPORT SECURITY CLASSIFICATION UNCLASSIFIED		1b. RESTRICTIVE MARKINGS	
2a. SECURITY CLASSIFICATION AUTHORITY		3. DISTRIBUTION / AVAILABILITY OF REPORT Approved for public release; distribution is unlimited	
2b. DECLASSIFICATION / DOWNGRADING SCHEDULE			
4. PERFORMING ORGANIZATION REPORT NUMBER(S)		5. MONITORING ORGANIZATION REPORT NUMBER(S)	
6a. NAME OF PERFORMING ORGANIZATION Naval Postgraduate School	6b. OFFICE SYMBOL (If applicable) Code 69	7a. NAME OF MONITORING ORGANIZATION Naval Postgraduate School	
6c. ADDRESS (City, State, and ZIP Code) Monterey, California 93943-5000		7b. ADDRESS (City, State, and ZIP Code) Monterey, California 93943-5000	
8a. NAME OF FUNDING / SPONSORING ORGANIZATION National Science Foundation	8b. OFFICE SYMBOL (If applicable)	9. PROCUREMENT INSTRUMENT IDENTIFICATION NUMBER CBT-8603582	
8c. ADDRESS (City, State, and ZIP Code) Washington, D.C. 20550		10. SOURCE OF FUNDING NUMBERS PROGRAM ELEMENT NO. PROJECT NO. TASK NO. WORK UNIT ACCESSION NO.	
11. TITLE (Include Security Classification) EFFECT OF VAPOR VELOCITY DURING CONDENSATION ON HORIZONTAL FINNED TUBES			
12. PERSONAL AUTHOR(S) Hopkins, Charles L. III			
13a. TYPE OF REPORT Master's Thesis	13b. TIME COVERED FROM TO	14. DATE OF REPORT (Year, Month, Day) 1988, December	15. PAGE COUNT 137
16. SUPPLEMENTARY NOTATION The views expressed in this thesis are those of the author and do not reflect the official policy or position of the Department of Defense or the U.S. Government.			
17. COSATI CODES FIELD GROUP SUB-GROUP		18. SUBJECT TERMS (Continue on reverse if necessary and identify by block number) Condensation; Vapor Velocity Effects, on Heat Transfer Coefficient; Finned Tubes, <i>these</i> <i>(N-Div)</i>	
19. ABSTRACT (Continue on reverse if necessary and identify by block number) Heat transfer measurements were made for condensation of R-113 and steam on a smooth tube and on three finned tubes with rectangular shape fins. These tubes had a fin height and width of 1.0 mm and spacings of 0.25, 1.5, and 4.0 mm (tubes A, B, and C respectively). Data were taken by increasing the vapor velocity from 0.4 to 1.9 m/s for R-113 and 4.8 to 31.3 m/s for steam. For both fluids, the improvement of the condensing heat-transfer coefficient with vapor velocity was smaller for the finned tubes than for the smooth tube. For R-113, the smooth tube experienced a 43 percent improvement with vapor velocity, whereas the finned tubes (tubes A, B and C respectively) experienced improvements of only 0, 5, and 10 percent. For steam, the smooth tube experienced a 62 percent improvement, whereas the finned tubes (tubes A, B and C respectively) experienced improvements of only 31, 11, and 9 percent. These test results show that, although finned			
20. DISTRIBUTION / AVAILABILITY OF ABSTRACT <input checked="" type="checkbox"/> UNCLASSIFIED/UNLIMITED <input type="checkbox"/> SAME AS RPT <input type="checkbox"/> NOTIC USERS		21. ABSTRACT SECURITY CLASSIFICATION Unclassified	
22a. NAME OF RESPONSIBLE INDIVIDUAL Prof. P.J. Marto		22b. TELEPHONE (Include Area Code) (408) 646-2989	22c. OFFICE SYMBOL Code 69Mx

DD FORM 1473, 84 MAR

83 APR edition may be used until exhausted.
All other editions are obsolete

SECURITY CLASSIFICATION OF THIS PAGE

U.S. Government Printing Office: 1986-608-24.
UNCLASSIFIED

UNCLASSIFIED

SECURITY CLASSIFICATION OF THIS PAGE

#19 -- ABSTRACT - (CONTINUED)

tubes can provide significant heat transfer enhancement over smooth tubes at low vapor velocities, the degree of enhancement becomes smaller as vapor velocity increases.



Accession For	
NTIS GRA&I	<input checked="checked" type="checkbox"/>
DTIC TAB	<input type="checkbox"/>
Unannounced	<input type="checkbox"/>
Justification	
By	
Distribution/	
Availability Codes	
Dist	Avail and/or Special
A-1	

UNCLASSIFIED

SECURITY CLASSIFICATION OF THIS PAGE

Approved for public release; distribution is unlimited

Effect of Vapor Velocity During Condensation
on Horizontal Finned Tubes

by

Charles Louis Hopkins III
Lieutenant Commander, United States Navy
B.S., University of Oklahoma, 1980

Submitted in partial fulfillment of the
requirements for the degree of

MASTER OF SCIENCE IN MECHANICAL ENGINEERING

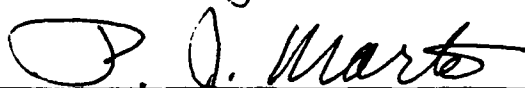
from the


NAVAL POSTGRADUATE SCHOOL
December 1988

Author:



C.L. Hopkins III

Approved by:


P.J. Marto, Thesis Co-advisor


A.S. Wanniarachchi, Thesis Co-advisor


A.J. Healey, Chairman
Department of Mechanical Engineering


G.E. Schacher,
Dean of Science and Engineering

ABSTRACT

Heat-transfer measurements were made for condensation of R-113 and steam on a smooth tube and on three finned tubes with rectangular shape fins. These tubes had a fin height and width of 1.0 mm and spacings of 0.25, 1.5, and 4.0 mm (tubes A, B, and C respectively). Data were taken by increasing the vapor velocity from 0.4 to 1.9 m/s for R-113 and 4.8 to 31.3 m/s for steam. For both fluids, the improvement of the condensing heat-transfer coefficient with vapor velocity was smaller for the finned tubes than for the smooth tube. For R-113, the smooth tube experienced a 32 percent improvement with vapor velocity, where the finned tubes (tubes A, B and C respectively) experienced improvements of only 0, 5 and 10 percent. For steam, the smooth tube experienced a 62 percent improvement, whereas the finned tubes (tubes A, B, and C respectively) experienced improvements of only 31, 11, and 9 percent. These test results show that, although finned tubes can provide significant heat transfer enhancement over smooth tubes at low vapor velocities, the degree of enhancement becomes smaller as vapor velocity increases.

TABLE OF CONTENTS

I.	INTRODUCTION -----	1
	A. BACKGROUND -----	1
	B. OBJECTIVES -----	6
II.	LITERATURE SURVEY -----	7
	A. GENERAL OBSERVATIONS -----	7
	B. EXPERIMENTAL AND THEORETICAL STUDIES -----	10
III.	DESCRIPTION OF APPARATUS -----	23
	A. SYSTEM OVERVIEW -----	23
	B. NEW TEST SECTION CONSTRUCTION -----	30
	C. INSTRUMENTATION -----	37
	D. SYSTEM INTEGRITY -----	39
	E. DATA ACQUISITION SYSTEM -----	40
	F. TUBES TESTED -----	41
IV.	SYSTEM OPERATION AND DATA REDUCTION -----	42
	A. SYSTEM OPERATION -----	42
	B. DATA REDUCTION -----	47
V.	RESULTS AND DISCUSSION -----	54
	A. INTRODUCTION -----	54
	B. EFFECTS OF VAPOR SHEAR ON HEAT TRANSFER PERFORMANCE -----	55
VI.	CONCLUSIONS AND RECOMMENDATIONS -----	80
	A. CONCLUSIONS -----	80
	B. RECOMMENDATIONS -----	81

APPENDIX A: SYSTEM STARTUP AND SHUTDOWN PROCEDURES ---	82
APPENDIX B: UNCERTAINTY ANALYSIS -----	84
APPENDIX C: LISTING OF RAW DATA -----	94
LIST OF REFERENCES -----	115
INITIAL DISTRIBUTION LIST -----	119

LIST OF TABLES

5.1	EFFECT OF VAPOR VELOCITY ON THE HEAT- TRANSFER PERFORMANCE FOR R-113 -----	65
5.2	EFFECT OF VAPOR VELOCITY ON THE HEAT- TRANSFER PERFORMANCE FOR STEAM -----	66

LIST OF FIGURES

2.1	A Cross-sectional View of a Finned Tube Showing Condensate Retention -----	9
3.1	Schematic of Test Apparatus -----	24
3.2	Schematic of Test Section -----	25
3.3	A Cross-sectional View of Test Section Showing Test Tube Installed -----	26
3.4	Purging System and Cooling Water Sump -----	28
3.5	Schematic of Mixing Chamber -----	29
3.6	A Photograph of Test Section--Side View -----	31
3.7	A Photograph of Test Section--Top View -----	32
3.8	A Photograph of Converging Nozzle with Windows Installed -----	34
3.9	A Photograph of Converging Nozzle--Side View ----	35
3.10	A Cross-sectional View of Test Section Showing Converging Nozzle Installation -----	36
5.1	Variation of Vapor-side Heat-transfer Coefficient with Temperature Drop Across the Condensate Film for a Smooth Tube for R-113 -----	56
5.2	Variation of Vapor-side Heat-transfer Coefficient with Temperature Drop Across the Condensate Film with $S = 0.25$ mm for R-113 -----	57
5.3	Variation of Vapor-side Heat-transfer Coefficient with Temperature Drop Across the Condensate Film with $S = 1.5$ mm for R-113 -----	58
5.4	Variation of Vapor-side Heat-transfer Coefficient with Temperature Drop Across the Condensate Film with $S = 4.0$ mm for R-113 -----	59

5.5	Variation of Vapor-side Heat-transfer Coefficient with Temperature Drop Across the Condensate Film for a Smooth Tube for Steam -----	61
5.6	Variation of Vapor-side Heat-transfer Coefficient with Temperature Drop Across the Condensate Film with $S = 0.25$ mm for Steam -----	62
5.7	Variation of Vapor-side Heat-transfer Coefficient with Temperature Drop Across the Condensate Film with $S = 1.5$ mm for Steam -----	63
5.8	Variation of Vapor-side Heat-transfer Coefficient with Temperature Drop Across the Condensate Film with $S = 4.0$ mm for Steam -----	64
5.9	Variation of NR and F for the Smooth Tube for R-113 -----	68
5.10	Variation of NR and F with $S = 0.25$ mm for R-113 -----	69
5.11	Variation of NR and F with $S = 1.5$ mm for R-113 -----	70
5.12	Variation of NR and F with $S = 4.0$ mm for R-113 -----	71
5.13	Variation of NR and F for a Smooth Tube and a Finned Tube ($S = 4.0$ mm) for R-113 -----	73
5.14	Variation of NR and F for the Smooth Tube for Steam -----	74
5.15	Variation of NR and F with $S = 0.25$ mm for Steam -----	75
5.16	Variation of NR and F with $S = 1.5$ mm for Steam -----	76
5.17	Variation of NR and F with $S = 4.0$ mm for Steam -----	77
5.18	Variation of NR and F for a Smooth Tube and a Finned Tube ($S = 1.5$ mm) for Steam -----	78

5.19	Variation of NR and F for the Smooth Tube with Both Fluids (R-113 and Steam) for This Research, $1.6 < G < 6$ -----	79
------	---	----

NOMENCLATURE

A_i	Tube inside heat-transfer surface area (m^2)
A_o	Tube outside heat-transfer surface area (m^2)
b	Fin spacing (mm)
C_i	Sieder-Tate type coefficient used in Equation (4.5)
C_p	Specific heat of cooling water (J/kgK)
D_i	Inside diameter of test tube (mm)
D_o	Root diameter of fin tubes or outside diameter of smooth tubes (mm)
E	Defined in Equation (2.3)
F	Defined in Equation (2.6)
G	Defined in Equation (2.10)
g	Acceleration due to gravity (m/s^2)
h_i	Inside heat-transfer coefficient (W/m^2K)
h_{Nu}	Nusselt's outside heat transfer coefficient (W/m^2K)
h_o	Outside condensity heat-transfer coefficient (W/m^2K)
h_{fg}	Specific enthalpy of vaporization (J/kg)
k_b	Thermal conductivity of cooling water at bulk mean temperature (W/mK)
k_f	Thermal conductivity of the condensate film (W/mK)
k_m	Thermal conductivity of the metal (W/mK)
LMTD	Log-mean-temperature difference defined in Equation (4.4)
\dot{m}	Mass flow rate of cooling water (kg/s)
m	Local condensation mass flux (Equation (2.14))
n	Exponent used in least squares fit Equation (5.1)

NR	The product of Nusselt number and (the negative square root of) two phase Reynolds number
Nu	Nusselt number
\overline{Nu}_T	Mean Nusselt number (uniform wall temperature analysis)
P^*	Defined in Equation (2.18)
Pr	Prandtl number of cooling water, $\mu C_p/k$
Q	Heat transfer rate (W)
q	Heat flux (W/m^2)
\tilde{Re}	Two phase Reynolds number given by $\rho_f U_\infty D_o / \mu_f$
R_o	Radius to the outside of the fin tips
R_w	Tube wall thermal resistance (Equation (4.1))
S	Fin spacing (mm)
T_{sat}	Saturation temperature of the fluid at system pressure (K)
T_{c_o}	Cooling water outlet temperature (K)
T_{c_i}	Cooling water inlet temperature (K)
U_o	Overall heat-transfer coefficient (W/m^2K)
U_∞	Free stream vapor velocity (m/s)
u_δ	Velocity at vapor-condensate interface (m/s)
X	Defined in Equation (2.9)

Greek Symbols

α_F	Fujii type coefficient used in Equation (4.10)
α_N	Nusselt type coefficient used in Equation (4.19)
β	Defined in Equation (4.11)
δ	Condensate film thickness
ΔT	Temperature difference across condensate film ($T_{sat} - T_{wall}$) (K)

ΔT_{cw}	Cooling water temperature difference ($T_{c_o}-T_{c_i}$) (K) in Equation (4.3)
ϵ_q	Enhancement ratio based on a constant heat flux
$\epsilon_{\Delta T}$	Enhancement ratio based on a constant temperature difference
λ	Latent heat (J/kg) used in Equation (2.3)
μ_b	Dynamic viscosity of the cooling water at bulk mean temperature ($N \cdot s/m^2$)
μ_f	Dynamic viscosity of the condensate at T_f ($N \cdot s/m^2$)
μ_w	Dynamic viscosity of the cooling water at inside wall temperature ($N \cdot s/m^2$)
μ_v	Dynamic viscosity of the vapor ($N \cdot s/m^2$)
Ω	Defined in Equation (4.6)
ψ	Condensate retention angle defined in Equation (2.1)
ρ_f	Density of the condensate at T_f (kg/m^3)
ρ_v	Density of the vapor at T_v (kg/m^3)
τ_δ	Shear stress at the condensate film surface
σ	Surface tension of the fluid (N/m)
θ	Fin tip half angle
ξ	Defined in Equation (2.13)

ACKNOWLEDGEMENTS

The author would like to express his sincere appreciation to Professor P.J. Marto and Professor A.S. Wanniarachchi for their guidance and support in completing this work.

The author would also like to offer special thanks to Mr. Jim Scholfield, Mr. Tom Christian for their instrumentation and computer hardware support, and special recognition to Mr. Charles Crow for his machinist's talents while manufacturing the high velocity test section.

Lastly the author would like to express his heart-felt thanks to his wife and children for the patience and support through the course of this thesis.

I. INTRODUCTION

A. BACKGROUND

Tactical considerations have forced our highly technological society to thoroughly investigate and understand fundamental heat-transfer mechanisms that occur during film condensation in naval steam plant main condensers. Due to its physical size, the heat-transfer characteristics of a steam plant main condenser have a direct impact on naval ship construction and the ability to efficiently accomplish the ship's mission. Designing marine propulsion plants with a high power density (maximum power with small size and weight) will reduce the ship's displacement and power required to achieve a given speed (power required is proportional to ship's displacement). This design philosophy creates more options for the ship's designer. Options such as increased ship capabilities due to a more powerful propulsion plant, improved accessibility in the engineering spaces, an increased weapons payload or any combination of these options are considerations made by the designer based on the ship's mission requirements.

Increased cooling capacities are required to support modern weapons and navigational electronics. The continued interest to reduce the size and weight of components on board ship goes beyond the propulsion system, and the same

considerations for the design of a steam plant main condenser can be applied to an air-conditioning and refrigeration condenser. A complete understanding of the basic heat-transfer equation that governs heat transfer will allow engineers to determine modifications that can be accomplished to enhance the ability to transfer heat. As early as 1861, Joule [Refs. 1,2] obtained measurements of heat transfer during condensation on the inside of a single vertical tube. Although the configuration of his apparatus is quite different than many contemporary testing techniques, the concepts that he developed can be utilized in modern heat transfer analysis. He calculated an overall heat-transfer coefficient U_o using the well-known relationships:

$$Q = \dot{m}c_p(T_{c_o} - T_{c_i}) \quad (1.1)$$

and

$$Q = U_o A_o (\text{LMTD}) \quad (1.2)$$

where LMTD is the log-mean-temperature difference.

The overall heat-transfer coefficient (U_o) is a function of the thermal resistances on the water side, the vapor side and the resistance through the tube wall. Generally, the thermal resistances on the water side and the vapor side are

most dominant and reducing either one of these thermal resistances will contribute to an improved overall heat-transfer coefficient. In fact, Sengupta [Ref. 3] reported that (for a conventional, smooth-tube steam condenser) approximately 56% of the total resistance is due to the water film resistance and approximately 22% is due to the steam film resistance.

Once the tube material and wall thickness are chosen for a particular operating environment, the tube wall resistance is a constant. Water-side enhancement is possible with turbulence promoters, twisted-tape inserts and deformation of the tube to promote a "roped" wall profile [Ref. 4]. Vapor-side enhancement techniques include the use of low integral fins, roped tubes, fluted tubes, drainage strips attached to the tubes and applied coatings to promote dropwise condensation [Refs. 5,6,7,8,9].

Increasing the performance or the effectiveness of the condenser can reduce the material and construction cost along with the size and weight. The heat-transfer equation (Equation 1.2) has several possibilities for improving condenser performance; they are: (a) increase the LMTD, (b) increase the heat-transfer area, or (c) increase the overall heat-transfer coefficient. The LMTD is determined by the specific power plant application and therefore cannot be considered as a method for improving condenser performance. Hence, condenser performance is essentially limited by the

total heat-transfer area and the overall heat-transfer coefficient.

Modern steam condensers are equipped with smooth tubes. In an effort to increase the heat-transfer rate per unit weight, the addition of integral fins to the tubes of the main condenser is an alternative under investigation. Wanniarachchi et al. [Ref. 10] reported that externally finned tubes have been widely used in the refrigeration industry for many years, and until recently, a common belief existed that such tubes would be unsuitable for use in steam condensers. Though without experimental support, this belief existed due to the considerable liquid retention (flooding) that occurs on the bottom of these tubes as a result of the relatively high surface tension of water (at 50°C, water has a surface tension of 0.068 N/m, while refrigerants have values of about 0.015 N/m).

However, after several years of research, recent data have shown that with the utilization of properly designed extended surfaces (i.e., increasing the effective heat-transfer area of the heat exchanger), significant improvements in steam-side heat transfer can be achieved. In fact, Yau et al. [Ref. 5] and Wanniarachchi et al. [Refs. 10,11] have shown that for condensation of steam, under most conditions, the heat-transfer performance of finned tubes exceeds the performance expected on the basis of area increase alone. This suggests that fluid surface tension

forces play an important role in the condensation process of both the flooded and unflooded portions of a finned tube by thinning the condensate film.

Another alternative to increasing heat-transfer area is the addition of extended surfaces on the water side of the tube. This method, while also increasing the heat-transfer area, will require additional pumping power due to increased frictional pressure drop and will substantially increase the difficulties associated with cleaning internally-fouled surfaces. Clearly, for marine use, the application of extended surfaces can be accomplished with greater repair and economic advantages to the external surface of the tube.

The large number of variables and physical mechanisms that take place during condensation on finned tubes precludes a simple theoretical treatment of this process. Parameters such as tube and fin geometry, surface tension forces, wall conduction effects and the interaction of gravitational forces lead to complex three-dimensional flow patterns. To further complicate the problem, the analysis of condensation on finned tubes must account for vapor shear forces and inundation effects (condensate falling from higher tubes), as these processes take place in actual use.

Until recently, almost all data on low integral-fin tubes have been obtained under low velocity vapor conditions. Condensation heat transfer research conducted at the Naval Postgraduate School has been limited, in almost

all cases, to vapor velocities less than 2.0 m/s for steam and R-113, whereas velocities for ethylene glycol have approached 10.0 m/s. However, very high vapor velocities can occur in actual condensers (i.e., 30-50 m/s in steam condensers), especially at the inlet regions. It is common practice to incorporate some over-design factor to account for the effects that cannot be computed directly. Vapor shear thins the condensate film and has been shown to increase performance of smooth tubes, but the effect on finned tubes requires additional investigation. Therefore, if the effect of high vapor shear on finned tubes is accurately known, this will help engineers to design enhanced surface condensers having more predictable heat duties.

B. OBJECTIVES

Major objectives for this thesis are:

1. Design and construct a new test section that will allow condensation measurements to be made at high vapor velocities.
2. Experimentally measure the effect of vapor velocity on the filmwise condensation heat-transfer coefficient on three finned tubes. These finned tubes have different fin spacings of 0.25, 1.5, and 4.0 mm, while they have equal fin heights and thicknesses of 1.0 mm.
3. Compare the results of item 2 above with those for a smooth tube. Also compare smooth-tube data with existing vapor-shear theoretical and experimental results.

II. LITERATURE SURVEY

A. GENERAL OBSERVATIONS

Condensation of vapor into liquid involves removing the enthalpy of vaporization. When the condensation process occurs in a filmwise mode, the individual drops of condensate coalesce to form a stable, continuous film on the heat-transfer surface. This continuous condensate film provides a resistance to heat transfer due to the relatively low thermal conductivity of the liquid, and the resistance increases as the film thickness increases. In general, the condensate film thickness (and therefore film resistance) on smooth horizontal tubes is small at the top of the tube and increases with peripheral distance to the bottom of the tube. Since the objective is to enhance heat transfer, it is necessary to reduce the film thickness, thereby reducing resistance to heat transfer. For the application of horizontal tubes, thinning of the condensate film may be accomplished by the use of finned surfaces, wire-wrapped or roped tubes, and drainage/porous strips. This research concentrates on the use of finned surfaces.

Close examination of a finned tube during condensation reveals two distinct regions: flooded and unflooded regions. Condensate flow between the fins is greatly affected by the ratio of surface tension forces to

gravitational forces. The surface tension forces perform a dual role on the behavior of the condensate film. First, these forces reduce the condensate film thickness at the fin tips and on the fin flanks in the unflooded region of the tube, thereby enhancing heat transfer. In this region, the condensate on the fin surface is driven by the combined effects of surface tension and gravitational forces into the fin root where it is drained primarily by gravity. Second, surface tension forces cause the condensate retention between the fins in the lower, flooded region of the tube and this decreases the effective heat-transfer area, thereby reducing heat transfer.

The flooded portion of the tube is defined by the retention angle (ψ) (Equation 2.1) which is the angle from the bottom centerline of the tube to the highest position on the tube where the interfin space is filled with condensate (see Figure 2.1).

$$\psi = \cos^{-1} \left[1 - \frac{2\sigma \cos \theta}{\rho g b R_o} \right] \quad (2.1)$$

Research conducted by Rudy and Webb [Ref. 12] on integral-fin tubes demonstrated that the retention angle increases (i.e., more flooding should occur) as the fin density increases or as the surface tension-to-density ratio of the fluid increases. They also reported that the difference between static and dynamic retention angles was

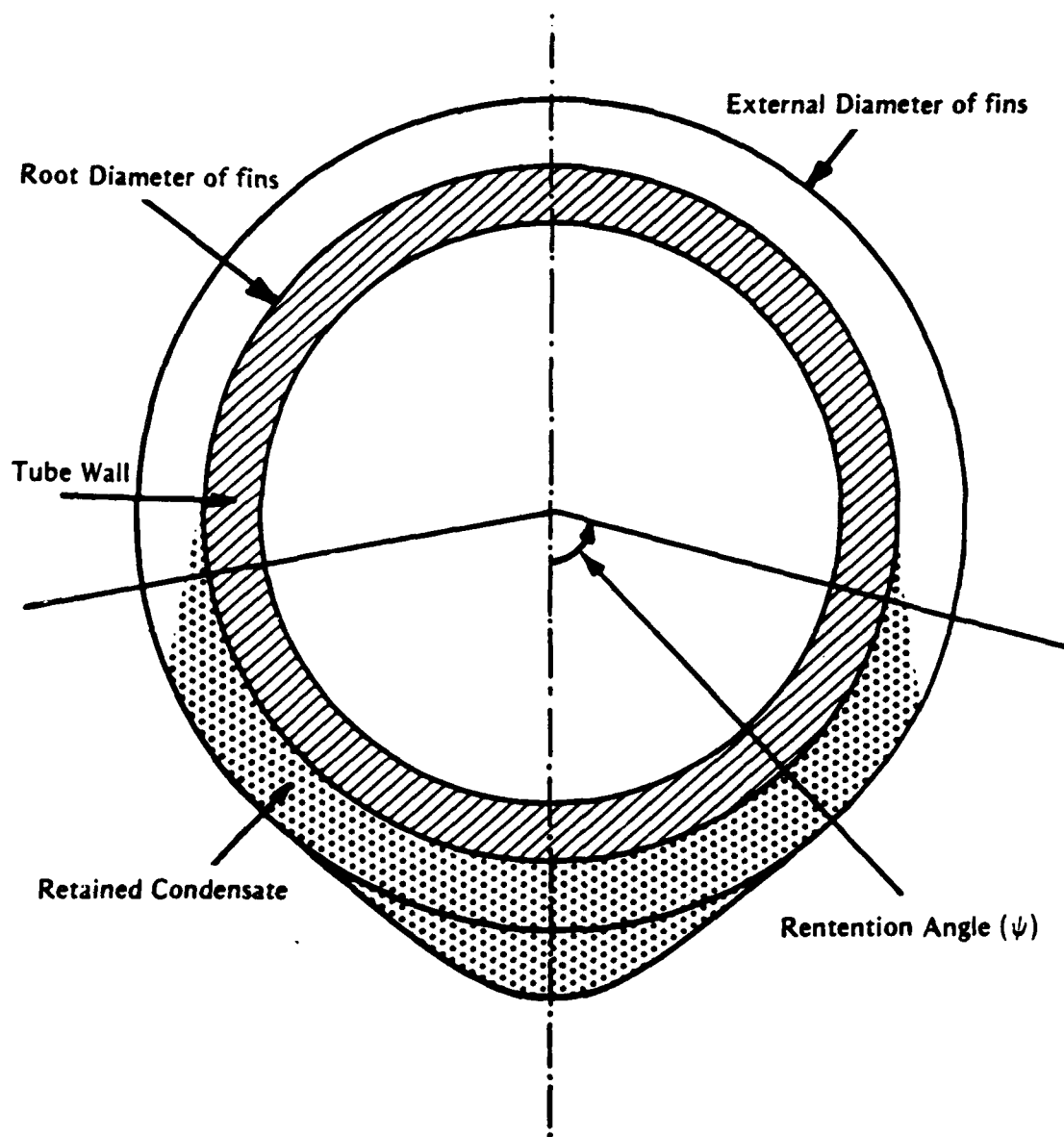


Figure 2.1 A Cross-sectional View of a Finned Tube Showing Condensate Retention

very small and when conducting tests with water, a significant portion of the tube surface was flooded. Numerous other researchers [Refs. 13,14,15,16] have conducted independent theoretical and experimental studies and have derived or verified the above equation for condensate retention angle. This equation has been shown to predict experimental data to within $\pm 10\%$. Cakan [Ref. 17] and Van Petten [Ref. 18] have given comprehensive literature reviews on the condensate-retention phenomenon, and no further discussion of this subject will be provided in this thesis.

It should, however, be noted that the above retention model does not account for vapor shear. It is possible that high vapor shear can have some effect on the condensate-retention angle. Since vapor shear tends to push condensate away from the upper portion of the tube, it may have a beneficial effect by reducing the retention angle. On the other hand, high vapor shear may retard condensate drainage from the bottom of the tube owing to the secondary flow patterns developed there, thus inhibiting the condensation process. Even though these effects can be small, a complete understanding will be needed through future research.

B. EXPERIMENTAL AND THEORETICAL STUDIES

1. Condensate Flow Regimes

Ishihara and Palen [Ref. 19] reported that the process of condensation can be divided into three

controlling regimes that apply to either smooth or finned tubes undergoing shell-side condensation as discussed below.

a. Gravity-Controlled Flow

In this regime, vapor shear forces are negligible and the liquid drains vertically downward under gravity. Laminar flow exists and therefore the Nusselt equation is applicable for smooth tubes and this equation may be adaptable for finned-tube applications. The properties of the liquid film are, in general, determined by gravity-dominated hydrodynamics. However, as mentioned above, in the case of finned tubes, surface tension forces can significantly influence liquid film properties at the region near the fin tips.

b. Shear-Controlled Flow

At high vapor velocity, the condensate film is normally turbulent and the film thickness is controlled by the shear force on the film and not by the effects of gravity. The classical Nusselt equation does not apply in this regime as it was developed for laminar film flow where the vapor shear effect is negligible (the Nusselt equation is too conservative at high vapor velocities). Also, in this regime, the condensing coefficient will be independent of the flow direction.

c. Transition Flow

There is a transition to shear-controlled flow as the vapor velocity increases. In the case of finned

tubes, as the condensate flow rate increases, the vapor-shear-created ripples and waves on the condensate film can lead to flooding of the fin space. Ishihara and Palen state that in this regime the vapor shear can have an insignificant effect on the condensing heat-transfer coefficient for finned tubes. Therefore, this regime is an area of study that occurs between the extremes of the gravity controlled flow and shear controlled flow regimes.

To distinguish which flow regime applies, Ishihara and Palen [Ref. 19] have recommended a shell-side flow parameter which consists of the ratio of the vapor shear force to the gravitational force on the fluid. On the other hand, diMarzo and Casarella [Ref. 20] distinguished flow regimes by using the ratio of shear stresses at the liquid-vapor interface and at the tube surface as a function of the Froude number.

2. Effects of Vapor Shear on Smooth Tubes

Nusselt's [Ref. 21] analysis for quiescent vapor condensing on a smooth horizontal tube with gravity-drained condensate resulted in the well-known expression for the condensing heat-transfer coefficient as given below:

$$h_{Nu} = 0.728 \left(\frac{E}{D_o \Delta T} \right)^{1/4}, \quad (2.2)$$

where

$$E = \frac{k_f^3 \rho_f (\rho_f - \rho_v) g \lambda}{\mu_f} \quad (2.3)$$

His approach neglected all but the viscous and gravity terms in the condensate momentum equation and all but the conduction term in the energy equation. In an effort to avoid the conservation equations for the vapor boundary layer, the shear stress at the condensate surface was also neglected. Since the Nusselt theory assumes the zero-vapor-velocity condition, it cannot be used reliably for designing actual condensers where reasonably high vapor shear exists. It does, however, serve as a conservative standard from which subsequent theories reference.

In 1966, Shekriladze and Gomelaui [Ref. 22] considered laminar film condensation on the external surface of a smooth horizontal cylinder in a transverse vapor flow. They reported that during the vapor-flow process, a number of unique conditions exists. They observed that as the vapor flows past a moving condensate film, vapor is removed from the vapor boundary-layer as a result of condensation. They also observed that the separation of the liquid boundary layer significantly alters the condensation rate over the tube surface beyond the separation point. In their analysis, they reported that downward vapor flow without separation of the boundary layer is possible for high velocities of incoming flow

(high rate of phase change) as the condensation of the vapor causes a suction effect sufficient to prevent separation. Their analysis further assumed that both the vapor and condensate boundary-layers are laminar, inertia forces may be neglected for vapor condensation on an isothermal surface and that the pressure gradient along the cylinder periphery may be neglected when compared to the momentum transferred by the condensing mass. Utilizing these assumptions and conditions, they arrived at the following result:

For the case of flow without separation and no body forces, they found:

$$Nu \tilde{Re}^{-1/2} = 0.9 , \quad (2.4)$$

where \tilde{Re} is a two-phase Reynolds number, given by

$$\rho_f U_\infty D_o / \mu_f .$$

For the case of flow without separation but with body forces, they found:

$$Nu \tilde{Re}^{-1/2} = 0.64 [(1 + (1 + 1.69F)^{1/2})^{1/2}]^{1/2} , \quad (2.5)$$

where

$$F = gD_o \mu_f h_{fg} / U_\infty^2 k_f \Delta T . \quad (2.6)$$

For velocities less than 10 m/s, for which they assumed no separation, satisfactory agreement between the theory and data was demonstrated (+/- 10%).

A possibility exists for the separation of the vapor boundary-layer, even though the vapor mass flux retards separation. This boundary-layer separation produces a sharp decrease in the heat-transfer rate over the portion of the cylinder beyond the separation point. The decrease in heat transfer beyond the separation point is the result of two effects. First, the vapor begins to flow in the opposite direction of gravity forces resulting in an increased film thickness. Second, the static pressure beyond the separation point is low when compared to the free-stream pressure, resulting in a decrease in actual temperature difference between the vapor and the cold wall. Shekriladze and Gomelaury [Ref. 22] also reported that approximately 35% of the total heat transfer occurs beyond a separation angle of 82°. To account for these effects, the mean heat-transfer coefficient for flow with separation (at an angle of approximately 82°), when compared to flow without separation should be lowered by 35%. For separation at 82°, they therefore adjusted Equation (2.5) to yield:

$$Nu \tilde{Re}^{-1/2} = 0.42 [1 + (1 + 1.69F)^{1/2}]^{1/2} \quad (2.7)$$

However, under actual operating conditions, separation may occur at any point from 82° to 180° . Therefore, Equations (2.5) and (2.7) represent the upper and lower limits for mean heat-transfer coefficients for condensation on a horizontal cylinder under the conditions of vapor flow with a separated boundary layer. Shekriladze and Gomelaouri [Ref. 22] utilized data from experiments conducted by Berman and Tumanov [Ref. 23] to illustrate the effects of Equations (2.5) and (2.7). At low vapor velocities (i.e., no boundary-layer separation) data fell near the upper curve corresponding to Equation (2.5), whereas the high vapor velocity (boundary-layer separation at approximately 82°) data approached the lower curve corresponding to Equation (2.7).

In 1972, Fujii et al. [Ref. 24] also investigated laminar filmwise condensation of downward-flowing vapor on a horizontal cylinder. They solved the two-phase boundary-layer equations with the assumption that the vapor outside the boundary layer can be treated as potential flow. Assuming that the effect of the pressure term in the condensate momentum equation is negligibly small (because the body force term is negligibly small when compared with the viscous term) and assuming no condensate boundary-layer separation, they developed the following expression for the average heat-transfer coefficient:

$$\text{Nu } \tilde{\text{Re}}^{-1/2} = X(1 + 0.276FX^{-4})^{1/4} , \quad (2.8)$$

where

$$X = 0.9(1 + 1/G)^{1/3} , \quad (2.9)$$

and

$$G = (\Delta T k_f / \mu_f h_{fg}) (\rho_f \mu_f / \rho_v \mu_v)^{1/2} . \quad (2.10)$$

It may be shown that for $G \gg 1$, the result becomes independent of G and also for $G \approx 10$, Equation (2.8) is in close agreement with the Shekriladze and Gomelaouri result, Equation (2.5). Their detailed numerical results agreed within $\pm 5\%$ when compared with Equation (2.8). In addition, their measured data, along with experimental data obtained from Berman and Tumanov [Ref. 23], agreed with Equation (2.8) to within $\pm 20\%$. They concluded that the theoretical and experimental results of the average heat-transfer coefficient were in fairly good agreement. They also concluded that with high incoming vapor velocity, the effect of the parameter G on the heat-transfer coefficients is significant, the effect of body force is negligible and that approximately 80% of the total condensation takes place on the upper half of the cylinder.

In 1979, Fujii et al. [Ref. 25] further investigated the more general case of vapor velocity by considering approach velocities other than vertically downward. As in the previous investigation, they neglected the inertia, convection and pressure terms in the condensate momentum equation. However, their analysis considered condensate boundary-layer separation and they arrived at the following empirical correlation:

$$Nu \tilde{Re}^{-1/2} = 0.96F^{1/5}, \quad 0.03 < F < 600 \quad (2.11)$$

They demonstrated that the solution for uniform wall heat flux agrees well with experimental results as far as the average heat-transfer coefficient is concerned. Using this correlation, if the variations in T_{sat} , ΔT_{cw} and cooling water velocity are not large, they determined that the scatter of data should be within $\pm 10\%$ according to the theoretical results and the accuracy of measurements.

In 1982, Lee and Rose [Ref. 26] used the Fujii-Truckenbrodt type of analysis (a modification of shear stresses at the condensate boundary layer based on potential flow theory), which predicts vapor boundary-layer separation and modified it (conservatively) by neglecting heat transfer beyond the separation point. Their results are represented by Equations (2.12) and (2.13):

$$\overline{NU}_T \tilde{Re}^{-1/2} = \xi(1 + 0.281F/\xi^4)^{1/4} , \quad (2.12)$$

where

$$\xi = 0.88(1 + 0.74/G)^{1/3} . \quad (2.13)$$

For the limiting case of low vapor velocity ($F \rightarrow \infty$), this equation approaches the Nusselt solution and for the case of high vapor velocity ($F \rightarrow 0$) and high condensation rate ($G \rightarrow \infty$), Equation (2.12) predicts a consistent behavior agreeing well with the numerical solutions for intermediate Nusselt numbers (constant wall-temperature case).

While previous studies of laminar film condensation from a vapor flowing over a smooth horizontal tube omitted the pressure-gradient term from the momentum balance for the condensate film, in 1984, Rose [Ref. 27] included this in his work. He showed that higher heat-transfer coefficients over the upper half of the tube can be achieved. He did, however, simplify the analysis in the following manner: he neglected inertia and convection terms, and used the infinite-condensation-rate asymptotic expression for the condensate shear stress,

$$\tau_\delta = m(U_\infty - u_\delta) \quad (2.14)$$

He also used the potential-flow-velocity distribution outside the vapor boundary layer, and he took the vapor velocity at the edge of the vapor boundary layer greater than the condensate velocity at the boundary layer. The results of his analysis showed that, when the term

$$\rho_v U_\infty^2 / \rho_f g D_o > 1/8 \quad (2.15)$$

the rate of increase of film thickness became infinite on the downstream half of the tube. But when the term

$$\rho_v U_\infty^2 / \rho_f g D_o < 1/8 \quad (2.16)$$

solutions could be obtained for the whole surface as the increase in the heat transfer for the upper half of the tube was essentially balanced by the decrease for the lower half. For the whole tube, Rose reported:

$$Nu Re^{-1/2} = \frac{0.64(1 + 1.81P^*)^{0.209}(1 + G^{-1})^{1/3} + 0.728F^{1/2}}{(1 + 3.51 F^{0.53} + F)^{1/4}} \quad (2.17)$$

where

$$P^* = \rho_v h_{fg} u_f / \rho_f k_f \Delta T \quad (2.18)$$

Equation (2.17) includes the effects of gravity, pressure gradient, and a correction for the surface shear stress

approximation. At low vapor velocities, Equation (2.17) approaches the Nusselt result and for high vapor velocities, it only considers heat transfer for the upper half of the tube and, for this reason, should yield conservative results.

Extensive research has been conducted to determine the effect of vapor velocity on the condensing heat-transfer coefficient for smooth horizontal tubes and this subject has been comprehensively reviewed by Rose in 1988 [Ref. 28]. This research has shown that as the vapor velocity increases, the heat-transfer coefficient can increase significantly. On the other hand, very little research has been published for vapor velocity effects on finned tubes.

3. Effects of Vapor Shear on Finned Tubes

This author knows of only three studies conducted to include the effects of vapor velocity on the condensing heat-transfer coefficient on horizontal finned tubes. Gogonin and Dorokhov [Ref. 29] measured the condensation heat transfer coefficients of Freon-21 on finned copper tubes with fins having a height of 1.5 mm and a spacing of 1.2 mm. They found a 20 percent improvement in the condensing heat-transfer coefficient as the vapor velocity increased to 8 m/s. However, a smooth tube under similar conditions resulted in a near 100 percent improvement. Based on the small enhancement observed for finned tubes,

they recommended that condenser tube bundles should be designed on the basis of a stationary vapor. In contrast to the observation of Gogonin and Dorokov, Yau et al. [Ref. 30] showed essentially the same influence of vapor velocity for both finned and smooth tubes when condensing steam. Notice, however, that they used only very low vapor velocities (0.5, 0.7, and 1.1 m/s). While still further, Flook [Ref. 31], testing with steam condensing on a finned copper tube (fin thickness and height equal to 1.0 mm and fin spacing equal to 1.5 mm) observed a 10 percent increase in the condensing heat-transfer coefficient as the vapor velocity was increased from 2 to 8 m/s.

III. DESCRIPTION OF APPARATUS

A. SYSTEM OVERVIEW

The test apparatus used for this research was essentially the same system used by Georgiadis [Ref. 32], Mitrou [Ref. 33], Lester [Ref. 34] and Van Petten [Ref. 18], with design modifications in the test section to provide a higher velocity environment. A schematic of the system is shown in Figure 3.1. Vapor was generated in a 304.8 mm (12.0 in) diameter Pyrex glass boiler which contains ten 4000-watt, 440-volt Watlow immersion heaters. The vapor formed in the boiler section flowed upward through a 304.8 mm (12.0 in) diameter to 152.4mm (6.0 in) diameter Pyrex reducing section, then through a 2.44 m (8.0 ft) long section of Pyrex pipe. The vapor then flowed through a 180 degree bend and into a 1.52 m (5 ft) long straightening section before finally entering a newly designed stainless-steel test section, which is shown in Figure 3.2. The condenser test tube was mounted horizontally in the test section as shown in Figure 3.3. Two rectangular Pyrex glass viewports were incorporated with the test section design modifications. The rectangular viewports permit visual observation of the condensing process on a single tube in the test section or will also allow observation of the condensing process on several in-line tubes. A portion of

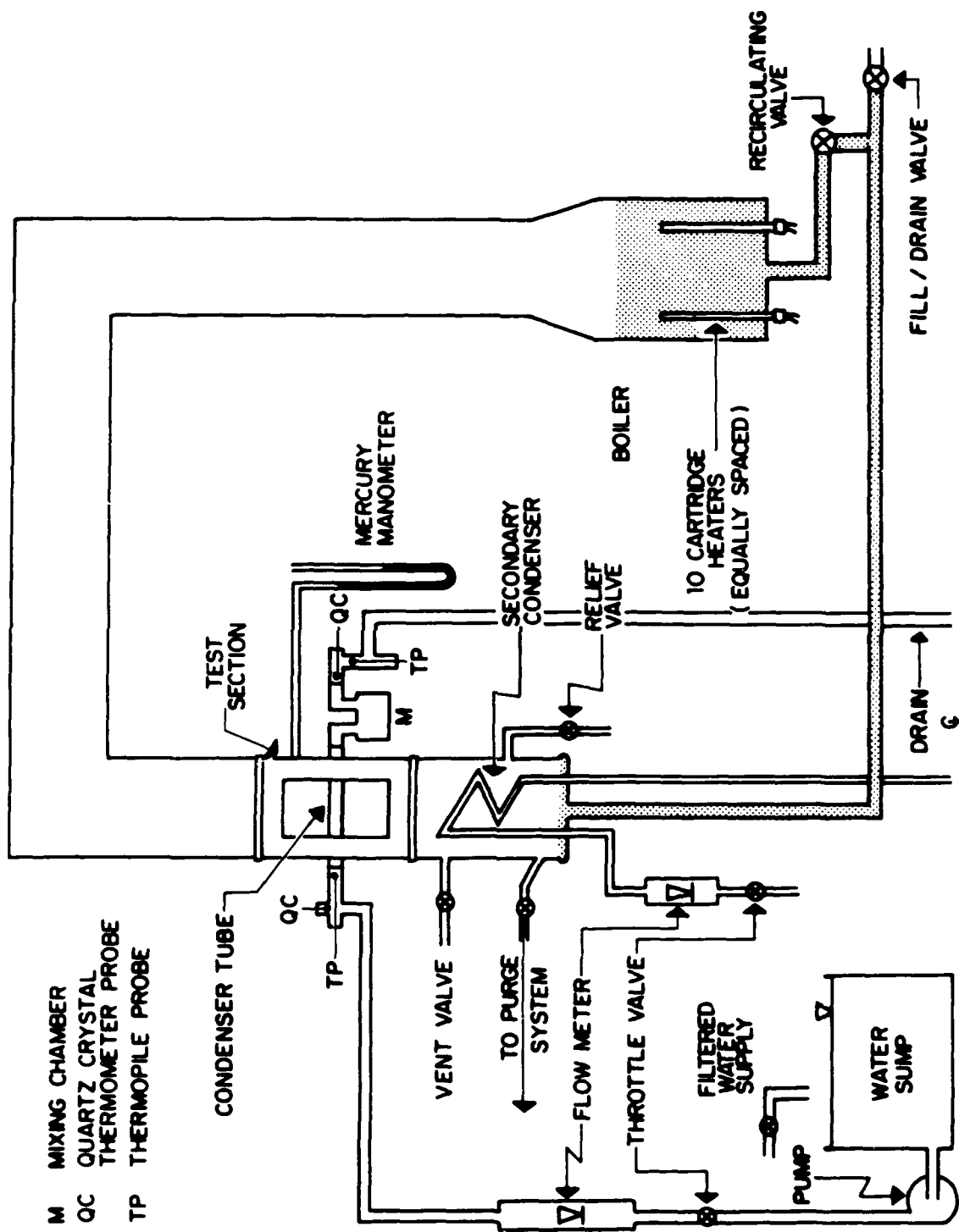


Figure 3.1 Schematic of Test Apparatus

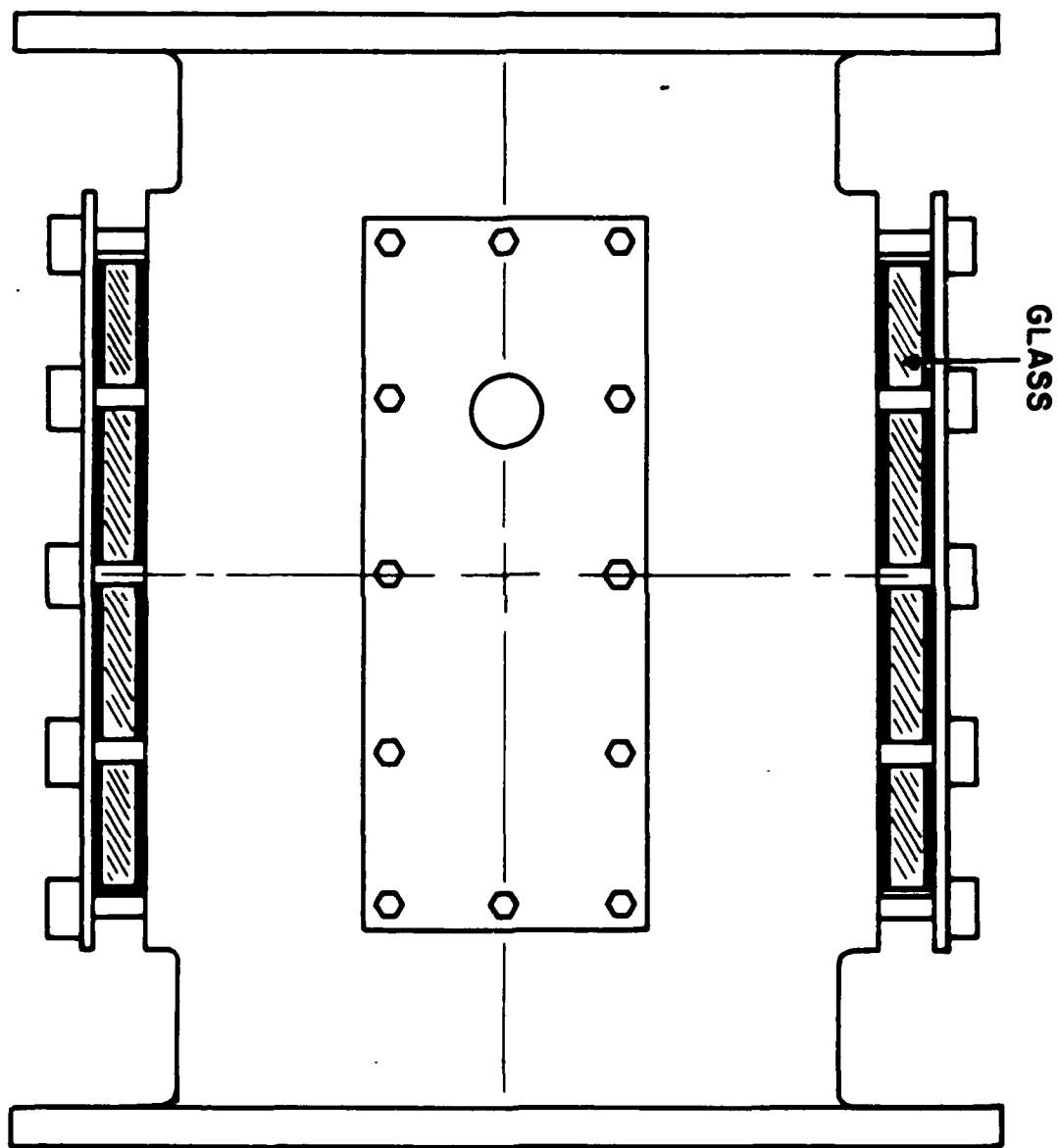


Figure 3.2 Schematic of Test Section

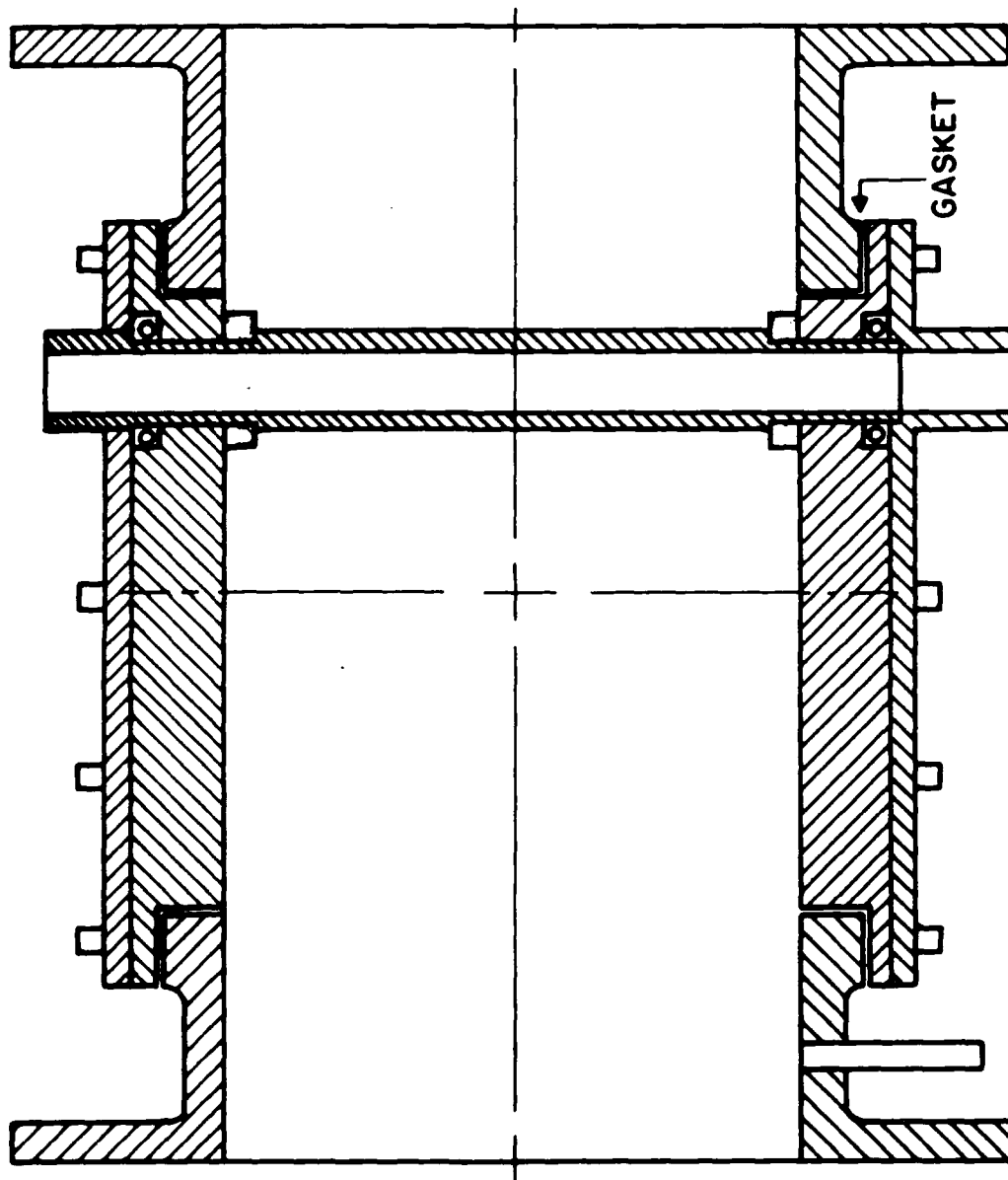


Figure 3.3 A Cross-sectional View of Test Section
Showing Test Tube Installed

the vapor condensed on the test tube, while the excess vapor travelled downward and condensed in the auxiliary condenser. The auxiliary condenser was constructed of two 9.5 mm (3/8 in) diameter, copper, water-cooled coils having a height of 457 mm (18 in). All condensate drained back to the boiler section by gravity, thereby completing the closed-loop cycle.

Cooling water for the test tube was provided on a single-pass basis by two centrifugal pumps connected in series. Water supplied to these pumps was provided through a large sump of approximately 0.4 m³ (Figure 3.4), which was filled with a continuous supply of filtered tap water. A throttle valve on the discharge of the second pump (and inlet to the flow meter) allowed the velocity of the water flowing through the test tube to be varied from 0.0 to 4.4 m/s (14.4 ft/sec). A mixing chamber (see Figure 3.5) on the cooling water outlet of the test tube was used for accurate measurement of the mean outlet temperature of the coolant. Cooling water for the auxiliary condenser was provided by a continuous supply of tap water through a flow meter. Throttling the flow of tap water through the auxiliary condenser was the primary method used to control the internal system pressure. For example, when the flow rate through the test tube was increased, the flow rate through the auxiliary condenser had to be decreased, thus maintaining the desired system pressure.

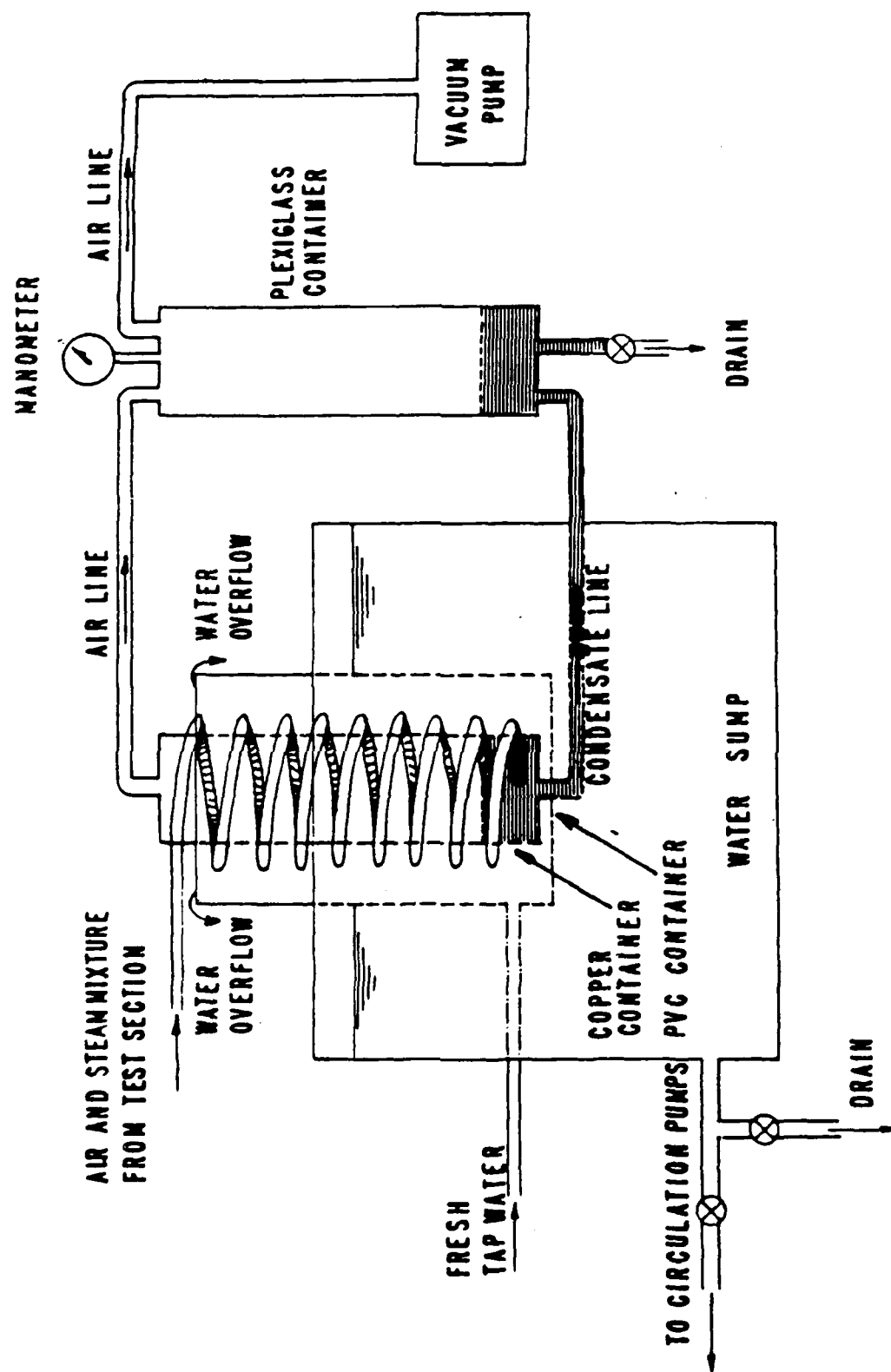


Figure 3.4 Purging System and Cooling Water Sump

STAINLESS STEEL MIXING CHAMBER

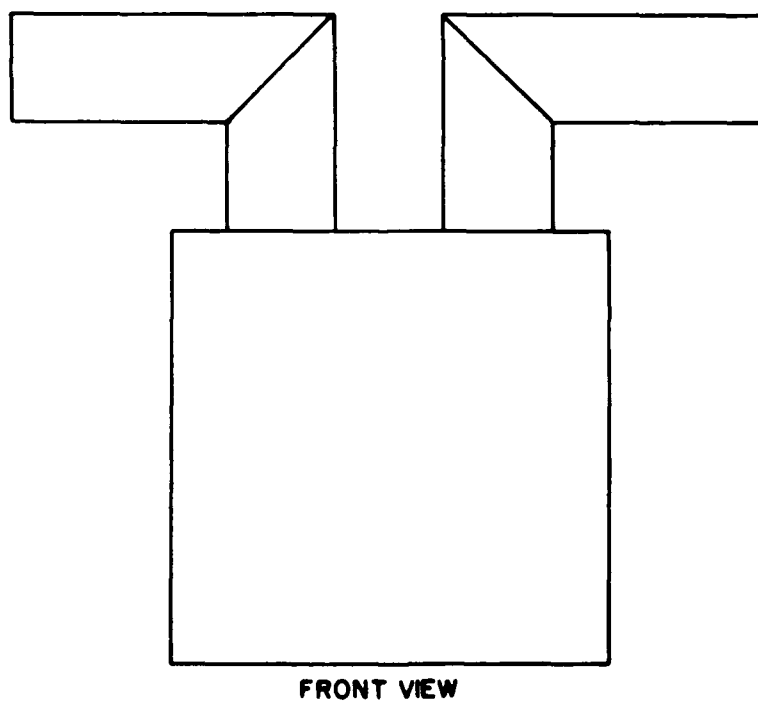
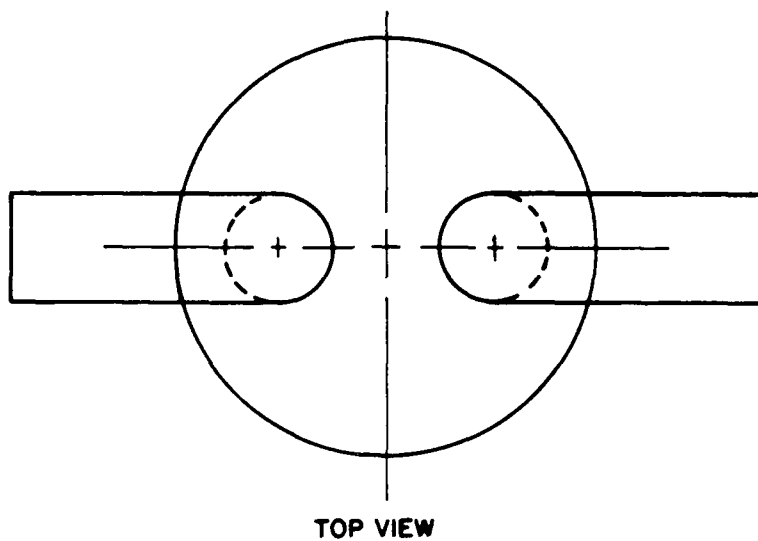


Figure 3.5 Schematic of Mixing Chamber

A vacuum pump was operated at the beginning of each test run to remove non-condensing gases from the test section. This purge system is shown schematically in Figure 3.4. During apparatus operation, the purge system would unavoidably draw small amounts of vapor along with trace amounts of air and non-condensing gases. Figure 3.4 illustrates how the purge system utilized still another condenser to condense the vapor carryover thereby minimizing contamination of the vacuum pump. Cooling water for this condenser was a continuous supply of filtered tap water before it entered the large sump. The condensate from this vapor was collected and later drained from the Plexiglas container.

B. NEW TEST SECTION CONSTRUCTION

A newly-designed test section was required to investigate the effects of vapor shear on the heat-transfer coefficient of a horizontally mounted integral-fin tube. The new test section was used for the testing and observation of one tube in a high-velocity environment. However, the test section was designed to support future testing of up to four tubes in a vertical row (to study condensate inundation effects). The new test section used for this investigation (Figures 3.6 and 3.7) was modelled from the test sections for previous research at the Naval Postgraduate School (when high vapor velocity was not a parameter under investigation).

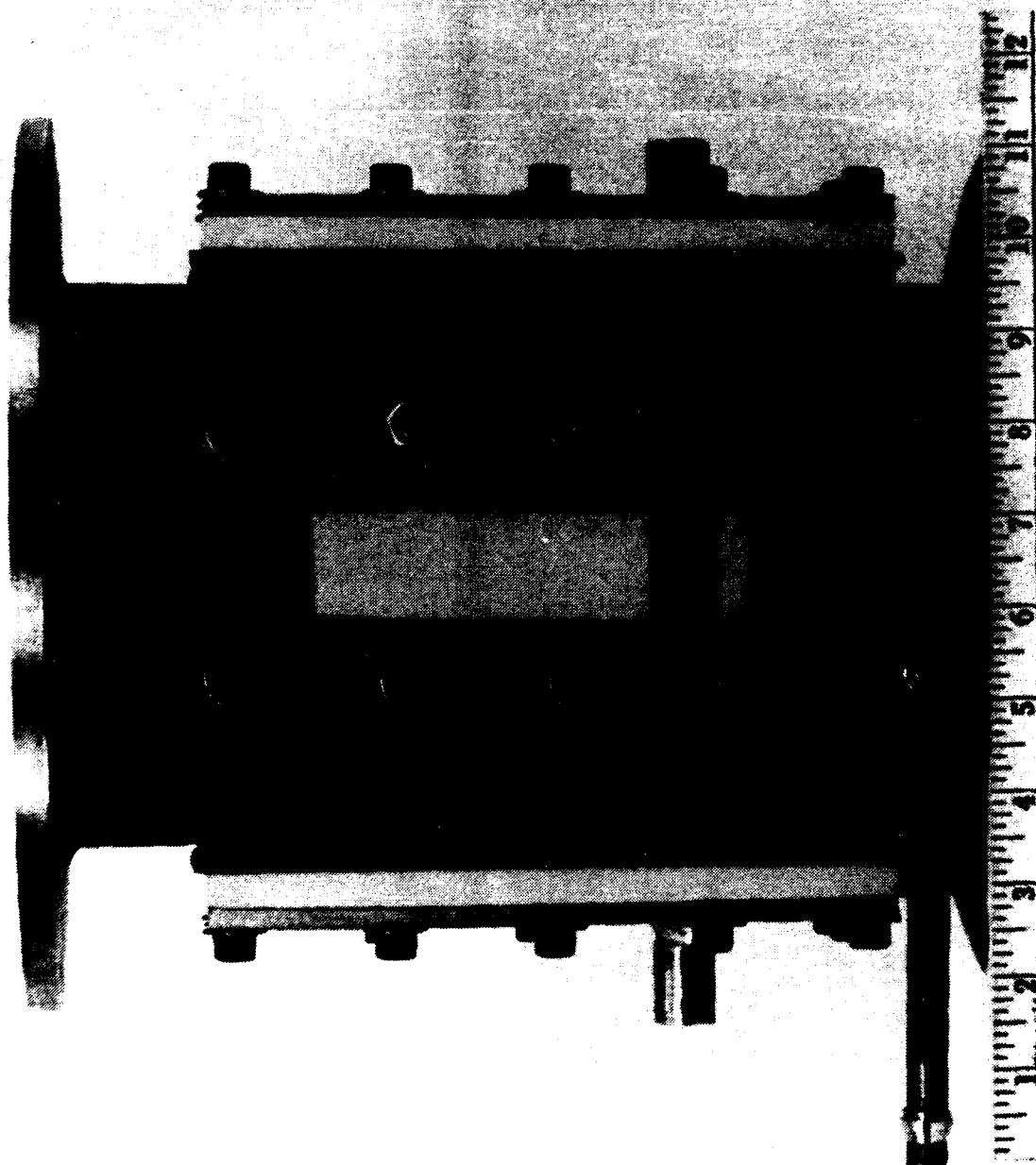


Figure 3.6 A Photograph of Test Section--Side View

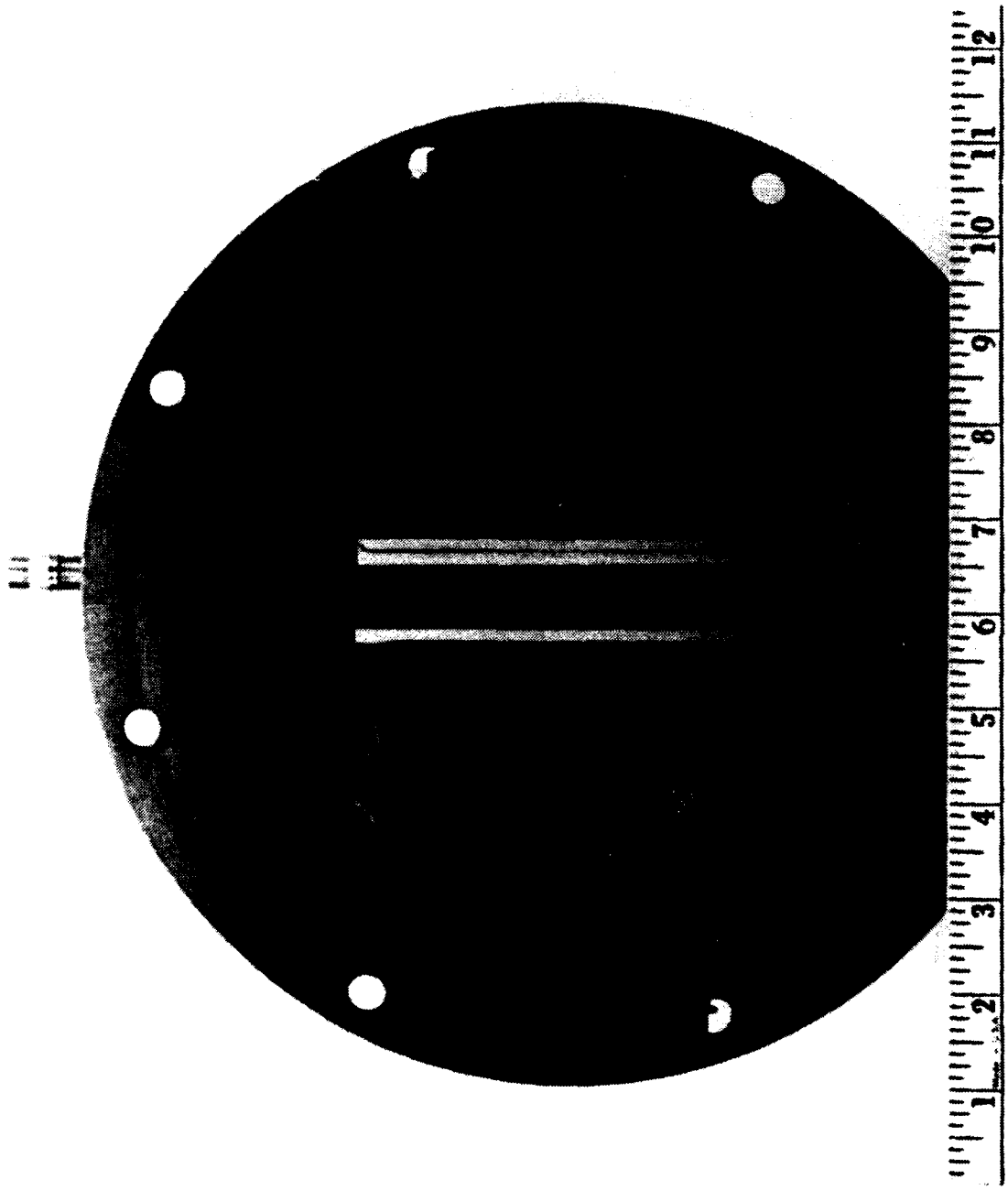


Figure 3.7 A Photograph of Test Section--Top View

The test section is 304.8 mm (12.9 in) long with an inner diameter of 157.5 mm (6.2 in). The high-velocity environment was created by a converging nozzle arrangement (shown in Figures 3.8-3.10) that reduced the cross-sectional flow area (from circular to rectangular) by a factor of 3.9. The vapor flow converged from a 157.5 mm (6.2 in) diameter header to a 31.6 mm (1.24 in) by 157.5 mm (6.2 in) rectangular channel within the test section. The channel width dimension was chosen to simulate a tube pitch to diameter ratio (P/D_o) of 1.25. Since the tube diameter was 19.05 mm, this pitch results in a fin tip clearance of 5.3 mm (0.21 in) on each side. To ensure two parallel channel faces, three spacers were installed in three locations along the channel. Stiffeners at the trailing edge of the channel centered it within the chamber as well as strengthened the thin metal structure. Viewing the condensing process on a tube was accomplished by installing Pyrex glass windows on the test section as well as along the channel walls. A smooth inner channel wall was accomplished by building a window frame on the outer channel wall that allowed the inner glass wall to align with the inner channel wall. In addition to providing a means to mount the glass, this frame also provided additional structural strengthening.

The effects of the vapor velocity profile on tube positioning within the flow-passage and consequently on the

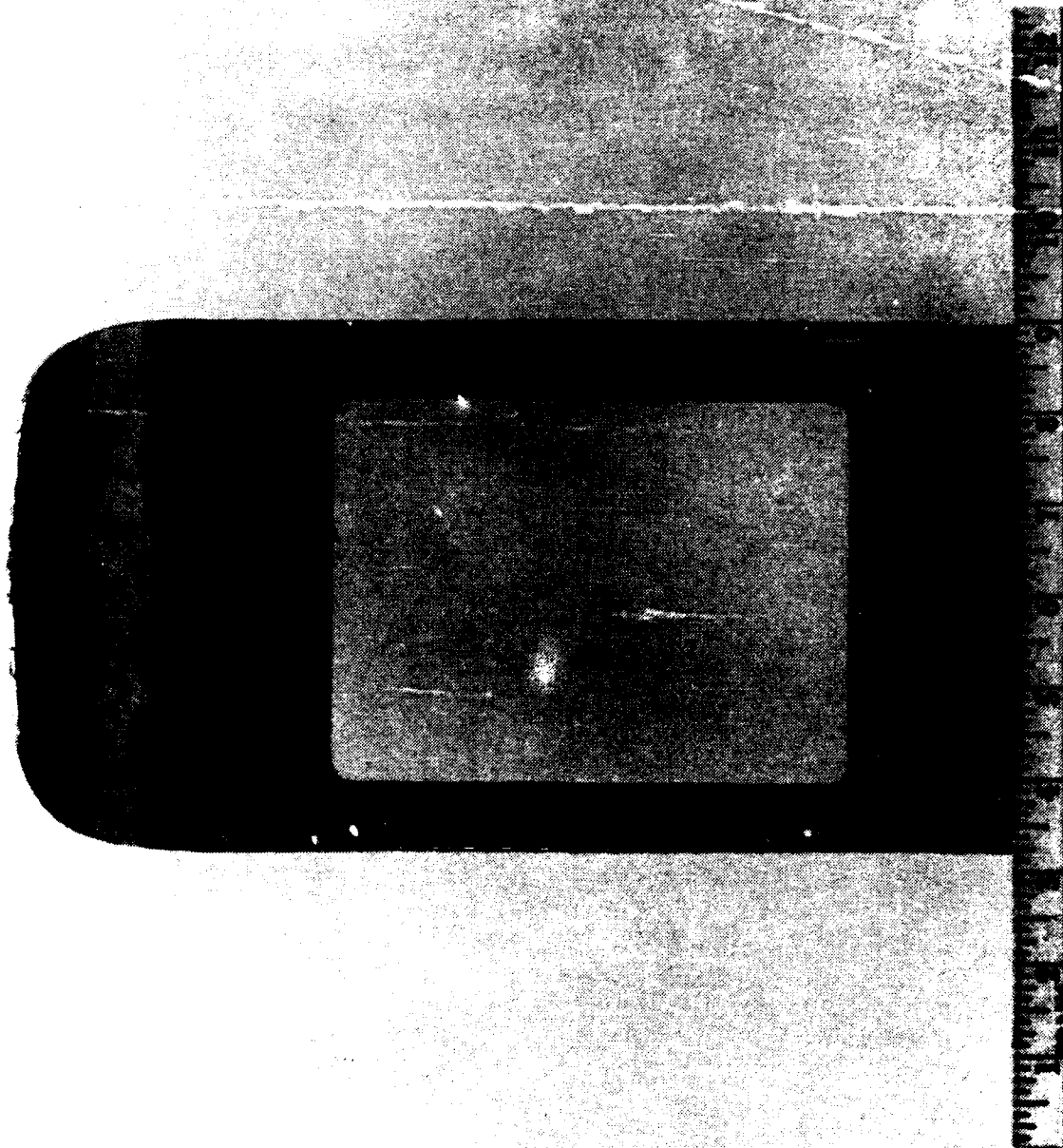


Figure 3.8 A Photograph of Converging Nozzle with Windows Installed

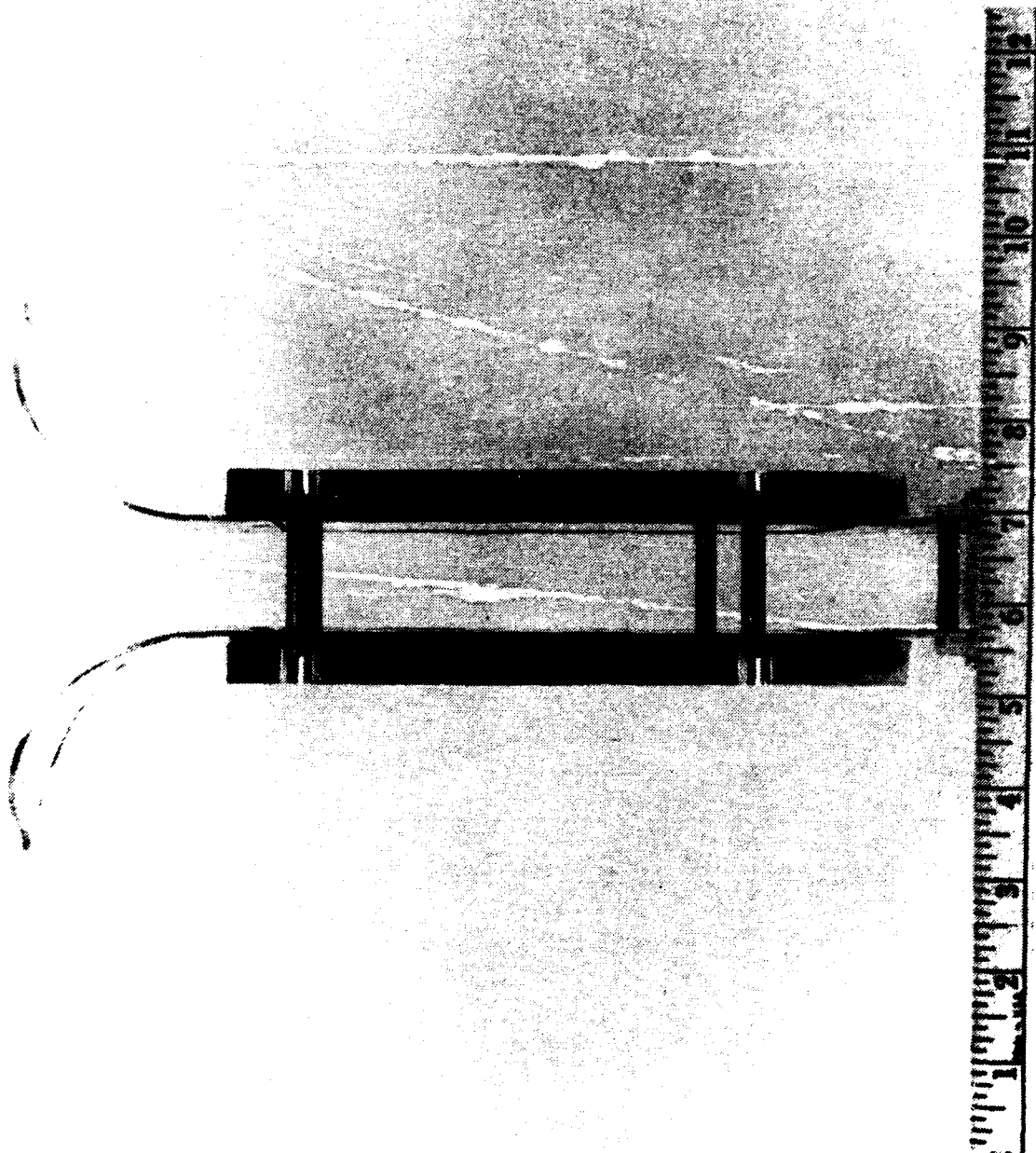


Figure 3.9 A Photograph of Converging Nozzle--Side View

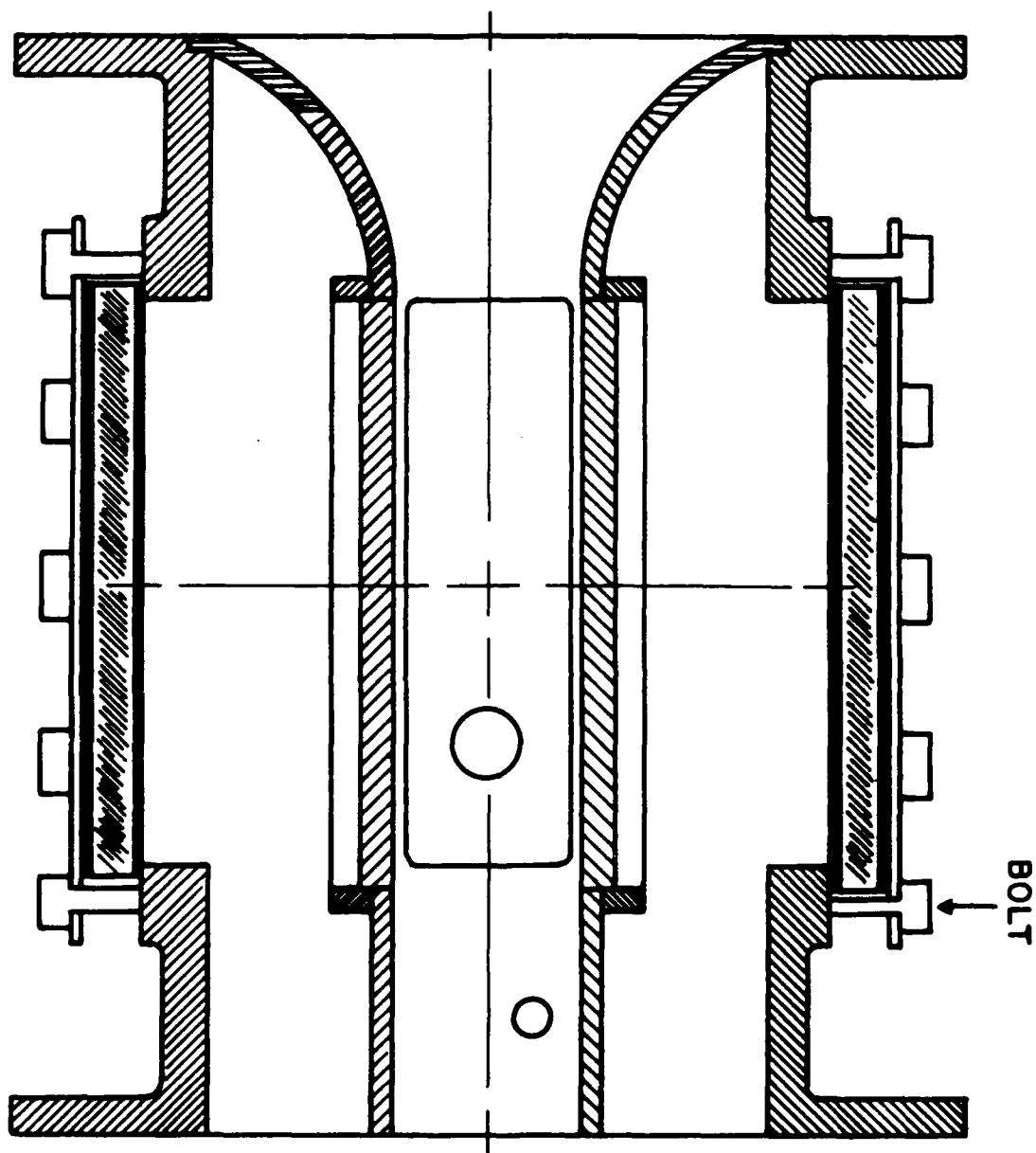


Figure 3.10 A Cross-sectional View of Test Section Showing Converging Nozzle Installation

heat-transfer performance, are unknown. Therefore, rectangular Teflon tube sheets were designed to support future testing of this effect as well as innundation effects. The rectangular tube sheets were held in place by aluminum backing plates. The tube was centered within the test section by installing two 0.79 mm (5/16 in) Teflon sleeves on each end of the tube, thus ensuring an active condensation length of 135 mm.

The tube cooling water connections were accomplished with two short sections of Tygon tubing. The inlet connection was made directly to the tube, while the outlet backing plate was fitted with a nipple (see Figure 3.3) for connection to the mixing chamber. The mixing chamber is a simple 76.2 mm (3.0 in) cylinder (see Figure 3.5) that provides turbulent mixing of the coolant for accurate temperature measurement.

C. INSTRUMENTATION

The electrical power input to the boiler immersion heaters was controlled by a panel-mounted potentiometer. The ambient vapor and condensate temperatures were measured using calibrated copper-constantan thermocouples made of 0.25 mm diameter wires. Two of them were used for vapor temperature, one for the condensate return temperature and one for the ambient temperature. These thermocouples agreed to within 0.1 K when compared with a platinum-resistance thermometer. The coolant temperature rise in the auxiliary

condenser was monitored with the use of a newly-added 10-junction, series-connected copper-constantan thermopile with a resolution of 0.003 K. The coolant temperature rise (monitored by the data-acquisition system) along with the auxiliary condenser flow rate (manually input by the operator) was utilized by a program to calculate the upstream vapor velocity. Since the most critical measurement during these tests is the temperature rise of coolant through the test tube, considerable attention was paid to obtaining the highest possible accuracy of this measurement. For this purpose, two independent temperature techniques were utilized: A Hewlett-Packard (HP) 2804A quartz thermometer with two probes having a resolution of 0.0001 K was used in addition to a 10-junction series connected copper-constantan thermopile with a resolution of 0.003 K. The test tube cooling water flow rate was measured using a calibrated rotameter and the value was manually entered into the computer. The cooling water flow rate through the auxiliary condenser was monitored by two parallel flow meters that allowed only one calibrated flow meter in service at any one time. The smaller flowmeter was utilized when obtaining low velocity data (for low boiler input power) while the large flow meter was utilized for obtaining the higher velocity data.

Absolute system pressure was determined by the use of a U-tube mercury-in-glass manometer (graduated in mm). The

manometer was connected to a pressure tap located below the test tube (Figure 3.10). At the beginning and at the end of each test run, an accurate pressure reading was manually entered into the computer. The measured system pressure and the saturation pressure corresponding to the measured vapor temperature were utilized to compute the concentration of any air that might be present. For this purpose, a Gibbs-Dalton ideal gas-mixture relationship was used. The computed non-condensing gas concentration was found to be within -0.10 to 0.0 percent. Such values revealed that major air leaks did not take place following the latest vacuum test on the apparatus. Note that the negative value for the non-condensing gas concentration represents the existence of vapor superheat, which arises mainly from the uncertainties associated with measured quantities.

D. SYSTEM INTEGRITY

Vacuum tightness for any condensing heat-transfer system, especially at low pressures similar to large steam-plant condensers (which operate at absolute pressures of about 50 mmHg), is very important. The reason for this is because even a small amount of air or other non-condensing gases present with the condensing vapor tends to accumulate at the liquid-vapor interface. When this phenomenon takes place, an added thermal resistance occurs at the interface which considerably degrades the heat-transfer performance. Therefore, in an effort to collect consistent and reliable

data, extreme care was taken to ensure a leak-tight apparatus. For example, during the early stages of this research and prior to data collection, all leaks were repaired. Subsequent to repairs, a vacuum test was conducted; a leak rate which corresponds to a pressure rise of about 4 mmHg in 24 hours at a pressure of about 12 mmHg absolute was measured and considered to be acceptable. Additionally, the vacuum pump was operated at selected intervals during the R-113 testing, and continually during the steam testing, effectively eliminating the accumulation of air and non-condensing gases within the apparatus.

E. DATA-ACQUISITION SYSTEM

An HP-9826A computer was used to control an HP-3497A Data-Acquisition System to monitor the system temperatures. While previous researchers at the Naval Postgraduate School used boiler power to determine the vapor velocity, this research used the total energy removed by the test and auxiliary condensers, together with the energy lost to the environment. Raw data were processed immediately using an assumed value for the Sieder-Tate-type coefficient (representing the tube side heat-transfer coefficient) and stored on a diskette for reprocessing at a later time. After all the sets were collected, the data were reprocessed using a new Sieder-Tate coefficient found by the modified Wilson method.

F. TUBES TESTED

For this research, three copper tubes having integral, rectangular-section fins and a smooth tube were tested. The finned tubes had dimensions of 1.0 mm for fin thickness and height and fin spacings of 0.25, 1.5 and 4.0 mm. These tubes were systematically tested at vapor velocities of 0.44, 0.65, 0.90, 1.2, 1.5, and 1.9 m/s for Freon-113 and 4.8, 13.1, 23.7, and 31.3 m/s for steam.

IV. SYSTEM OPERATION AND DATA REDUCTION

A. SYSTEM OPERATION

1. For R-113 as Working Fluid

Subsequent to the installation of a clean tube, the system was started in accordance with the procedures listed in Appendix A. During startup, the purge pump was operated at selected intervals to remove non-condensing gases. The system was allowed to reach steady-state conditions as indicated by a stabilized test-section temperature of 48.5°C and a variation in the tube coolant temperature rise of ± 0.005 K as indicated by the quartz thermometers. In an effort to provide near equally-spaced heat flux data points, two sets of data were taken for each of the following coolant flow rates: 20% (1.6 m/s), 26% (1.49 m/s), 35% (1.97 m/s), 45% (2.51 m/s), 54% (3.0 m/s), 62% (3.43 m/s), 70% (3.86 m/s), 80% (4.4 m/s) and again at 20% to show repeatability within each run. These same flow rates were used for additional runs as the vapor velocity was increased to the following values: 0.44, 0.65, 0.90, 1.22, 1.46, and 1.92 m/s. As the cooling water flow rate through the test tube was changed, the system experienced a slight change in pressure. In an effort to maintain a constant system pressure, the flow rate through the auxiliary condenser was adjusted. For example, when the flow rate through the test

tube was increased, the flow rate through the auxiliary condenser had to be decreased, thus maintaining the desired internal system pressure. To test each tube with the range of vapor velocities listed above, two auxiliary condenser flow meters were used: a 1/2 in rotameter for accurate auxiliary condenser flow measurements at low vapor velocities and a 1 in rotameter for the flow measurements at high vapor velocities. All tubes tested were manufactured from copper which is a highly conductive material. Therefore, the time interval required to achieve steady-state conditions after the tube coolant flow rate changed was approximately two minutes and the entire run of 18 data sets (at a constant vapor velocity) was completed in about an hour.

After steady-state conditions were reached, the operator would be prompted by the computer to enter the tube flow rate and auxiliary condenser flow rate. Upon entering these values, the software would gather and store all thermocouple and quartz thermometer readings. The initial and final data sets of each run were used to verify that no non-condensing gases were present. To demonstrate repeatability, two runs were accomplished at each vapor velocity.

2. For Steam as Working Fluid

The condensation process of steam on a copper tube could occur under a partial dropwise mode (a more effective

mode than the filmwise condensation mode) due to the poor wetting characteristics with water. Since all of the tubes tested were manufactured from copper, and since the purpose of the research was to investigate the effect of vapor velocity with filmwise condensation, each tube was prepared in the following manner to ensure that filmwise condensation took place:

1. Clean the internal and external surface of the tube with distilled water.
2. Place the tube in a steam bath.
3. Heat and stir a solution of equal volumes of ethyl alcohol and sodium hydroxide. When the solution is watery, apply a coating to the external tube surface using a tooth brush.
4. If the tube has not been previously treated, apply a new coating every 15 minutes for approximately one hour to oxidize the outside surface (a black oxide layer). If the tube has been previously treated, apply a coating every ten minutes for a period of 30 minutes to reestablish the oxide layer and remove contaminants.
5. Thoroughly rinse the tube with distilled water to remove excess solution, and install it in the system as soon as possible for testing.

Georgiadis [Ref. 32] reported that the black oxide layer produced exhibits high wetting characteristics with negligible thermal resistance.

An investigation conducted by Search [Ref. 3] revealed that the water-side thermal resistance contributes to as much as 56% of the overall thermal resistance (as compared to 22% for the steam film resistance). Therefore, any fluctuations or deviations in the water-side resistance

will result in an even greater discrepancy in the condensing heat transfer coefficient. Therefore, to improve the accuracy on the condensing heat-transfer coefficient, through the enhancement of the inside heat-transfer coefficient, a spiral insert was used. The spiral insert consisted of a 6.4-mm-diameter stainless-steel rod, with a 3.2-mm-copper wire (with a 20 mm pitch) wrapped around and soldered to the rod. To avoid conductance from the tube wall to the insert, the wrapped insert was machined down to give a clearance of 0.5 mm between the outer wire diameter and the inner tube wall.

Following installation of a clean tube and insert, the system was again started in accordance with Appendix A. However, the system was warmed up differently for steam (vacuum testing) than for R-113 (near-atmospheric testing) in that heaters were energized to warm the distilled water to the approximate operating temperature then the purge pump was started and operated continuously. Steady-state conditions were achieved when the variation in the tube coolant temperature rise was ± 0.005 K and steam temperature stabilized at 48.5°C . Two sets of steam data were obtained using the same tube coolant flow rates (as with the R-113 data) to provide near-equally-spaced heat flux values (18 data points per run). Steam testing also employed the two auxiliary condenser flow meters used for R-113 testing. The vapor velocity for steam testing was

systematically increased by boiler input power to the following values: 4.8, 13.1, 23.7, and 31.3 m/s.

After steady-state conditions were achieved (approximately two minutes after adjusting flow rates), the operator would be prompted by the computer to enter the tube-water flow rate and the auxiliary condenser flow rate. The computer would then automatically gather and store all thermocouple and quartz thermometer data. The same fluctuations in steam pressure with tube flow rate were experienced (as with R-113) and the auxiliary condenser flow rate was adjusted accordingly.

As discussed in Chapter III, rectangular viewports were provided for visual observation of the condensing process in a high-vapor-velocity environment. During steam testing, the appearance of the film was verified and if there was evidence of dropwise condensation, the run was discontinued and the data were discarded. However, at high vapor velocities and consequently high condensation rates, it was very easy to maintain a complete film as typically demonstrated by less than a three percent disagreement in the steam-side heat-transfer coefficient between initial and final data sets.

To demonstrate repeatability, two runs at different vapor velocities (usually a high and then a low vapor velocity) were accomplished on each tube before treating the tube again. The next time that tube was tested, the same

two vapor velocities were used. However, the order of the vapor velocities were reversed (i.e., low vapor velocity followed by high vapor velocity). In each case, the results compared within three percent.

B. DATA REDUCTION

The overall thermal resistance ($1/U_O A_O$) is the summation of the individual thermal resistances of the water-side, wall and vapor-side resistances (neglecting fouling resistance) and can be expressed as:

$$\frac{1}{U_O A_O} = \frac{1}{h_i A_i} + \frac{R_w}{A_O} + \frac{1}{h_O A_O} , \quad (4.1)$$

where

$$R_w = \frac{D_O \ln \left[\frac{D_O}{D_i} \right]}{2 k_m} , \quad (4.2)$$

and the overall thermal resistance can be computed with the following equations:

$$Q = \dot{m} C_p \Delta T_{cw} = U_O A_O [LMTD] , \quad (4.3)$$

where

$$LMTD = \frac{T_{c_o} - T_{c_i}}{\ln \left[\frac{T_{sat} - T_{c_i}}{T_{sat} - T_{c_o}} \right]} . \quad (4.4)$$

The calculation of U_o is the first step in the determination of the inside and outside heat-transfer coefficients (h_i and h_o , respectively).

The Modified Wilson Plot method was utilized to process all the filmwise condensation data. The inside heat-transfer coefficient is determined by a Sieder-Tate-type equation:

$$h_i = C_i \frac{k_b}{D_i} Re^{0.8} Pr^{1/3} \left[\frac{\mu_b}{\mu_w} \right]^{0.14} = C_i \Omega, \quad (4.5)$$

where

$$\Omega = \frac{k_b}{D_i} Re^{0.8} Pr^{1/3} \left[\frac{\mu_b}{\mu_w} \right]^{0.14} \quad (4.6)$$

Previous research at the Naval Postgraduate School has utilized Nusselt's equation to determine the outside heat-transfer coefficient for film condensation on smooth horizontal tubes. This equation is given by:

$$h_{Nu} = 0.655 \left[\frac{k_f^3 \rho_f^2 g h_{fg}}{\mu_f D_o q} \right]^{1/3} \quad (4.7)$$

where the subscript f on the fluid properties indicates that they are calculated at the local film temperature.

Nusselt's assumptions include a zero-vapor-shear condition, which results in a leading coefficient of 0.655. However, in a high-vapor-shear environment, a larger leading

coefficient (say α_N) will result, which has to be determined iteratively via the Modified Wilson Plot Technique. The Nusselt relation will be used as a reference for this research.

As pointed out in Chapter II, to account for high vapor-shear, Fujii et al. [Ref. 25] developed a correlation that accounts for the variation of the outside heat-transfer coefficient on a smooth tube with vapor velocity. It is given by (also Equation (2.11))

$$\text{Nu } \tilde{\text{Re}}^{-1/2} = 0.96 F^{1/5} , \quad (4.8)$$

where

$$F = g D_o \mu_f h_{fg} / U_\infty^2 k_f \Delta T . \quad (4.9)$$

Equations (4.8) and (4.9) may be re-written to express h_o as a function of heat flux and vapor velocity as given by:

$$h_o = \alpha_F \left[\frac{g h_{fg}}{q} \right]^{1/4} [\mu_f^{-3} D_o^{-3} \rho_f^5 U_\infty]^{1/8} k_f = \alpha_F \beta , \quad (4.10)$$

where

$$\beta = \left[\frac{g h_{fg}}{q} \right]^{1/4} [\mu_f^{-3} D_o^{-3} \rho_f^5 U_\infty]^{1/8} k_f . \quad (4.11)$$

Substituting Equations (4.5) and (4.10) into Equation (4.1), several algebraic steps may be followed to get:

$$\frac{1}{U_O} = \frac{A_O}{A_i C_i \Omega} + R_w + \frac{1}{\alpha_F \beta} , \quad (4.12)$$

$$[\frac{1}{U_O} - R_w] \beta = \frac{A_O \beta}{A_i C_i \Omega} + \frac{1}{\alpha_F} . \quad (4.13)$$

Equation (4.13) can be expressed in a linear form as given below:

$$Y = mX + b ,$$

where

$$Y = [\frac{1}{U_O} - R_w] \beta , \quad (4.14)$$

$$X = \frac{A_O \beta}{A_i \Omega} , \quad (4.15)$$

$$m = \frac{1}{C_i} , \quad (4.16)$$

$$b = \frac{1}{\alpha_F} . \quad (4.17)$$

where the coefficient values of C_i and α_F are defined by Equations (4.5) and (4.10) respectively. An iterative process was utilized to obtain C_i and α_F by fitting a least-squares line to the data points in each run (i.e., for

the different water velocities). Notice that the slope of the Modified Wilson plot line gives the inverse of C_i , while the intercept gives the inverse of α_F . Iteration of these coefficients is continued until convergence is within $\pm 0.1\%$ between two successive values. The inside heat-transfer coefficient (h_i) was then determined using Equation (4.5). Since the overall heat-transfer coefficient (U_o) was known with the use of Equation (4.3), Equation (4.1) was rearranged to determine the outside heat-transfer coefficient by subtracting the wall and inside resistances from the overall resistance.

$$\frac{1}{h_o} = \frac{1}{U_o} - \frac{A_o}{A_i h_i} - R_w \quad (4.18)$$

For this research, enhancement is defined (for a smooth or finned tube) as the ratio of outside heat-transfer coefficient for the tube tested (in a high-vapor-shear environment) to that of the outside heat-transfer coefficient for a smooth tube in a zero-vapor-velocity environment (Nusselt theory) at the same heat flux.

With this definition, the ratio of Equations (4.10) to (4.7) would not yield a simple expression. As a result, an alternative procedure was used to determine the outside heat-transfer coefficient using the Nusselt-type expression given below:

$$h_o = \alpha_F \beta = \alpha_N \left[\frac{k_f^3 \rho_f^2 g h_{fg}}{\mu_f D_o q} \right]^{1/3} \quad (4.19)$$

With Equation (4.19), the enhancement (for constant heat flux) created by vapor shear is given by

$$\epsilon_q = \alpha_N / 0.655 \quad (4.20)$$

To determine α_N the following procedure was used: The software utilized for this research allows the operator the option of processing or reprocessing the raw data using the Fujii et al. [Ref. 25] relationship to account for high vapor shear. The computer prompts the operator to enter the vapor velocity and again uses the Modified Wilson plot technique to determine a Sieder-Tate-type coefficient (C_i) with high vapor shear and a value of α_F . The new value of C_i is then forced to remain constant while reprocessing the original data again, but this time the operator uses the Nusselt theory (the reference for zero vapor shear) to arrive at a new coefficient, α_N . α_N is then used in Equation (4.19) to determine h_o . Finally, the enhancement is determined from the ratio of Equations (4.19) to (4.7) (i.e., $\alpha_N / 0.655$). This method of re-processing the original data provides an assessment of the heat-transfer performance in a high vapor shear environment. Notice that the above-mentioned scheme of finding C_i using the Fujii et al. [Ref.

25] correlation, and then forcing this C_i to find an α_N value is justified by the fact that Equation (4.10) cannot be evaluated for zero vapor velocity. It is worth mentioning that the C_i found by the two methods (Nusselt and Fujii) agreed within +/- 5%.

As discussed by Masuda and Rose [Ref. 35], the enhancement ratio used for a constant temperature drop across the condensate film ($\Delta T = T_{\text{sat}} - T_{\text{wo}}$) can be expressed as:

$$\epsilon_{\Delta T} = \epsilon_q^{3/4} \quad (4.21)$$

V. RESULTS AND DISCUSSION

A. INTRODUCTION

Data were obtained for a smooth tube and three integral-fin tubes utilizing the procedures described in Chapter IV. The three finned tubes tested had a fin thickness and fin height of 1.0 mm and fin spacings of 0.25, 1.5, and 4.0 mm. For simplicity, these tubes will be referred to as tubes A, B, and C, respectively. For R-113, data were obtained at near-atmospheric conditions whereas steam data were obtained at 87 mmHg (1.7 psia). As described in Chapter IV, testing was accomplished with six vapor velocities for R-113 and four vapor velocities for steam. Complete filmwise condensation was maintained for all data runs with both fluids and the non-condensing gas concentration was essentially zero (within the accuracy of measurements). To demonstrate repeatability with R-113, two sets of data were taken at each coolant velocity. When testing with steam, the initial runs on the smooth tube were accomplished at a low vapor velocity to show agreement with previous investigations and to establish a reference as the vapor velocity was increased. The initial two runs were accomplished at two different vapor velocities (usually a high value followed by a low value). Then the tube was removed and re-treated while another tube was being tested.

The next time that the first tube was tested, the order of the two velocities was switched. Notice that this switching was used to demonstrate that the data were not affected by partial dropwise condensation when using steam as the working fluid. It is common practice to maximize the inside heat-transfer coefficient if the primary emphasis is on the outside heat-transfer coefficient. Similarly, the outside heat-transfer coefficient must be maximized if the inside coefficient is to be measured. However, as discussed in Chapter IV, this investigation uses the Modified Wilson plot technique, which gives both inside and outside heat-transfer coefficients simultaneously. For this reason, it is clear that the two resistances must be made approximately equal to obtain accurate coefficients. Based on this requirement, it was necessary to boost the inside heat-transfer coefficient through the use of a spiral insert when using steam as the working fluid, while no insert was used for R-113.

B. EFFECTS OF VAPOR VELOCITY ON HEAT TRANSFER PERFORMANCE

Figures 5.1 through 5.4 show the variations of the vapor-side heat-transfer coefficient with the temperature drop across the condensate film for all four tubes with R-113. In these figures, vapor velocity is shown as a parameter. For comparison purposes, a curve representing Nusselt theory is also shown. Also shown in these figures are the uncertainty bands computed for typical data sets

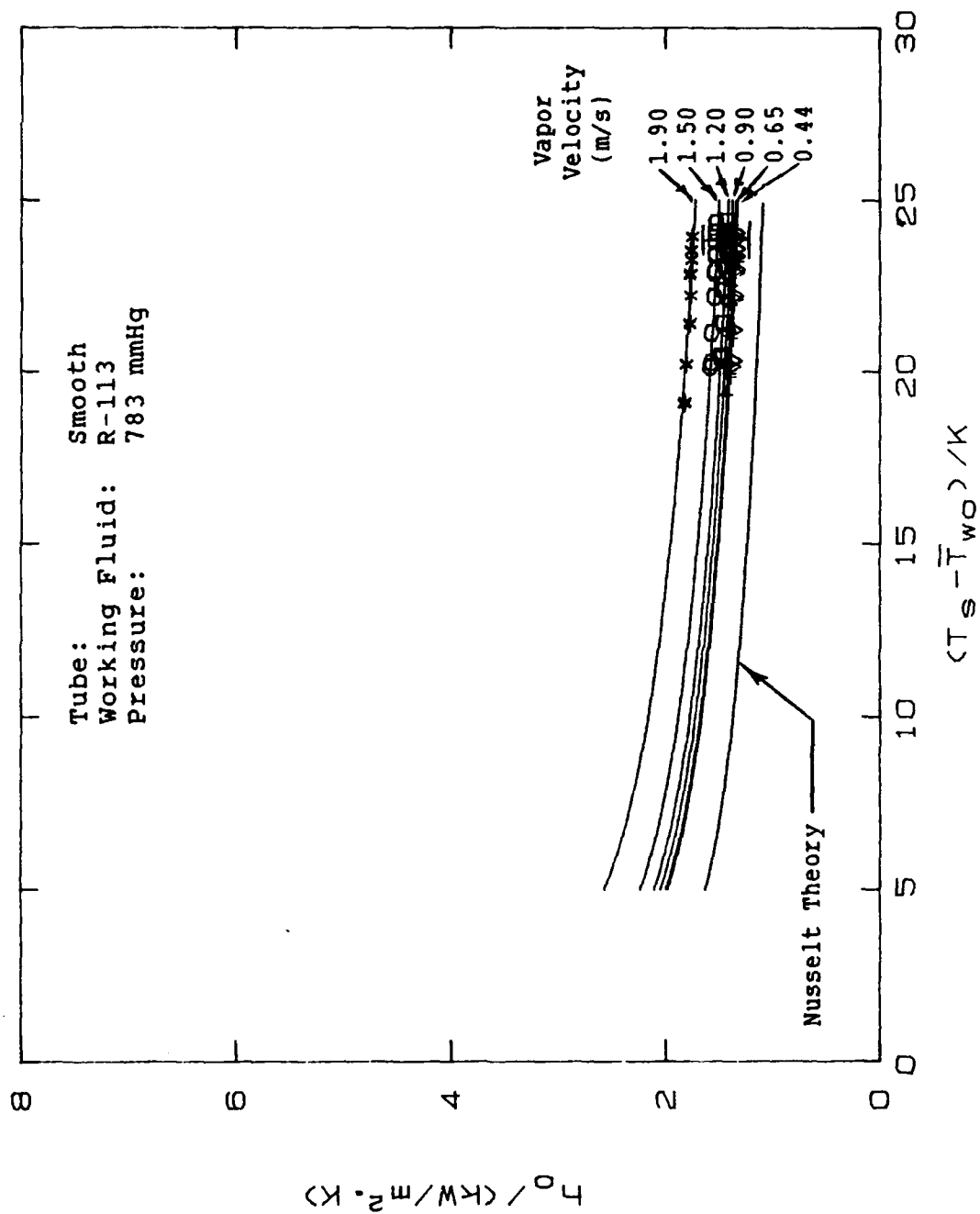


Figure 5.1 Variation of Vapor-side Heat-transfer Coefficient with Temperature Drop Across the Condensate Film for a Smooth Tube for R-113

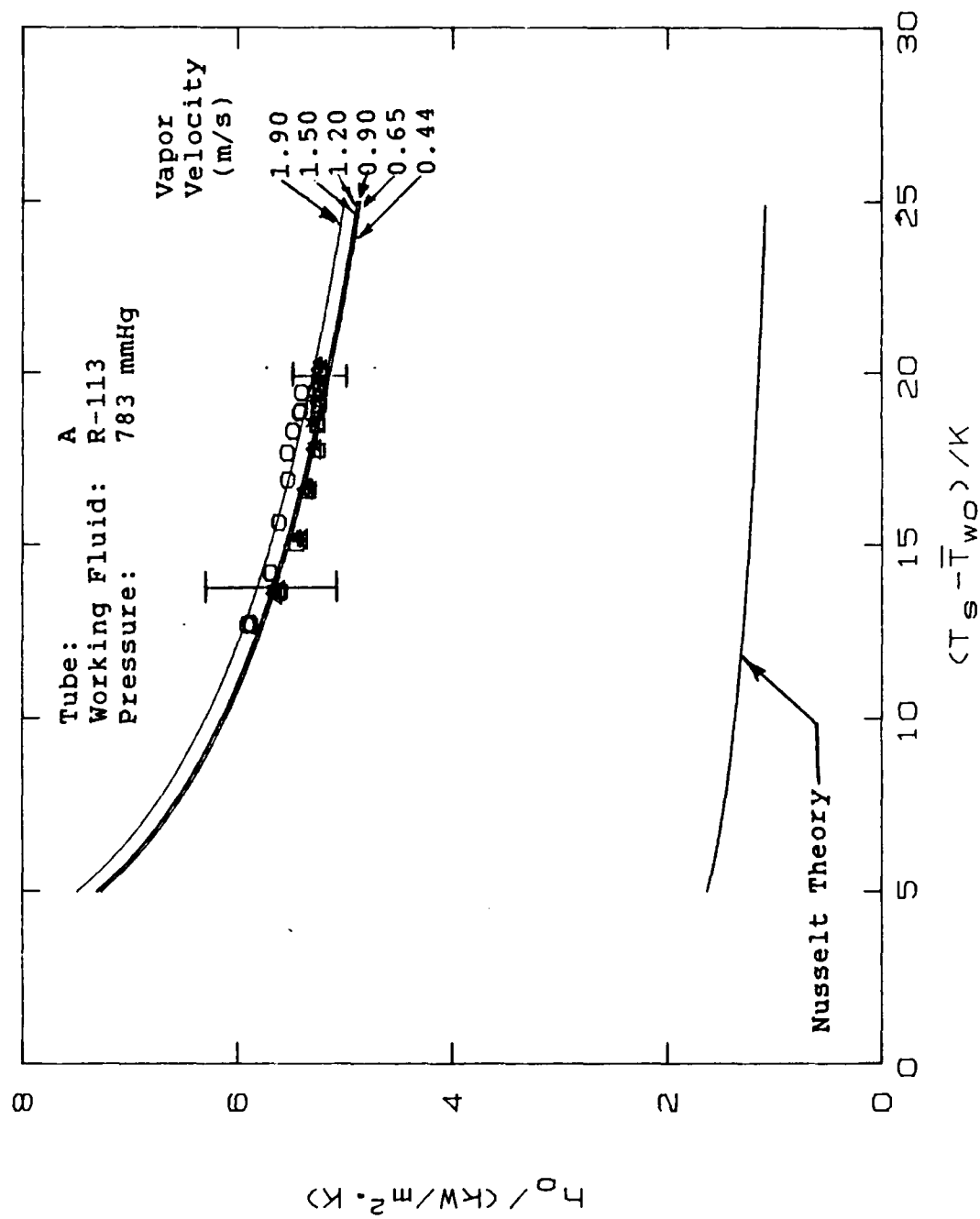


Figure 5.2 Variation of Vapor-side Heat-transfer Coefficient with Temperature Drop Across the Condensate Film with $S = 0.25$ mm for R-113

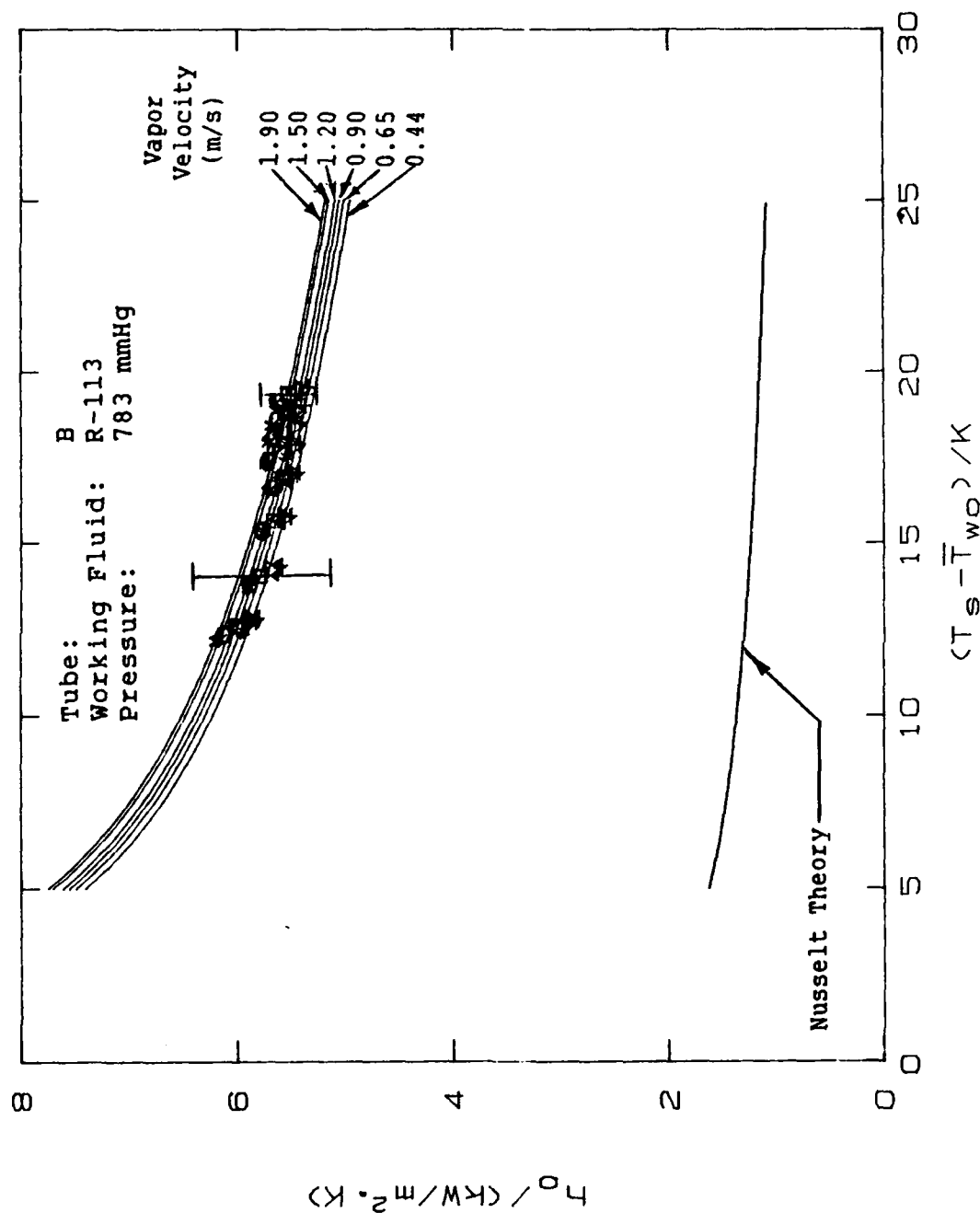


Figure 5.3 Variation of Vapor-side Heat-transfer Coefficient with Temperature Drop Across the Condensate Film with $S = 1.5$ mm for R-113

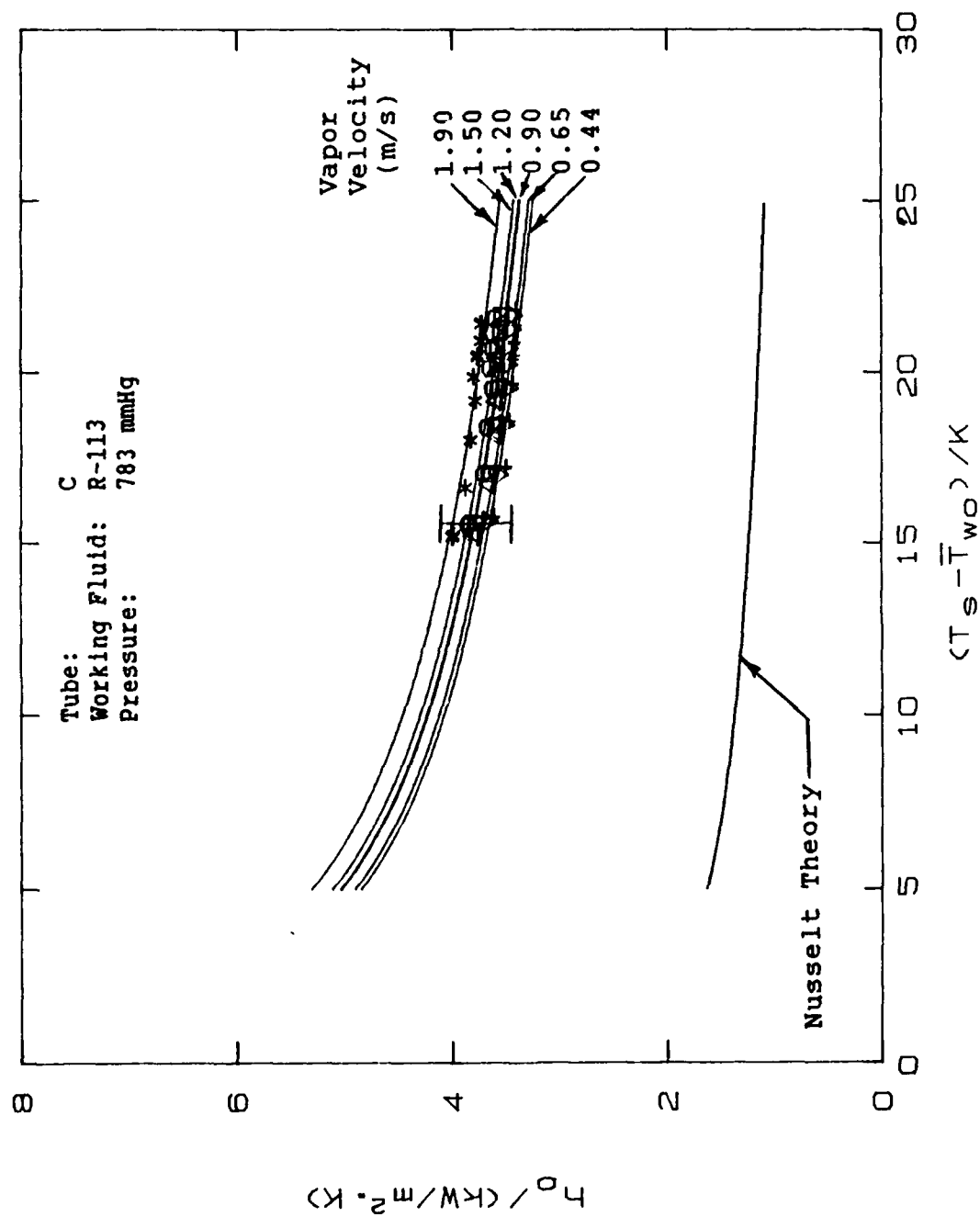


Figure 5.4 Variation of Vapor-side Heat-transfer Coefficient with Temperature Drop Across the Condensate Film with $S = 4.0$ mm for R-113

using the uncertainty analysis outlined in Appendix B. Notice that the repeatability of data (for the same conditions) was much better than the ranges suggested by these uncertainty bands. In each case, the vapor-side heat-transfer coefficient shows a clear trend with vapor velocity (i.e., h_o increases as the vapor velocity increases).

The least-squares-fit curves shown in these figures were generated in accordance with the following expression:

$$q = a \Delta T^n \quad (5.1)$$

As pointed out by Yau et al. [Ref. 36], slightly better fits to the data points were possible by computing an exponent (n) for each data run. In fact the computed n values varied between 0.70 and 0.73 for steam and between 0.80 and 0.81 for R-113. These n values are in very good agreement with Yau et al., who reported values between 0.7 and 0.8. Recall that enhancement created by the effect of vapor velocity was defined in Chapter IV (Equation (4.19)) as $\epsilon_q = \alpha_N/0.655$. Notice that this equation is possible only if the exponent (n) discussed above is set equal to 0.75. Therefore, least-squares fits shown in Figures 5.1 through 5.4 were based on an exponent value (n) of 0.75.

Data taken on these same four tubes with steam as the working fluid are plotted in Figures 5.5 through 5.8 using the same format just described. Once again, the increase in

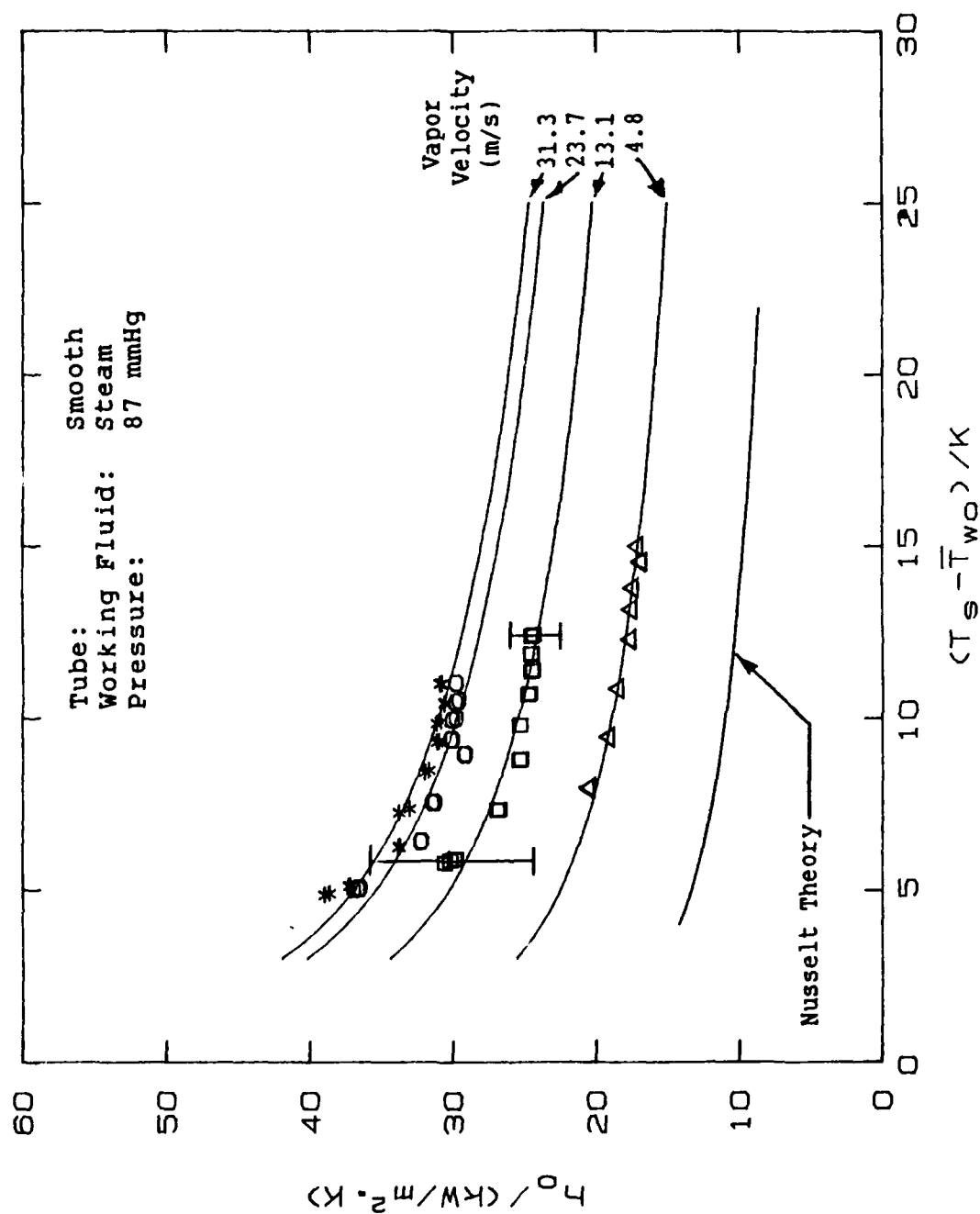


Figure 5.5 Variation of Vapor-side Heat-transfer Coefficient with Temperature Drop Across the Condensate Film for a Smooth Tube for Steam

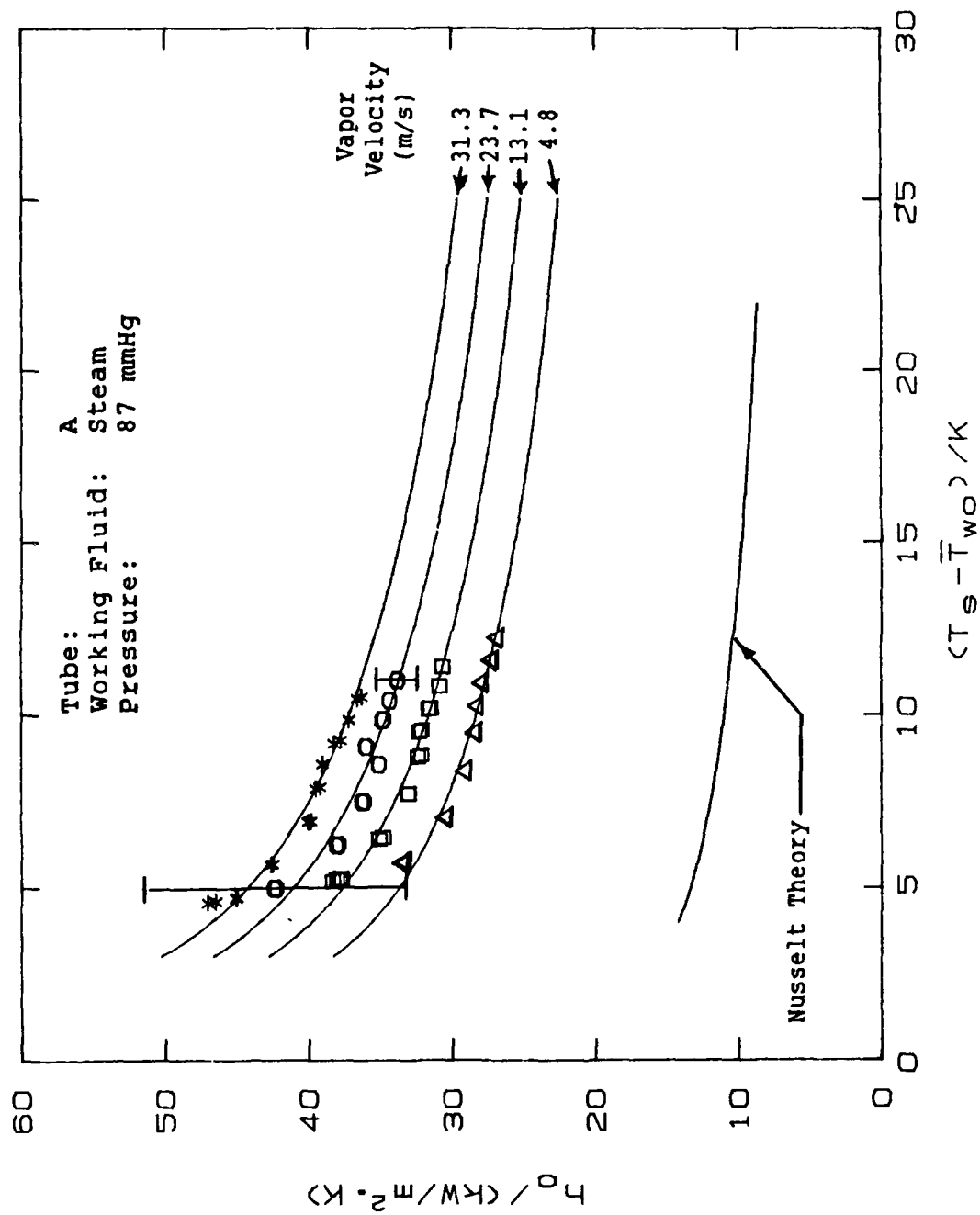


Figure 5.6 Variation of Vapor-side Heat-transfer Coefficient with Temperature Drop Across the Condensate Film with $S = 0.25$ mm for Steam

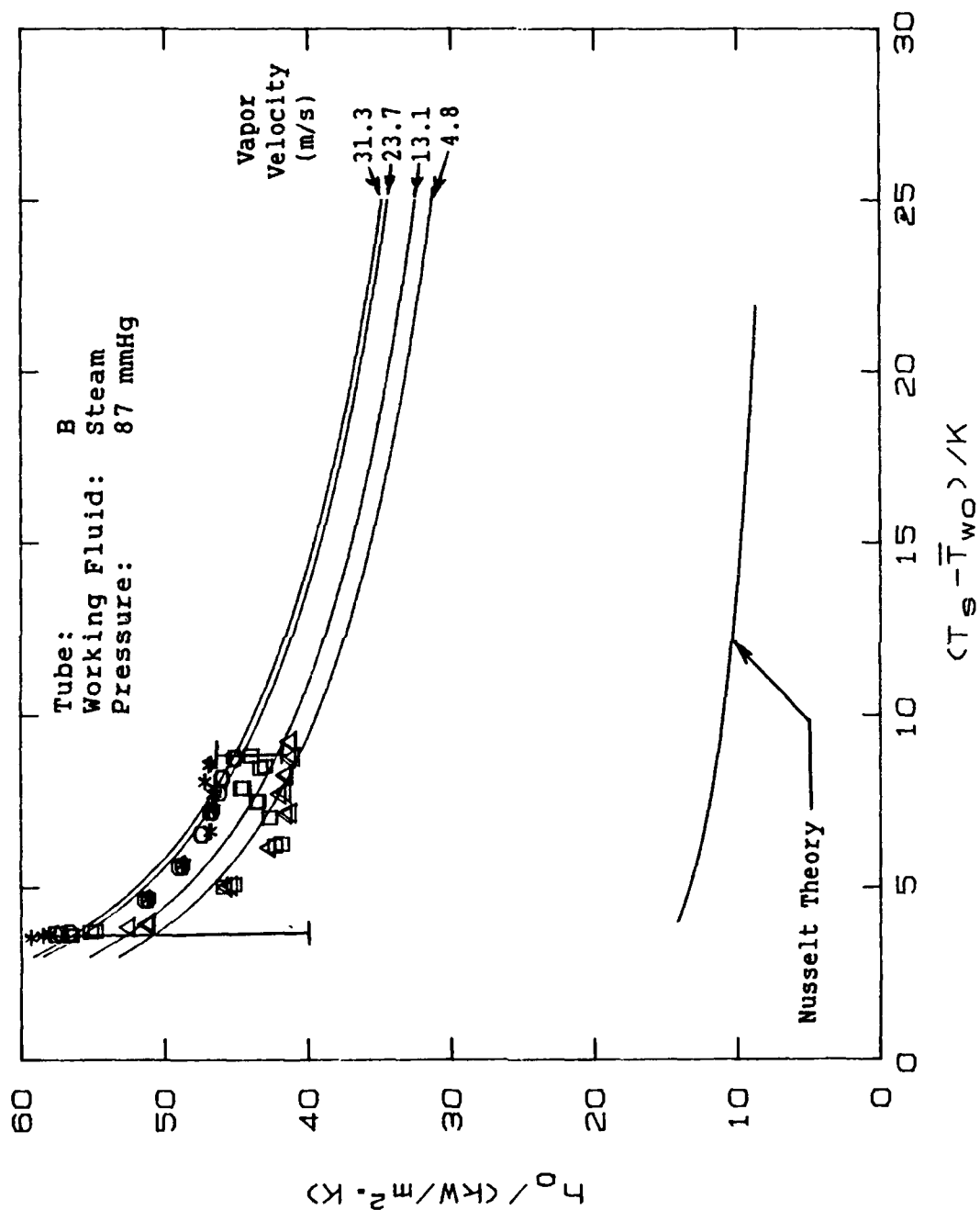


Figure 5.7 Variation of Vapor-side Heat-transfer Coefficient with Temperature Drop Across the Condensate Film with $S = 1.5$ mm for Steam

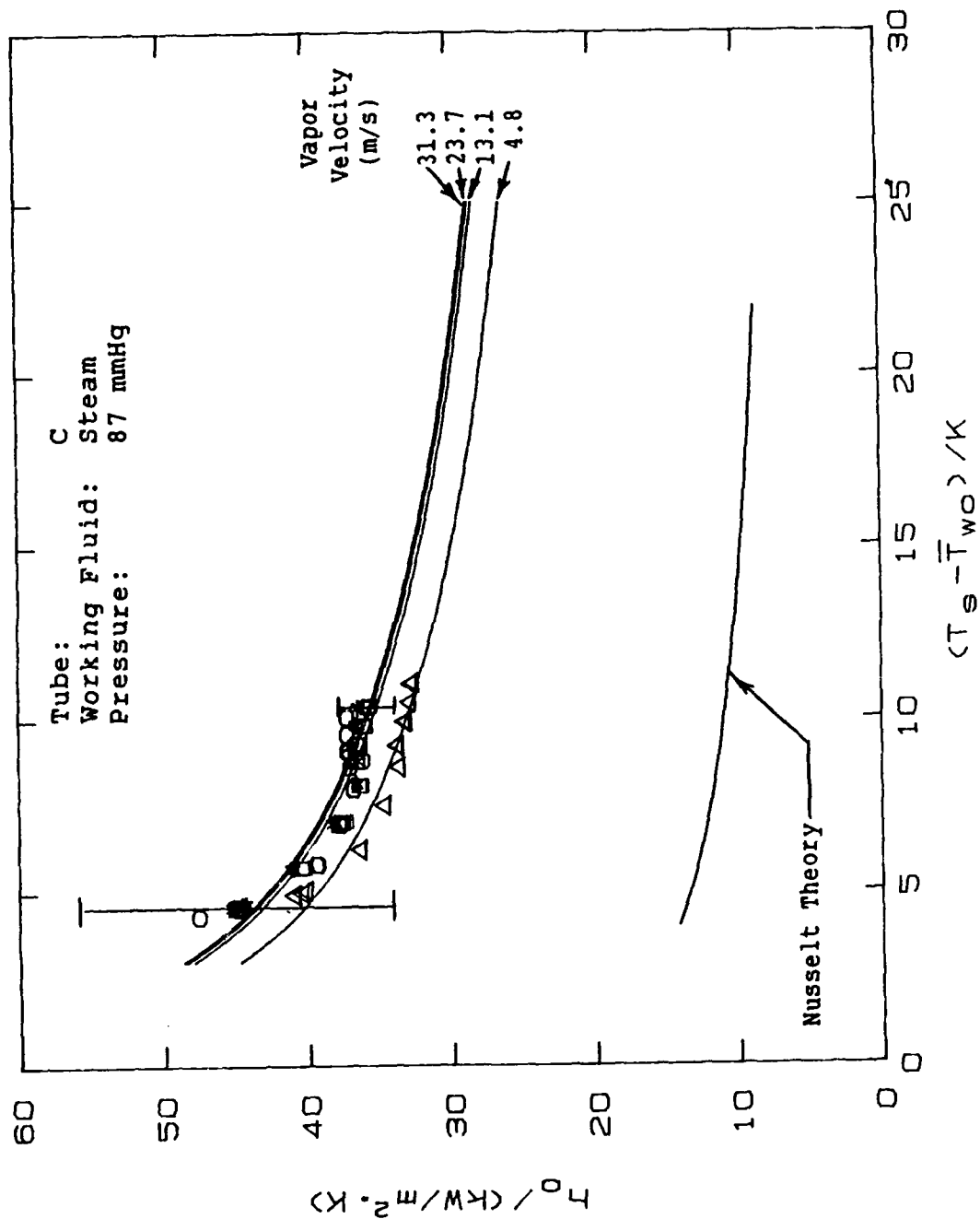


Figure 5.8 Variation of Vapor-side Heat-transfer Coefficient with Temperature Drop Across the Condensate Film with $S = 4.0 \text{ mm}$ for Steam

vapor velocity increases the vapor-side heat-transfer coefficient. Notice that the effect of vapor velocity is the largest for the smooth tube.

The results observed in these figures are summarized, in the form of the enhancement ratio at constant temperature difference ($\epsilon_{\Delta T} = \epsilon_q^{3/4}$), in Tables 5.1 and 5.2 for R-113 and steam respectively. As can be seen, for R-113, the

TABLE 5.1
EFFECT OF VAPOR VELOCITY ON THE HEAT-
TRANSFER PERFORMANCE FOR R-113

<u>VAPOR VELOCITY (M/S)</u>	<u>ENHANCEMENT BASED ON CONDENSATE FILM ΔT SMOOTH</u>	<u>A</u>	<u>B</u>	<u>C</u>
0.44	1.164	4.383	4.452	2.903
0.65	1.183	-	4.503	2.937
0.90	1.224	4.364	4.541	3.013
1.22	1.259	4.360	4.576	3.019
1.46	1.337	4.500	4.632	3.063
1.92	1.537	4.388	4.660	3.179
% IMPROVEMENT	32	0	5	10

smooth tube results in a 32 percent improvement in the outside heat-transfer coefficient when the vapor velocity was increased from 0.44 to 1.9 m/s. However, the improvement with vapor velocity was smaller for the finned tubes. In fact, the improvements are 0, 5, and 10 percent for tubes A, B, and C, respectively. This trend is in

TABLE 5.2

EFFECT OF VAPOR VELOCITY ON THE HEAT-
TRANSFER PERFORMANCE FOR STEAM

VAPOR VELOCITY (M/S)	ENHANCEMENT BASED ON CONDENSATE FILM ΔT			
	<u>SMOOTH</u>	<u>A</u>	<u>B</u>	<u>C</u>
4.8	1.780	2.639	3.649	3.073
13.1	2.376	2.939	3.779	3.293
23.7	2.766	3.201	4.002	3.334
31.3	2.885	3.445	4.046	3.337
% ENHANCEMENT	62	31	11	9

agreement with the results reported by Gogonin and Dorokhov [Ref. 29], who also showed smaller improvements for finned tubes than for smooth tubes. Furthermore, the improvement is seen to increase with increasing fin spacing for R-113. This trend can be explained by the fact that as the fin spacing increases, the finned tube more closely resembles a smooth tube.

Table 5.2 shows a 62 percent improvement for the smooth tube, with steam as the working fluid, when the vapor velocity increases from 4.8 to 31.3 m/s. Once again, the effect of velocity on the finned tubes is not as large as on the smooth tube. The observed improvements are 31, 11, and 9 percent for tubes A, B, and C, respectively. In contrast to the trend seen for R-113, these data show less improvement as fin spacing increases. The exact reason for this different trend is not completely known, but can

possibly be explained by the considerable flooding that occurs on these tubes with steam as the working fluid, in contrast to R-113, which has such a small value of surface tension. Notice that tube A (which has a tube spacing of 0.25 mm) was completely flooded by water but was less than half flooded by R-113.

Previous research conducted for high vapor velocity on smooth tubes, which was summarized by Rose [Ref. 28], has displayed data by plotting $NuRe^{-1/2}$ versus F (these two terms are defined in Chapter II and from this point on will be referred to as NR and F , respectively). Figures 5.9 through 5.12 show the variation of NR and F for the smooth tube and tubes A, B, and C, respectively, for R-113 as the working fluid. For comparison purposes, curves representing Nusselt theory (Equation (2.2)) and the Fujii et al. [Ref. 25] theory (Equation (2.11)) are also shown. In each case, the data show a consistent trend. As the vapor velocity increases (i.e., F decreases) the data slope downward. More specifically, for a smooth tube, as the vapor velocity decreases ($F \rightarrow \infty$), the data approach the Nusselt correlation and as the vapor velocity increases ($F \rightarrow 0$), the data depart from the Nusselt correlation, indicating an enhancement in outside heat-transfer coefficient. This trend can be explained by recalling that the Nusselt correlation was developed with the zero-vapor-shear assumption. Therefore, a departure from Nusselt's theory

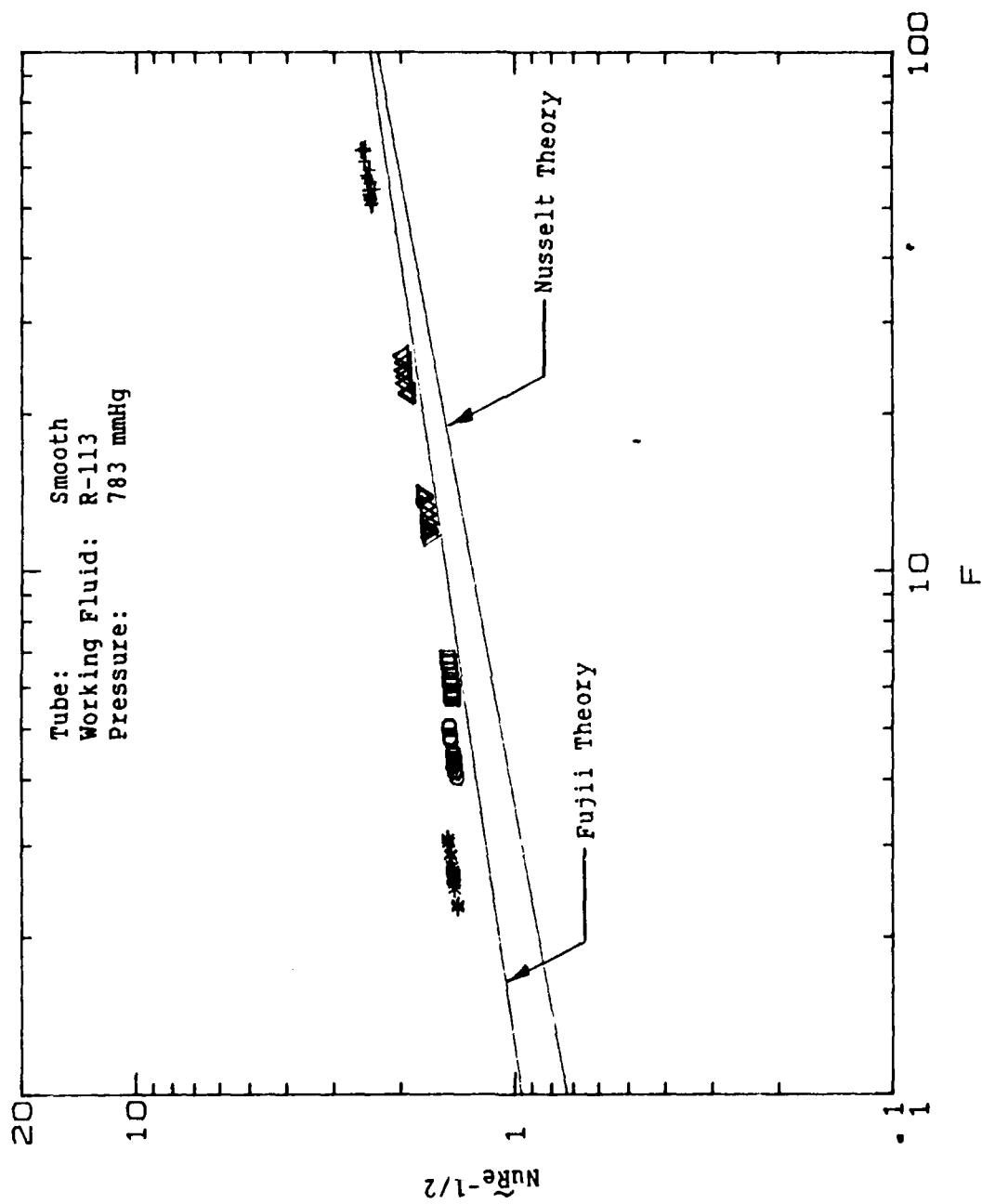


Figure 5.9 Variation of NR and F for the Smooth Tube for R-113

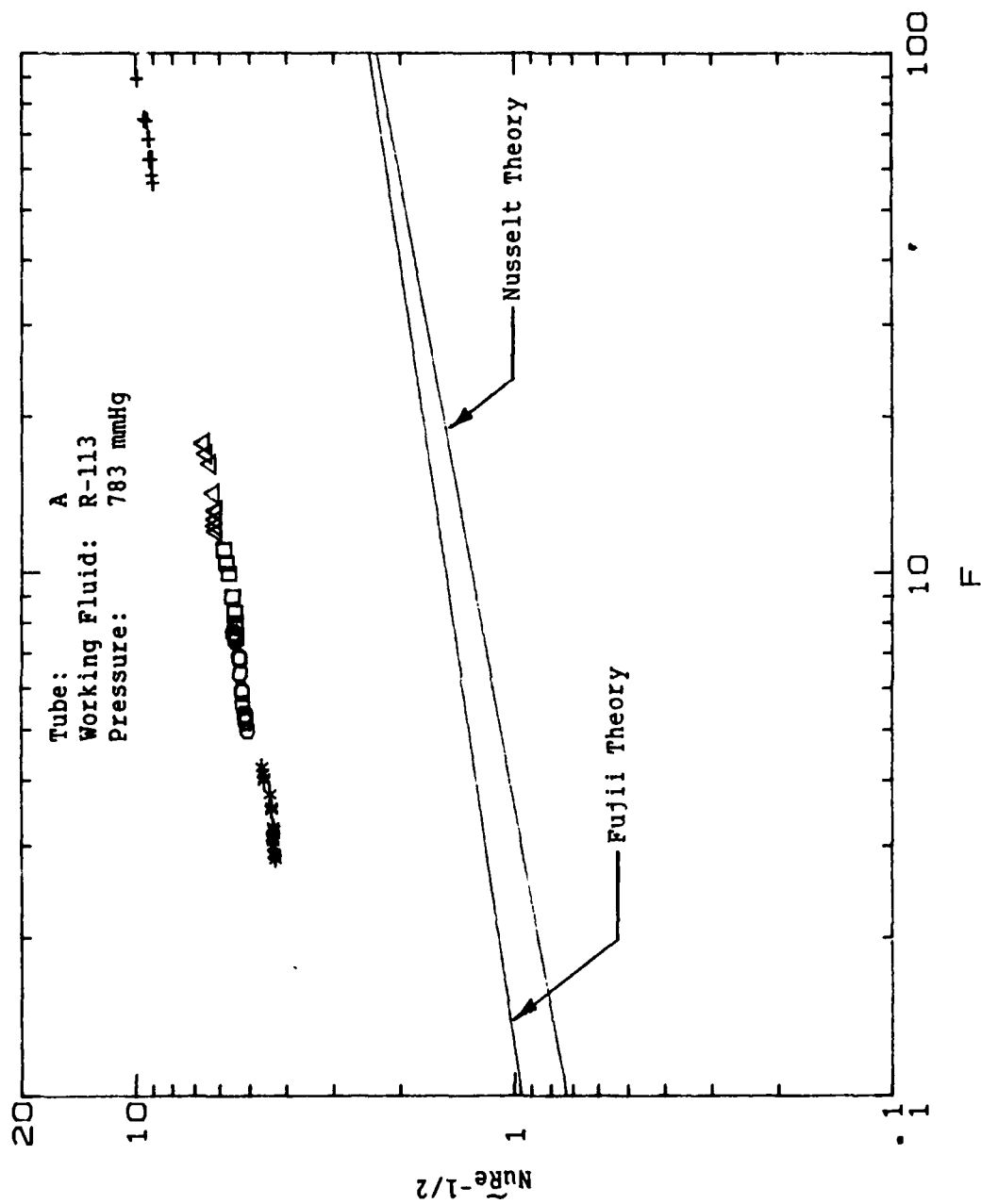


Figure 5.10 Variation of NR and F with $S = 0.25$ mm for R-113

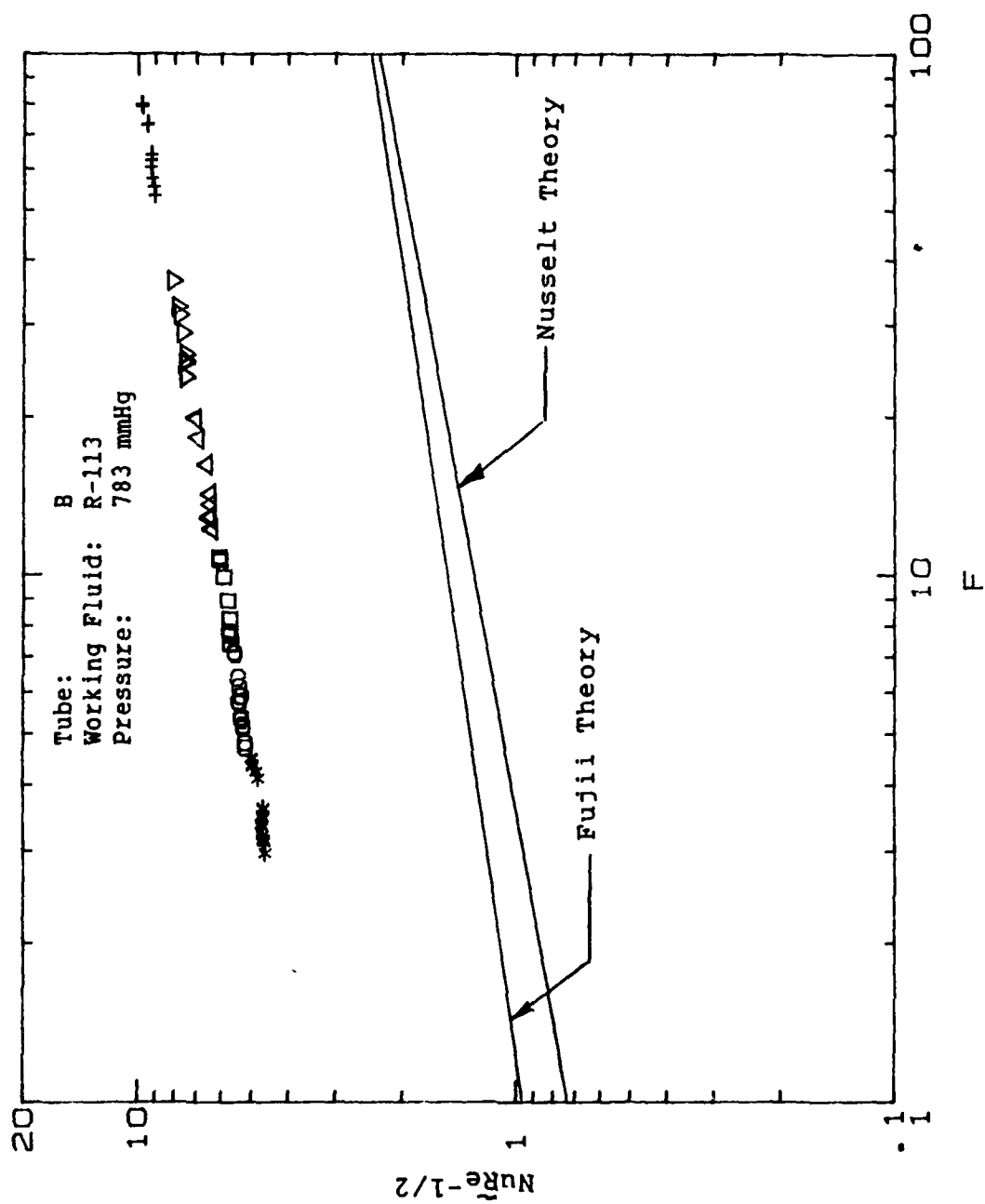


Figure 5.11 Variation of NR and F with $S = 1.5$ mm for R-113

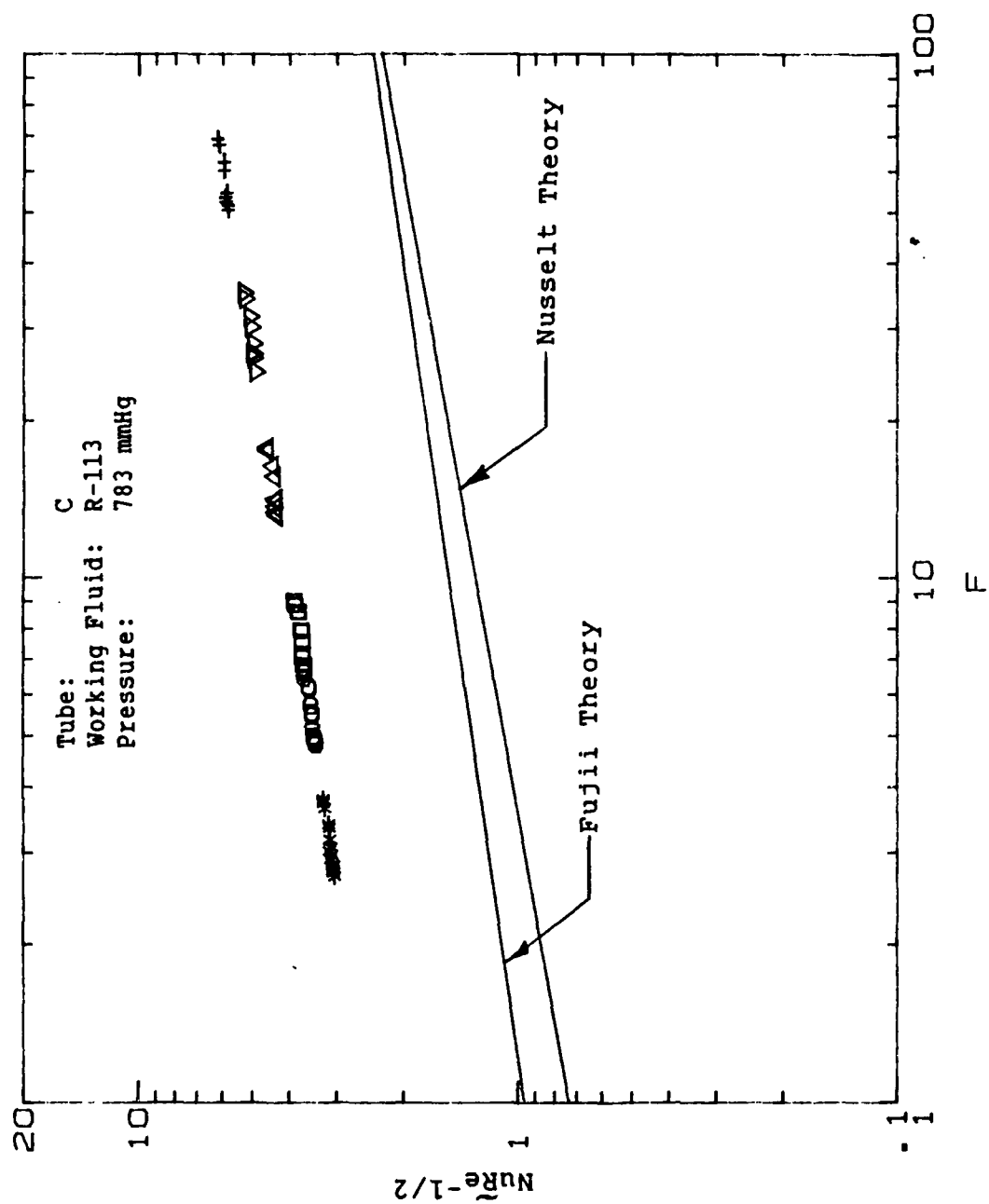


Figure 5.12 Variation of NR and F with S = 4.0 mm for R-113

is expected at high vapor velocities. Notice that the same trends can be observed for data taken on finned tubes A, B, and C, respectively. Again, the data slope downward, but with a steeper slope than for the smooth tube. This trend is readily observed when data for a finned tube are superimposed onto the same plot as the smooth tube (Figure 5.13). The separation of the data at low vapor velocities ($F \rightarrow \infty$) is an example of the enhancement obtained when using finned tubes in a quiescent vapor. However, as the vapor velocity increases, the data for the smooth and finned tube converge, indicating that finned tube performance approaches smooth tube performance at high vapor velocities. This trend was observed for all finned tubes tested with R-113 as the working fluid and is in agreement with the results of Gogonin and Dorokhov [Ref. 29].

Data taken on these four tubes with steam as the working fluid are plotted in Figures 5.14 through 5.17 using the same format described above. The data for the smooth tube show the same trends as described above for R-113: As vapor velocity increases, the data departs from Nusselt's theory. Enhancement due to finned surfaces was clearly observed and the finned tube data converge toward the smooth tube data at high velocities (Figure 5.18), confirming the previously observed results of Gogonin and Dorokhov [Ref. 29] for R-21.

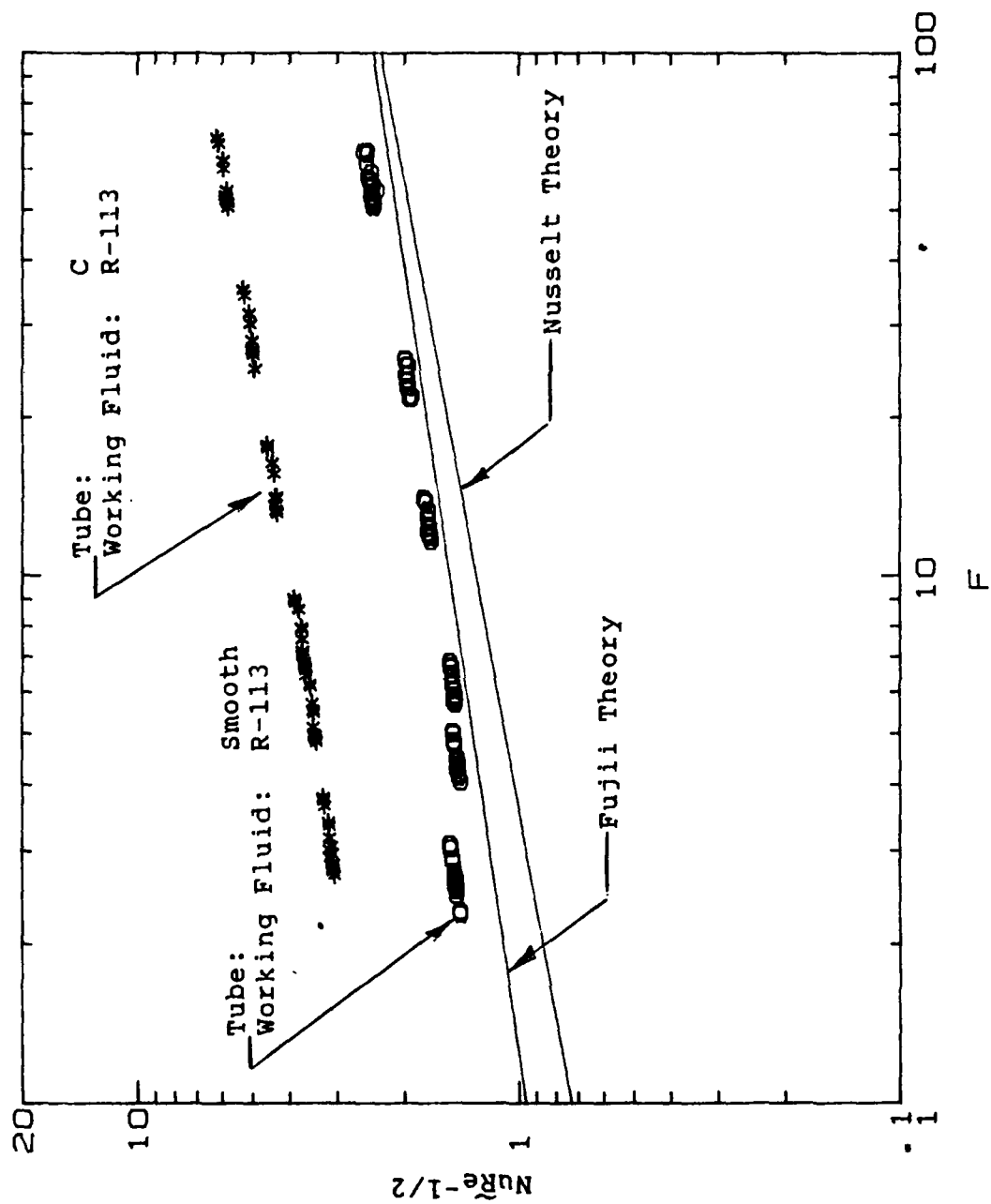


Figure 5.13 Variation of NR and F for a Smooth Tube and a Finned Tube ($S = 4.0$ mm) for R-113

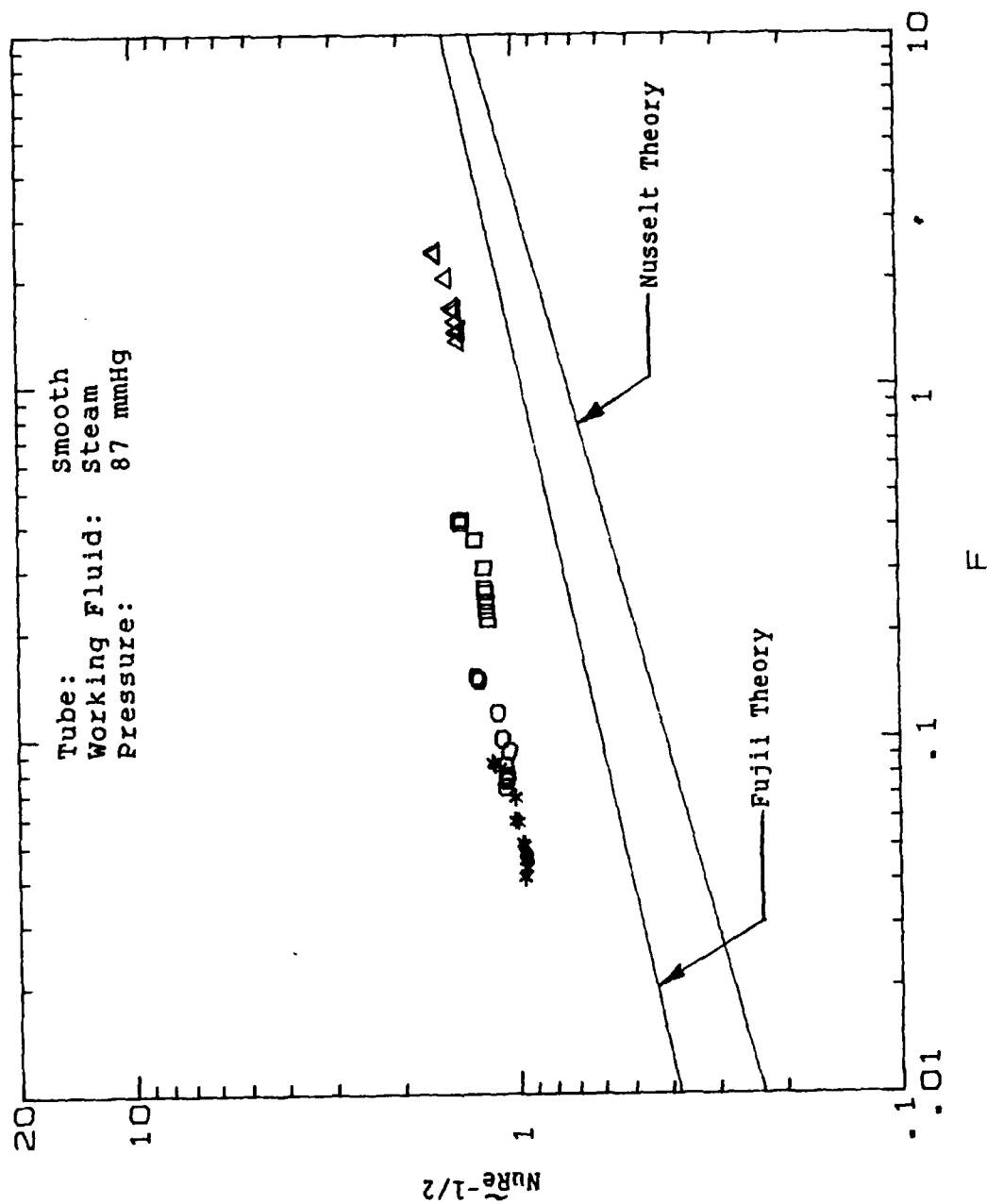


Figure 5.14 Variation of Nu and F for the Smooth Tube for Steam

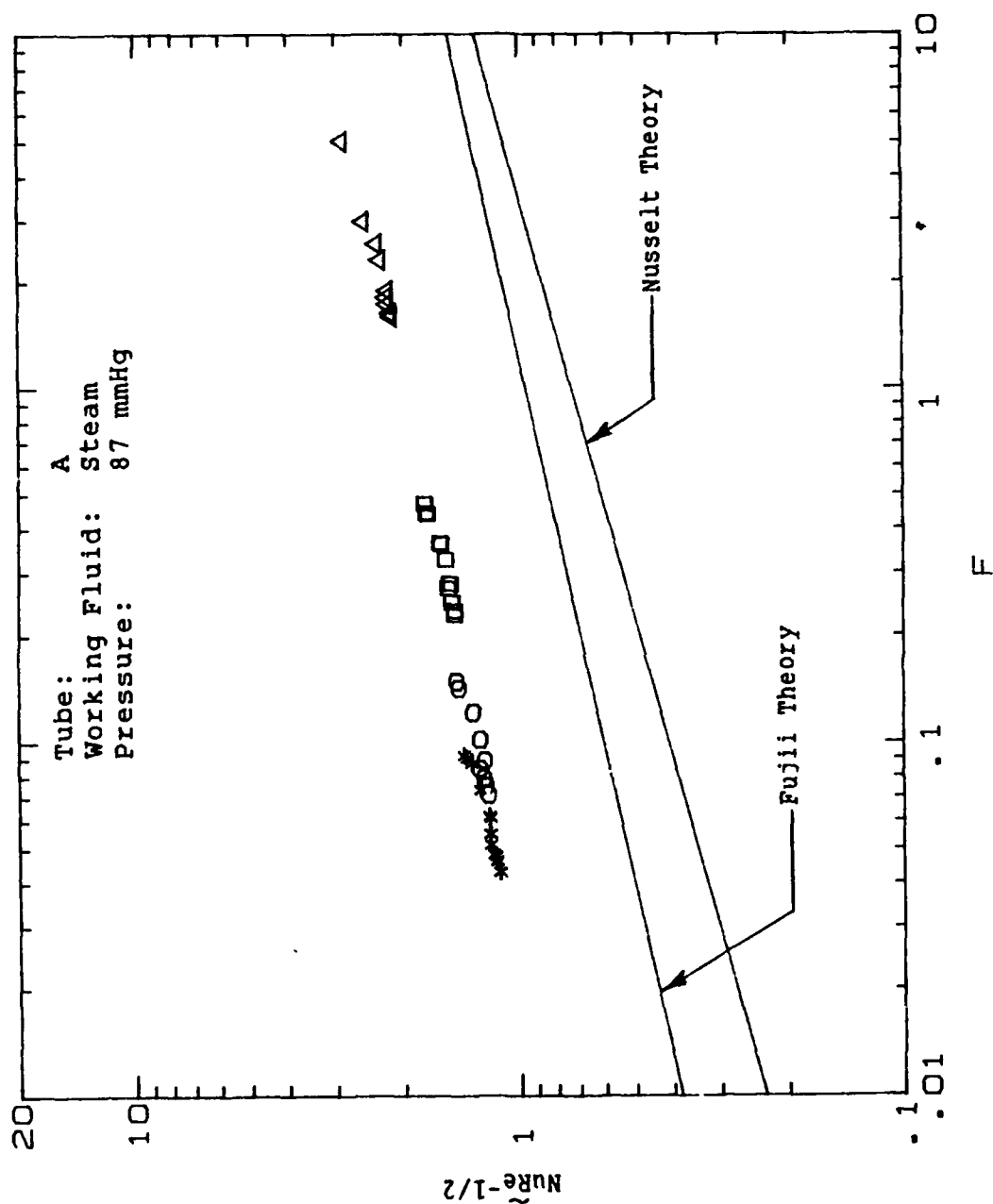


Figure 5.15 Variation of NR and F with $S = 0.25$ mm for Steam

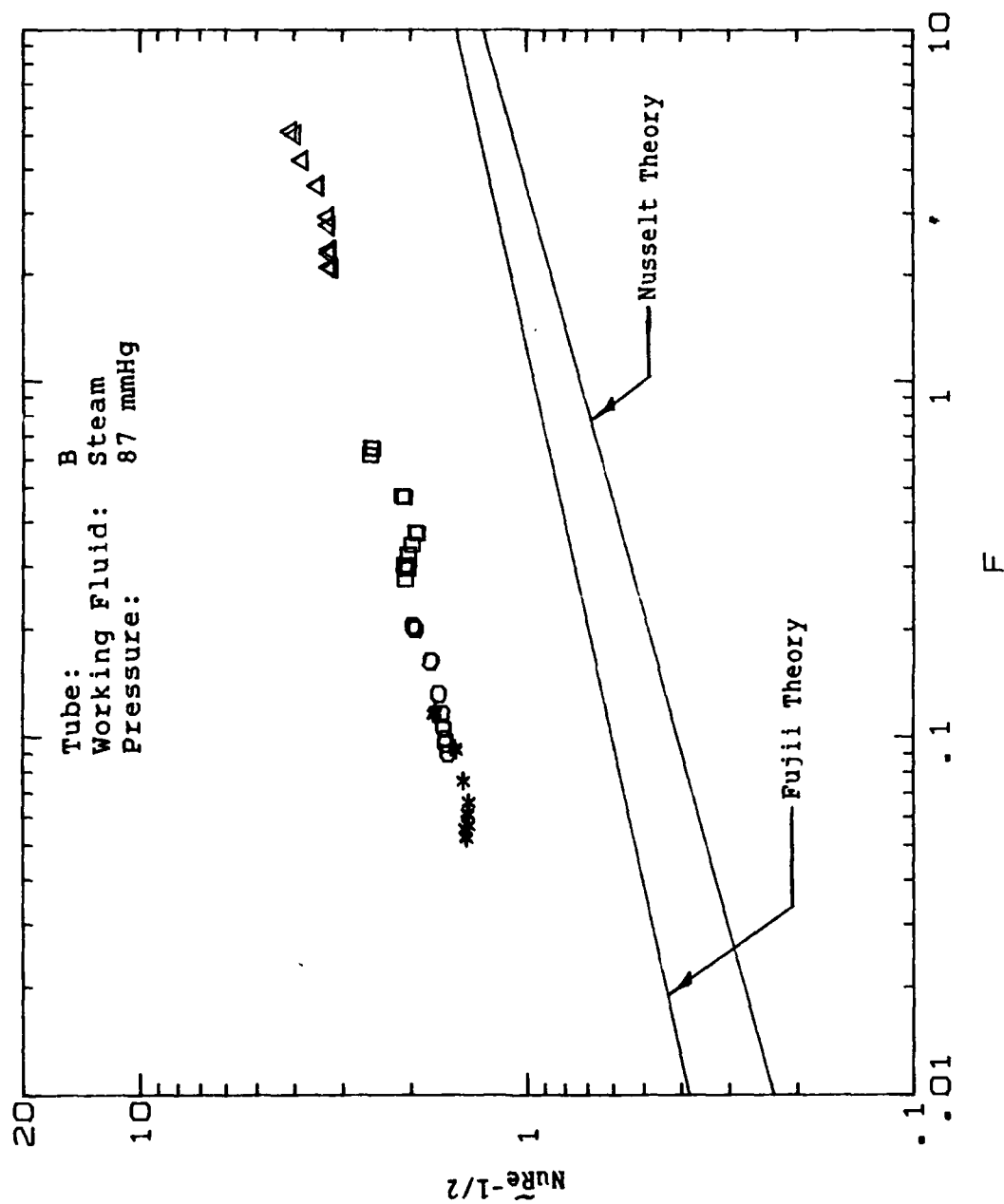


Figure 5.16 Variation of NR and F with S = 1.5 mm for Steam

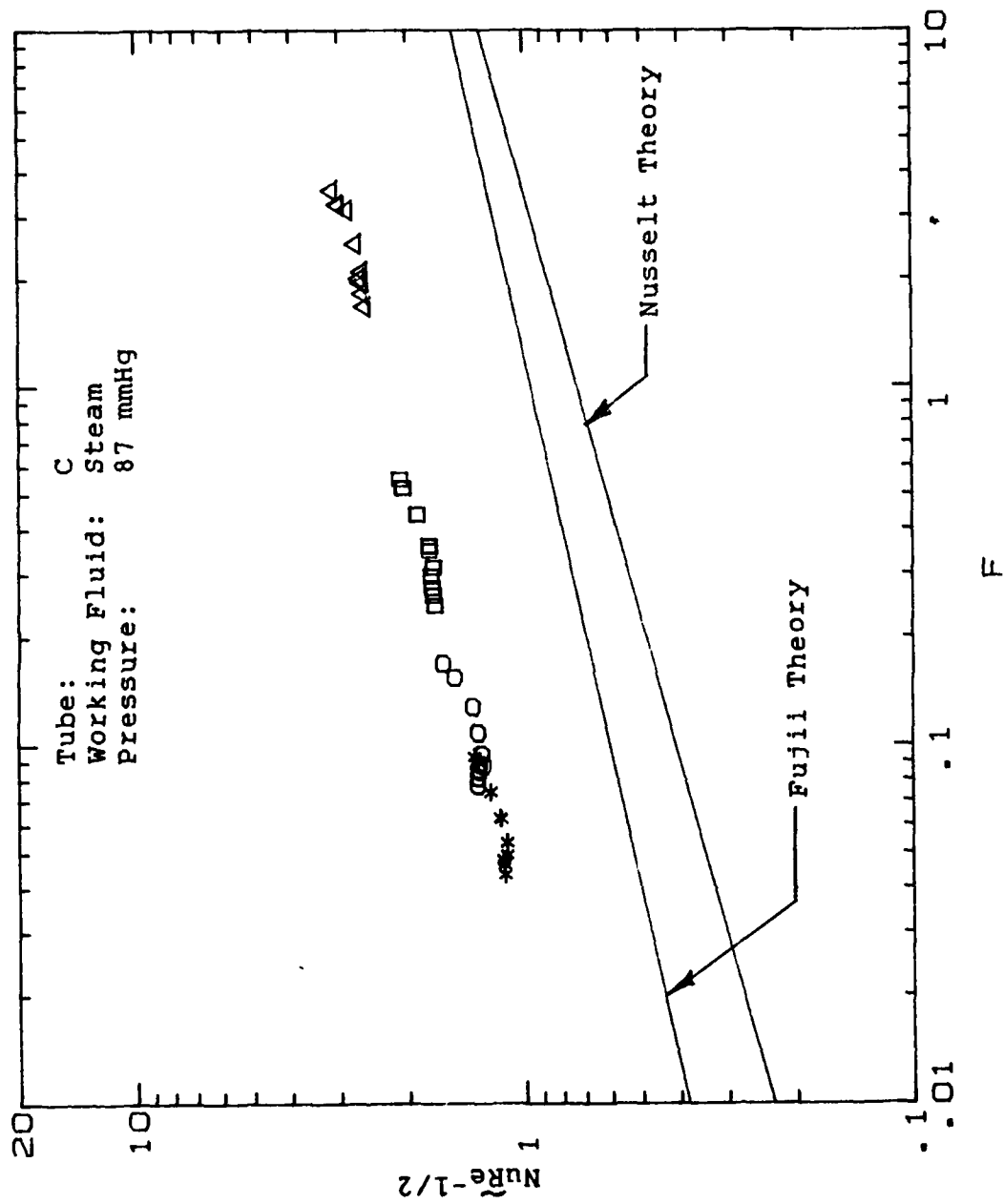


Figure 5.17 Variation of NR and F with S = 4.0 mm for Steam

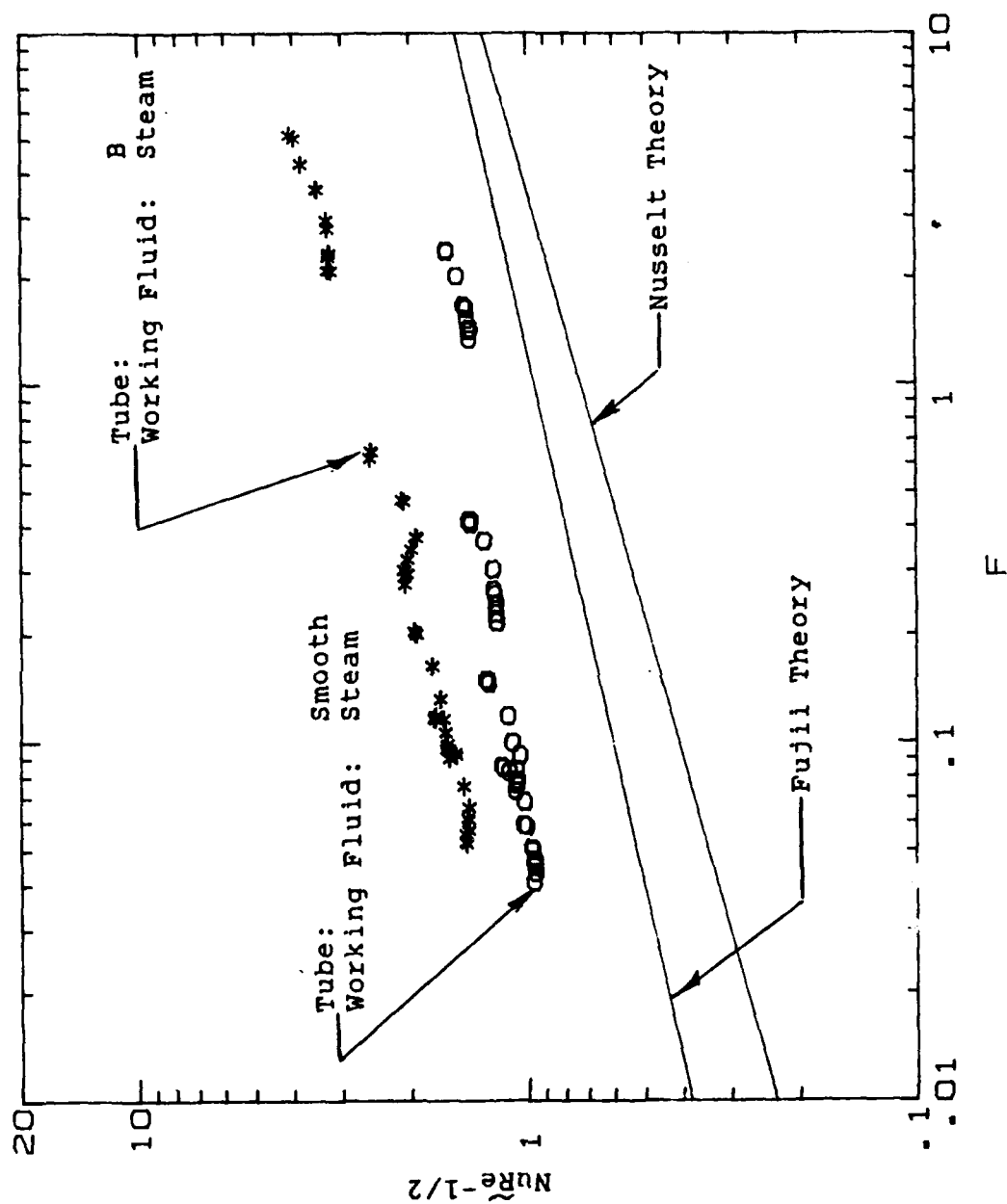


Figure 5.18 Variation of Nu and F for a Smooth Tube and a Finned Tube ($S = 1.5$ mm) for Steam

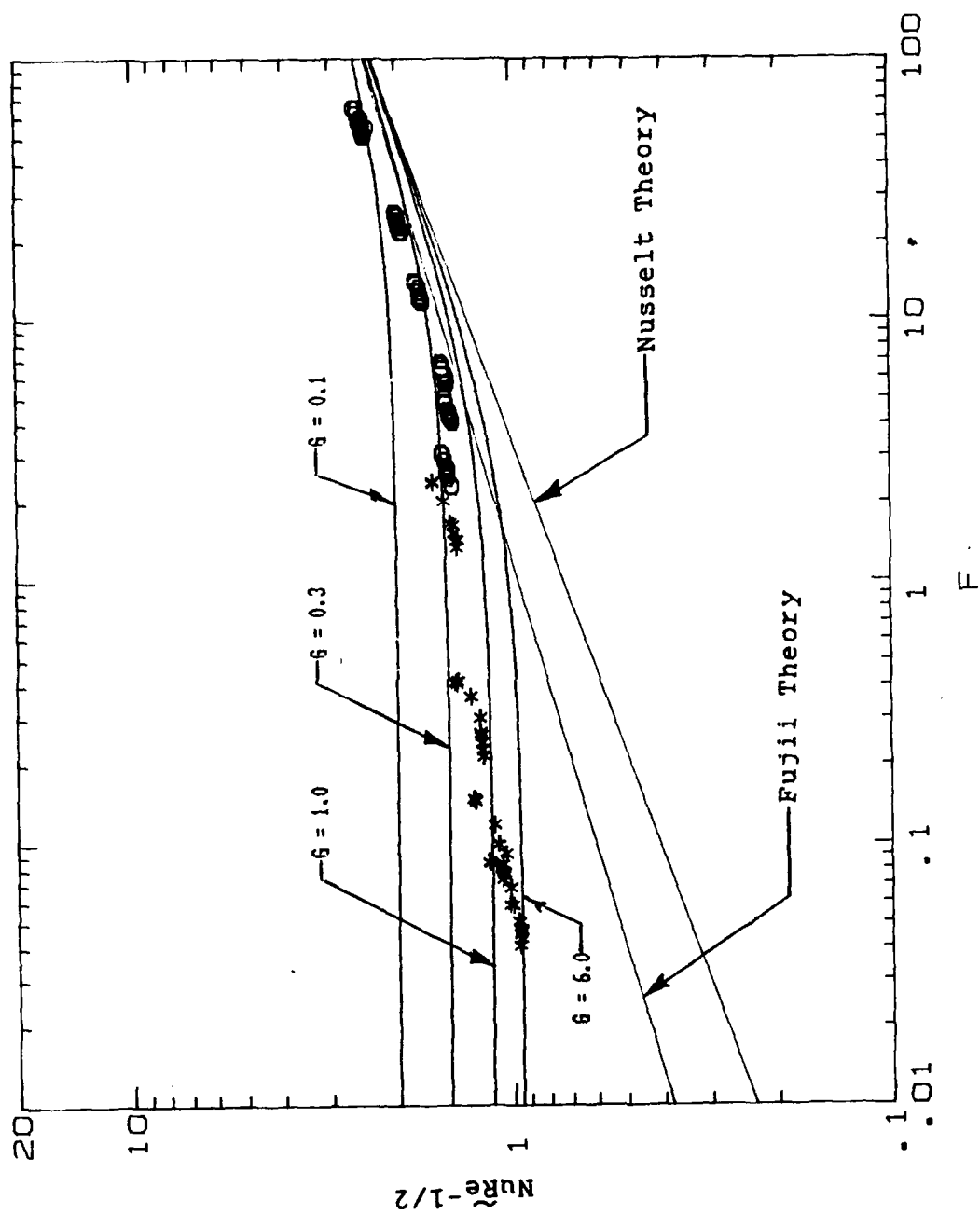


Figure 5.19 Variation of NR and F for the Smooth Tube with Both Fluids (R-113 and Steam) for This Research, $1.6 < G < 6$

VI. CONCLUSIONS AND RECOMMENDATIONS

A. CONCLUSIONS

To investigate the effects of vapor velocity on the condensing heat-transfer coefficient, a new test section was designed and built. The maximum vapor velocities achieved (just upstream of the test tube) were 1.9 m/s for R-113 and 31.3 m/s for steam.

High vapor shear data were taken and compared for a smooth tube and three finned tubes. The finned tubes had fin dimensions of 1.0 mm for thickness and height with spacings of 0.25, 1.5, and 4.0 mm. For the two fluids tested, the smooth tube experienced the largest percent increase in the outside heat-transfer coefficient with increase in vapor velocity (32 percent for R-113 and 62 percent for steam).

The variation of $NuRe^{-1/2}$ versus F was examined for both R-113 and steam and consistent trends were observed. For smooth tubes at low vapor velocities (i.e., large F), the data approached the Nusselt correlation and at high vapor velocities (i.e., small F), the data departed from the Nusselt correlation indicating an enhancement in outside heat transfer coefficient. For finned tubes, the separation of the data from smooth tube data at low vapor velocities clearly displayed finned tube enhancement. As vapor

velocity increased, the finned tube data sloped downward, but at a steeper slope than the smooth tube data, indicating that finned tube performance approaches smooth tube performance at high vapor velocities.

For the two fluids tested, the finned tubes showed opposite trends in performance. For example, with R-113 as the working fluid, tube performance increased as fin spacing increased. Whereas with steam as the working fluid, tube performance decreased as fin spacing increased. The exact reason for this trend is not known at this time and will require further investigation.

Data obtained for smooth tubes (Figure 5.19) can be accurately but somewhat conservatively predicted by Equation (2.8). For this research, $1.6 < G < 6$.

B. RECOMMENDATIONS

1. Systematically test tubes with different fin geometries in an attempt to obtain the optimum geometry in a high vapor shear environment.
2. Move the test tubes within the test chamber to investigate the effect of the vapor velocity profile on tube performance.
3. Obtain higher velocity data by reducing the width of the converging channel.
4. Install and test several in-line tubes and investigate inundation effects in a high velocity environment.
5. Modify the test chamber to remove air and non-condensibles from the baffled area between the channel window and the test section window.
6. Modify the test chamber to defog the channel and test chamber windows.

AD-A205 072

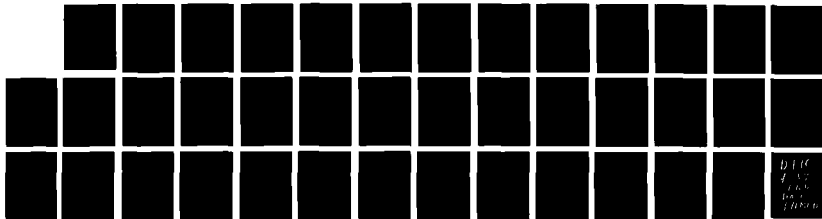
EFFECT OF VAPOR VELOCITY DURING CONDENSATION ON
HORIZONTAL FINNED TUBES(U) NAVAL POSTGRADUATE SCHOOL
MONTEREY CA C R HOPKINS DEC 88

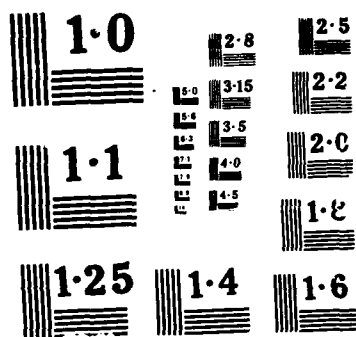
2/2

UNCLASSIFIED

F/G 20/13

NL





APPENDIX A

SYSTEM START-UP AND SHUT-DOWN PROCEDURES

The system is started in the following manner:

1. Ensure that the liquid level in the boiler is four to six inches above the heating elements.
2. Check the oil level in the purge pump and check to insure that the system vent valve is shut.
3. Turn on the data acquisition system, computer and printer. Load the interactive program entitled DRP13G.
4. Open the fill valve for the tube coolant water sump.
5. When the sump is full, start the circulation pumps and adjust tube flow rate to 20%.
6. Open the isolation valve and adjust coolant flow through the auxiliary condenser to at least 50% for start-up. Flow will be adjusted during start-up to eventually achieve steady state conditions.
7. Energize heaters and adjust voltage to approximately 50 volts for system warm-up. Note that system pressure should be carefully monitored (with the data acquisition system and mercury manometer). Auxiliary condenser flow rate and voltage should be carefully adjusted to prevent an over-pressure condition during warm-up.
8. When testing with Freon, operate the purge pump at selected intervals (for approximately five seconds). At

steady state conditions, the pressure is maintained slightly above atmospheric by adjusting the auxiliary condenser flow. When testing with steam, the distilled water is warmed to the approximate operating temperature in the boiler. Then the vacuum pump is started and operated continuously throughout the testing. At steady state conditions, a vacuum is maintained by the condensing process and by the removal of non-condensable gases using the purge system.

The system is secured in the following manner:

1. Isolate and secure the purge system.
2. Secure power to boiler heating elements.
3. Circulate water through the auxiliary condenser and test tube allowing the system to cool down.
4. When the system has cooled (about 15 minutes), secure water to auxiliary condenser, secure circulating pumps and secure water to the sump.
5. Turn off the computer, data acquisition system and printer.

APPENDIX B

UNCERTAINTY ANALYSIS

Uncertainties are always introduced when taking measurements. They are a function of the accuracy and calibration of the measuring instrument as well as the operator's experience. For this research, numerical data were used with theoretical formulations to determine the vapor-side heat-transfer coefficient. Therefore, the final result may be severely distorted due to error propagation during the many computational steps. When evaluating the final results, it may be unwise to accept experimental results when uncertainties are large. The uncertainty of a computation can be determined by using the following equation proposed by Kline and McClintok [Ref. 37]:

$$W_R = \left\{ \left[\frac{\delta R}{\delta X_1} W_1 \right]^2 + \left[\frac{\delta R}{\delta X_2} W_2 \right]^2 + \dots + \left[\frac{\delta R}{\delta X_N} W_N \right]^2 \right\}^{1/2} \quad (B.1)$$

where:

R = the result of the calculation;

W_R = the uncertainty of the result;

X_1, X_2, \dots, X_N = the measured independent variables;

W_1, W_2, \dots, W_N = the uncertainties in the measured variables.

A more complete discussion of the development of the uncertainty analysis used for this research is given by Georgiadis [Ref. 32]. Uncertainties associated with various quantities during this research were obtained using the uncertainty program provided by Mitrou [Ref. 33], and are listed below.

DATA FOR THE UNCERTAINTY ANALYSIS:

File Name: S90R19
 Pressure Condition: Atmospheric (101 kPa)
 Vapor Temperature = 48.46 (Deg C)
 Water Flow Rate (%) = 20.00
 Water Velocity = 1.16 (m/s)
 Heat Flux = 3.112E+04 (W/m^2)
 Tube-metal thermal conduc. = 385.0 (W/m.K)
 Sieder-Tate constant = 0.0345

UNCERTAINTY ANALYSIS:

VARIABLE	PERCENT UNCERTAINTY
Mass Flow Rate, Md	3.00
Reynolds Number, Re	3.10
Heat Flux, q	3.50
Log-Mean-Tem Diff, LMTD	1.75
Wall Resistance, Rw	2.67
Overall H.T.C., Uo	3.91
Water-Side H.T.C., Hi	9.05
Vapor-Side H.T.C., Ho	5.86

DATA FOR THE UNCERTAINTY ANALYSIS:

File Name: S90R19
 Pressure Condition: Atmospheric (101 kPa)
 Vapor Temperature = 48.43 (Deg C)
 Water Flow Rate (%) = 80.00
 Water Velocity = 4.40 (m/s)
 Heat Flux = 3.220E+04 (W/m^2)
 Tube-metal thermal conduc. = 385.0 (W/m.K)
 Sieder-Tate constant = 0.0345

UNCERTAINTY ANALYSIS:

VARIABLE	PERCENT UNCERTAINTY
Mass Flow Rate, Md	0.79
Reynolds Number, Re	1.10
Heat Flux, q	6.47
Log-Mean-Tem Diff, LMTD	6.41
Wall Resistance, Rw	2.67
Overall H.T.C., Uo	9.11
Water-Side H.T.C., Hi	8.75
Vapor-Side H.T.C., Ho	10.08

DATA FOR THE UNCERTAINTY ANALYSIS:

File Name: FA90R51
 Pressure Condition: Atmospheric (101 kPa)
 Vapor Temperature = 48.49 (Deg C)
 Water Flow Rate (%) = 20.00
 Water Velocity = 1.16 (m/s)
 Heat Flux = 7.804E+04 (W/m^2)
 Tube-metal thermal conduc. = 385.0 (W/m.K)
 Sieder-Tate constant = 0.0421

UNCERTAINTY ANALYSIS:

VARIABLE	PERCENT UNCERTAINTY
Mass Flow Rate, Md	3.00
Reynolds Number, Re	3.10
Heat Flux, q	3.11
Log-Mean-Tem Diff, LMTD	.70
Wall Resistance, Rw	2.67
Overall H.T.C., Uo	3.19
Water-Side H.T.C., Hi	7.55
Vapor-Side H.T.C., Ho	9.65

DATA FOR THE UNCERTAINTY ANALYSIS:

File Name: FA90R51
 Pressure Condition: Atmospheric (101 kPa)
 Vapor Temperature = 48.40 (Deg C)
 Water Flow Rate (%) = 80.00
 Water Velocity = 4.40 (m/s)
 Heat Flux = 1.028E+05 (W/m^2)
 Tube-metal thermal conduc. = 385.0 (W/m.K)
 Sieder-Tate constant = 0.0421

UNCERTAINTY ANALYSIS:

VARIABLE	PERCENT UNCERTAINTY
Mass Flow Rate, Md	0.79
Reynolds Number, Re	1.10
Heat Flux, q	2.20
Log-Mean-Tem Diff, LMTD	2.01
Wall Resistance, Rw	2.67
Overall H.T.C., Uo	2.98
Water-Side H.T.C., Hi	7.19
Vapor-Side H.T.C., Ho	4.57

DATA FOR THE UNCERTAINTY ANALYSIS:

File Name: FB80R39
 Pressure Condition: Atmospheric (101 kPa)
 Vapor Temperature = 48.45 (Deg C)
 Water Flow Rate (%) = 20.00
 Water Velocity = 1.16 (m/s)
 Heat Flux = 7.670E+04 (W/m^2)
 Tube-metal thermal conduc. = 385.0 (W/m.K)
 Sieder-Tate constant = 0.0363

UNCERTAINTY ANALYSIS:

VARIABLE	PERCENT UNCERTAINTY
Mass Flow Rate, Md	3.00
Reynolds Number, Re	3.10
Heat Flux, q	3.11
Log-Mean-Tem Diff, LMTD	.72
Wall Resistance, Rw	2.67
Overall H.T.C., Uo	3.19
Water-Side H.T.C., Hi	8.64
Vapor-Side H.T.C., Ho	12.48

DATA FOR THE UNCERTAINTY ANALYSIS:

File Name: FB80R39
 Pressure Condition: Atmospheric (101 kPa)
 Vapor Temperature = 48.50 (Deg C)
 Water Flow Rate (%) = 80.00
 Water Velocity = 4.40 (m/s)
 Heat Flux = 1.043E+05 (W/m^2)
 Tube-metal thermal conduc. = 385.0 (W/m.K)
 Sieder-Tate constant = 0.0363

UNCERTAINTY ANALYSIS:

VARIABLE	PERCENT UNCERTAINTY
Mass Flow Rate, Md	0.79
Reynolds Number, Re	1.10
Heat Flux, q	2.18
Log-Mean-Tem Diff, LMTD	1.98
Wall Resistance, Rw	2.67
Overall H.T.C., Uo	2.94
Water-Side H.T.C., Hi	8.32
Vapor-Side H.T.C., Ho	5.15

DATA FOR THE UNCERTAINTY ANALYSIS:

File Name: FC90R28
 Pressure Condition: Atmospheric (101 kPa)
 Vapor Temperature = 48.47 (Deg C)
 Water Flow Rate (%) = 20.00
 Water Velocity = 1.16 (m/s)
 Heat Flux = 6.020E+04 (W/m^2)
 Tube-metal thermal conduc. = 385.0 (W/m.K)
 Sieder-Tate constant = 0.0362

UNCERTAINTY ANALYSIS:

VARIABLE	PERCENT UNCERTAINTY
Mass Flow Rate, Md	3.00
Reynolds Number, Re	3.10
Heat Flux, q	3.16
Log-Mean-Tem Diff, LMTD	.91
Wall Resistance, Rw	2.67
Overall H.T.C., Uo	3.29
Water-Side H.T.C., Hi	8.66
Vapor-Side H.T.C., Ho	8.80

DATA FOR THE UNCERTAINTY ANALYSIS:

File Name: FC90R28
 Pressure Condition: Atmospheric (101 kPa)
 Vapor Temperature = 48.44 (Deg C)
 Water Flow Rate (%) = 80.00
 Water Velocity = 4.40 (m/s)
 Heat Flux = 7.452E+04 (W/m^2)
 Tube-metal thermal conduc. = 385.0 (W/m.K)
 Sieder-Tate constant = 0.0362

UNCERTAINTY ANALYSIS:

VARIABLE	PERCENT UNCERTAINTY
Mass Flow Rate, Md	0.79
Reynolds Number, Re	1.10
Heat Flux, q	2.91
Log-Mean-Tem Diff, LMTD	2.77
Wall Resistance, Rw	2.67
Overall H.T.C., Uo	4.02
Water-Side H.T.C., Hi	8.34
Vapor-Side H.T.C., Ho	5.44

DATA FOR THE UNCERTAINTY ANALYSIS:

File Name: S120S17
 Pressure Condition: Vacuum (11 kPa)
 Vapor Temperature = 48.34 (Deg C)
 Water Flow Rate (%) = 20.00
 Water Velocity = 1.16 (m/s)
 Heat Flux = 1.769E+05 (W/m^2)
 Tube-metal thermal conduc. = 385.0 (W/m.K)
 Sieder-Tate constant = 0.0624

UNCERTAINTY ANALYSIS:

VARIABLE	PERCENT UNCERTAINTY
Mass Flow Rate, Md	3.00
Reynolds Number, Re	3.10
Heat Flux, q	3.05
Log-Mean-Tem Diff, LMTD	.32
Wall Resistance, Rw	2.67
Overall H.T.C., Uo	3.06
Water-Side H.T.C., Hi	4.07
Vapor-Side H.T.C., Ho	19.00

DATA FOR THE UNCERTAINTY ANALYSIS:

File Name: S120S17
 Pressure Condition: Vacuum (11 kPa)
 Vapor Temperature = 48.37 (Deg C)
 Water Flow Rate (%) = 80.00
 Water Velocity = 4.40 (m/s)
 Heat Flux = 2.995E+05 (W/m^2)
 Tube-metal thermal conduc. = 385.0 (W/m.K)
 Sieder-Tate constant = 0.0624

UNCERTAINTY ANALYSIS:

VARIABLE	PERCENT UNCERTAINTY
Mass Flow Rate, Md	0.79
Reynolds Number, Re	1.10
Heat Flux, q	1.14
Log-Mean-Tem Diff, LMTD	.69
Wall Resistance, Rw	2.67
Overall H.T.C., Uo	1.33
Water-Side H.T.C., H	3.35
Vapor-Side H.T.C., Hu	4.34

DATA FOR THE UNCERTAINTY ANALYSIS:

File Name: FA160S13
 Pressure Condition: Vacuum (11 kPa)
 Vapor Temperature = 48.39 (Deg C)
 Water Flow Rate (%) = 20.00
 Water Velocity = 1.16 (m/s)
 Heat Flux = 2.104E+05 (W/m^2)
 Tube-metal thermal conduc. = 385.0 (W/m.K)
 Sieder-Tate constant = 0.0739

UNCERTAINTY ANALYSIS:

VARIABLE	PERCENT UNCERTAINTY
Mass Flow Rate, Md	3.00
Reynolds Number, Re	3.10
Heat Flux, q	3.04
Log-Mean-Tem Diff, LMTD	.28
Wall Resistance, Rw	2.67
Overall H.T.C., Uo	3.06
Water-Side H.T.C., Hi	3.69
Vapor-Side H.T.C., Ho	21.26

DATA FOR THE UNCERTAINTY ANALYSIS:

File Name: FA160S13
 Pressure Condition: Vacuum (11 kPa)
 Vapor Temperature = 48.35 (Deg C)
 Water Flow Rate (%) = 80.00
 Water Velocity = 4.40 (m/s)
 Heat Flux = 3.670E+05 (W/m^2)
 Tube-metal thermal conduc. = 385.0 (W/m.K)
 Sieder-Tate constant = 0.0739

UNCERTAINTY ANALYSIS:

VARIABLE	PERCENT UNCERTAINTY
Mass Flow Rate, Md	0.79
Reynolds Number, Re	1.11
Heat Flux, q	1.07
Log-Mean-Tem Diff, LMTD	.57
Wall Resistance, Rw	2.67
Overall H.T.C., Uo	1.21
Water-Side H.T.C., Hi	2.87
Vapor-Side H.T.C., Ho	4.40

DATA FOR THE UNCERTAINTY ANALYSIS:

File Name: FB120S19
 Pressure Condition: Vacuum (11 kPa)
 Vapor Temperature = 48.54 (Deg C)
 Water Flow Rate (%) = 20.00
 Water Velocity = 1.16 (m/s)
 Heat Flux = 2.049E+05 (W/m^2)
 Tube-metal thermal conduc. = 385.0 (W/m.K)
 Sieder-Tate constant = 0.0652

UNCERTAINTY ANALYSIS:

VARIABLE	PERCENT UNCERTAINTY
Mass Flow Rate, Md	3.00
Reynolds Number, Re	3.10
Heat Flux, q	3.04
Log-Mean-Tem Diff, LMTD	.28
Wall Resistance, Rw	2.67
Overall H.T.C., Uo	3.06
Water-Side H.T.C., Hi	3.96
Vapor-Side H.T.C., Ho	31.18

DATA FOR THE UNCERTAINTY ANALYSIS:

File Name: FB120S19
 Pressure Condition: Vacuum (11 kPa)
 Vapor Temperature = 48.39 (Deg C)
 Water Flow Rate (%) = 80.00
 Water Velocity = 4.40 (m/s)
 Heat Flux = 3.855E+05 (W/m^2)
 Tube-metal thermal conduc. = 385.0 (W/m.K)
 Sieder-Tate constant = 0.0652

UNCERTAINTY ANALYSIS:

VARIABLE	PERCENT UNCERTAINTY
Mass Flow Rate, Md	0.79
Reynolds Number, Re	1.10
Heat Flux, q	1.05
Log-Mean-Tem Diff, LMTD	.54
Wall Resistance, Rw	2.67
Overall H.T.C., Uo	1.18
Water-Side H.T.C., Hi	3.21
Vapor-Side H.T.C., Ho	6.35

DATA FOR THE UNCERTAINTY ANALYSIS:

File Name: FC120S23
 Pressure Condition: Vacuum (11 kPa)
 Vapor Temperature = 48.41 (Deg C)
 Water Flow Rate (%) = 20.00
 Water Velocity = 1.16 (m/s)
 Heat Flux = 2.045E+05 (W/m^2)
 Tube-metal thermal conduc. = 385.0 (W/m.K)
 Sieder-Tate constant = 0.0687

UNCERTAINTY ANALYSIS:

VARIABLE	PERCENT UNCERTAINTY
Mass Flow Rate, Md	3.00
Reynolds Number, Re	3.10
Heat Flux, q	3.04
Log-Mean-Tem Diff, LMTD	.28
Wall Resistance, Rw	2.67
Overall H.T.C., Uo	3.06
Water-Side H.T.C., Hi	3.84
Vapor-Side H.T.C., Ho	24.41

DATA FOR THE UNCERTAINTY ANALYSIS:

File Name: FC120S23
 Pressure Condition: Vacuum (11 kPa)
 Vapor Temperature = 48.34 (Deg C)
 Water Flow Rate (%) = 80.00
 Water Velocity = 4.40 (m/s)
 Heat Flux = 3.669E+05 (W/m^2)
 Tube-metal thermal conduc. = 385.0 (W/m.K)
 Sieder-Tate constant = 0.0687

UNCERTAINTY ANALYSIS:

VARIABLE	PERCENT UNCERTAINTY
Mass Flow Rate, Md	0.79
Reynolds Number, Re	1.10
Heat Flux, q	1.07
Log-Mean-Tem Diff, LMTD	.57
Wall Resistance, Rw	2.67
Overall H.T.C., Uo	1.21
Water-Side H.T.C., Hi	3.07
Vapor-Side H.T.C., Ho	5.05

APPENDIX C

LISTING OF RAW DATA

This appendix contains the raw data for R-113 and steam presented in this investigation.

R-113 Data

File Name: S112R21
Pressure Condition: Atmospheric
Vapor Velocity: 1.9 (m/s)

Data #	Vw (m/s)	Tin (C)	Tout (C)	Ts (C)
1	0.74	21.56	22.02	48.43
2	0.74	21.56	22.02	48.39
3	0.94	21.35	21.72	48.43
4	0.94	21.35	21.72	48.46
5	1.25	21.15	21.44	48.39
6	1.25	21.15	21.44	48.46
7	1.59	21.01	21.25	48.37
8	1.59	21.01	21.25	48.38
9	1.90	20.93	21.14	48.42
10	1.90	20.93	21.14	48.47
11	2.18	20.87	21.06	48.46
12	2.18	20.88	21.06	48.47
13	2.45	20.83	21.00	48.41
14	2.45	20.83	21.00	48.40
15	2.79	20.79	20.93	48.46
16	2.79	20.79	20.93	48.45
17	0.74	21.55	22.00	48.44
18	0.74	21.55	22.01	48.41

File Name: S100R20
Pressure Condition: Atmospheric
Vapor Velocity: 1.5 (m/s)

Data #	Vw (m/s)	Tin (C)	Tout (C)	Ts (C)
1	0.74	21.93	22.34	48.41
2	0.74	21.92	22.34	48.45
3	0.94	21.71	22.05	48.41
4	0.94	21.71	22.04	48.44
5	1.25	21.51	21.77	48.45
6	1.25	21.51	21.77	48.44
7	1.59	21.37	21.59	48.37
8	1.59	21.37	21.58	48.45
9	1.90	21.28	21.46	48.45
10	1.90	21.28	21.46	48.39
11	2.18	21.22	21.38	48.46
12	2.45	21.17	21.31	48.46
13	2.45	21.17	21.31	48.48
14	2.79	21.12	21.25	48.46
15	2.79	21.12	21.25	48.47
16	0.74	21.86	22.28	48.42
17	0.74	21.81	22.22	48.48

File Name: S90R19
 Pressure Condition: Atmospheric
 Vapor Velocity: 1.3 (m/s)

Data #	Vw (m/s)	Tin (C)	Tout (C)	Ts (C)
1	0.74	22.03	22.42	48.46
2	0.74	22.02	22.42	48.50
3	0.94	21.80	22.12	48.49
4	0.94	21.80	22.12	48.50
5	1.25	21.59	21.84	48.48
6	1.25	21.59	21.85	48.45
7	1.59	21.46	21.66	48.40
8	1.59	21.45	21.66	48.38
9	1.90	21.37	21.54	48.44
10	1.90	21.37	21.54	48.43
11	2.18	21.31	21.46	48.39
12	2.18	21.31	21.47	48.46
13	2.45	21.27	21.40	48.40
14	2.45	21.26	21.40	48.42
15	2.79	21.22	21.34	48.42
16	2.79	21.21	21.33	48.43
17	0.74	21.97	22.37	48.49
18	0.74	21.97	22.37	48.45

File Name: S80R17
 Pressure Condition: Atmospheric
 Vapor Velocity: 0.9 (m/s)

Data #	Vw (m/s)	Tin (C)	Tout (C)	Ts (C)
1	0.74	22.47	22.85	48.48
2	0.74	22.46	22.84	48.41
3	0.94	22.23	22.54	48.49
4	0.94	22.23	22.53	48.51
5	1.25	22.02	22.27	48.48
6	1.25	22.02	22.26	48.43
7	1.59	21.87	22.07	48.43
8	1.59	21.87	22.06	48.51
9	1.90	21.77	21.94	48.47
10	1.90	21.77	21.93	48.42
11	2.18	21.69	21.84	48.40
12	2.18	21.69	21.83	48.46
13	2.45	21.63	21.76	48.46
14	2.45	21.63	21.76	48.47
15	2.79	21.57	21.69	48.39
16	2.79	21.57	21.68	48.48
17	0.74	22.31	22.69	48.45
18	0.74	22.30	22.69	48.48

File Name: S70R15
 Pressure Condition: Atmospheric
 Vapor Velocity: 0.6 (m/s)

Data #	Vw (m/s)	Tin (C)	Tout (C)	Ts (C)
1	0.74	22.17	22.54	48.36
2	0.74	22.17	22.54	48.33
3	0.94	22.05	22.34	48.38
4	0.94	22.05	22.35	48.38
5	1.25	21.89	22.13	48.37
6	1.25	21.89	22.13	48.47
7	1.59	21.79	21.98	48.43
8	1.59	21.79	21.98	48.54
9	1.90	21.73	21.89	48.55
10	1.90	21.73	21.89	48.51
11	2.18	21.72	21.86	48.44
12	2.18	21.73	21.87	48.43
13	2.45	21.69	21.82	48.47
14	2.45	21.70	21.82	48.47
15	2.79	21.67	21.79	48.43
16	2.79	21.68	21.79	48.43
17	0.74	22.47	22.84	48.44
18	0.74	22.47	22.83	48.46

File Name: S60R11
 Pressure Condition: Atmospheric
 Vapor Velocity: 0.4 (m/s)

Data #	Vw (m/s)	Tin (C)	Tout (C)	Ts (C)
1	0.74	22.62	22.98	48.77
2	0.74	22.62	22.98	48.14
3	0.94	22.45	22.74	48.09
4	0.94	22.45	22.74	48.82
5	1.25	22.28	22.51	48.01
6	1.25	22.28	22.51	48.08
7	1.59	22.16	22.34	48.08
8	1.59	22.16	22.34	48.05
9	1.90	22.08	22.24	48.82
10	1.90	22.08	22.24	48.19
11	2.18	22.03	22.17	48.68
12	2.18	22.03	22.17	48.65
13	2.45	21.99	22.12	48.23
14	2.45	21.99	22.12	48.09
15	2.79	21.95	22.06	48.56
16	2.79	21.95	22.06	48.51
17	0.74	22.68	23.04	48.71
18	0.74	22.68	23.04	48.19

File Name: FA112R48
 Pressure Condition: Atmospheric
 Vapor Velocity: 1.9 (m/s)

Data #	Vw (m/s)	Tin (C)	Tout (C)	Ts (C)
1	0.74	21.71	22.73	48.44
2	0.74	21.72	22.73	48.44
3	0.94	21.50	22.34	48.43
4	0.94	21.50	22.34	48.43
5	1.25	21.31	22.00	48.44
6	1.25	21.32	22.00	48.45
7	1.59	21.19	21.76	48.40
8	1.59	21.19	21.76	48.40
9	1.90	21.11	21.61	48.32
10	1.90	21.11	21.61	48.36
11	2.18	21.05	21.50	48.44
12	2.18	21.05	21.50	48.46
13	2.45	21.01	21.42	48.48
14	2.45	21.01	21.42	48.48
15	2.79	20.97	21.33	48.47
16	2.79	20.97	21.33	48.45
17	0.74	21.72	22.73	48.44
18	0.74	21.71	22.73	48.44

File Name: FA100R50
 Pressure Condition: Atmospheric
 Vapor Velocity: 1.5 (m/s)

Data #	Vw (m/s)	Tin (C)	Tout (C)	Ts (C)
1	0.74	21.95	22.93	48.44
2	0.74	21.95	22.93	48.46
3	0.94	21.73	22.56	48.45
4	0.94	21.73	22.56	48.45
5	1.25	21.54	22.22	48.42
6	1.25	21.54	22.22	48.42
7	1.59	21.42	21.98	48.43
8	1.59	21.42	21.99	48.44
9	1.90	21.35	21.85	48.43
10	1.90	21.35	21.85	48.42
11	2.18	21.30	21.75	48.42
12	2.18	21.30	21.75	48.45
13	2.45	21.27	21.67	48.45
14	2.45	21.27	21.67	48.41
15	2.79	21.23	21.59	48.47
16	2.79	21.23	21.60	48.50
17	0.74	22.02	23.00	48.40
18	0.74	22.02	23.00	48.42

File Name: FA90R51
 Pressure Condition: Atmospheric
 Vapor Velocity: 1.2 (m/s)

Data #	Vw (m/s)	Tin (C)	Tout (C)	Ts (C)
1	0.74	22.17	23.18	48.49
2	0.74	22.17	23.18	48.50
3	0.94	21.96	22.80	48.44
4	0.94	21.96	22.80	48.42
5	1.25	21.76	22.45	48.46
6	1.25	21.76	22.45	48.48
7	1.59	21.63	22.20	48.46
8	1.59	21.63	22.20	48.47
9	1.90	21.55	22.04	48.43
10	1.90	21.55	22.04	48.41
11	2.18	21.49	21.93	48.43
12	2.18	21.49	21.93	48.45
13	2.45	21.44	21.85	48.48
14	2.45	21.44	21.85	48.47
15	2.79	21.40	21.76	48.42
16	2.79	21.40	21.76	48.40
17	0.74	22.15	23.15	48.44
18	0.74	22.15	23.15	48.43

File Name: FA80R53
 Pressure Condition: Atmospheric
 Vapor Velocity: 0.9 (m/s)

Data #	Vw (m/s)	Tin (C)	Tout (C)	Ts (C)
1	0.74	22.02	23.02	48.38
2	0.74	22.02	23.02	48.38
3	0.94	21.79	22.63	48.47
4	0.94	21.79	22.63	48.49
5	1.25	21.60	22.29	48.51
6	1.25	21.60	22.29	48.51
7	1.59	21.46	22.03	48.45
8	1.59	21.46	22.03	48.44
9	1.90	21.37	21.86	48.42
10	1.90	21.37	21.86	48.45
11	2.18	21.31	21.75	48.50
12	2.18	21.31	21.75	48.49
13	2.45	21.26	21.67	48.47
14	2.45	21.26	21.66	48.47
15	2.79	21.21	21.57	48.44
16	2.79	21.20	21.57	48.43
17	0.74	21.93	22.94	48.41
18	0.74	21.93	22.94	48.42

File Name: FA60R55
Pressure Condition: Atmospheric
Vapor Velocity: 0.4 (m/s)

Data #	Vw (m/s)	Tin (C)	Tout (C)	Ts (C)
1	0.74	21.77	22.78	48.38
2	0.74	21.76	22.77	48.38
3	0.94	21.54	22.38	48.42
4	0.94	21.54	22.38	48.43
5	1.25	21.34	22.04	48.45
6	1.25	21.35	22.03	48.47
7	1.59	21.21	21.79	48.45
8	1.59	21.21	21.78	48.45
9	1.90	21.12	21.62	48.51
10	1.90	21.12	21.62	48.51
11	2.18	21.06	21.52	48.46
12	2.18	21.06	21.52	48.45
13	2.45	21.01	21.42	48.48
14	2.45	21.02	21.42	48.48
15	2.79	20.97	21.33	48.48
16	2.79	20.97	21.33	48.46
17	0.74	21.71	22.72	48.42
18	0.74	21.71	22.73	48.43

File Name: FB112R45
 Pressure Condition: Atmospheric
 Vapor Velocity: 1.9 (m/s)

Data #	Vw (m/s)	Tin (C)	Tout (C)	Ts (C)
1	0.74	21.80	22.79	48.45
2	0.74	21.80	22.79	48.47
3	0.94	21.57	22.40	48.42
4	0.94	21.57	22.40	48.40
5	1.25	21.38	22.06	48.41
6	1.25	21.38	22.06	48.47
7	1.59	21.25	21.82	48.46
8	1.59	21.24	21.82	48.42
9	1.90	21.16	21.67	48.41
10	1.90	21.16	21.67	48.44
11	2.18	21.11	21.57	48.41
12	2.18	21.11	21.57	48.48
13	2.45	21.07	21.48	48.37
14	2.45	21.07	21.48	48.37
15	2.79	21.03	21.40	48.48
16	2.79	21.03	21.40	48.49
17	0.74	21.78	22.77	48.42
18	0.74	21.78	22.77	48.49

File Name: FB100R43
 Pressure Condition: Atmospheric
 Vapor Velocity: 1.5 (m/s)

Data #	Vw (m/s)	Tin (C)	Tout (C)	Ts (C)
1	0.74	21.81	22.80	48.47
2	0.74	21.81	22.80	48.48
3	0.94	21.59	22.42	48.43
4	0.94	21.59	22.42	48.38
5	1.25	21.40	22.08	48.40
6	1.25	21.40	22.08	48.46
7	1.59	21.27	21.84	48.45
8	1.59	21.27	21.84	48.38
9	1.90	21.19	21.70	48.39
10	1.90	21.19	21.70	48.45
11	2.18	21.14	21.59	48.42
12	2.18	21.14	21.59	48.44
13	2.45	21.10	21.51	48.40
14	2.45	21.10	21.51	48.44
15	2.79	21.05	21.43	48.40
16	2.79	21.06	21.43	48.40
17	0.74	21.81	22.80	48.48
18	0.74	21.81	22.80	48.48

File Name: FB90R42
 Pressure Condition: Atmospheric
 Vapor Velocity: 1.2 (m/s)

Data #	Vw (m/s)	Tin (C)	Tout (C)	Ts (C)
1	0.74	21.77	22.77	48.50
2	0.74	21.77	22.77	48.46
3	0.94	21.57	22.41	48.39
4	0.94	21.57	22.41	48.44
5	1.25	21.39	22.07	48.48
6	1.25	21.39	22.07	48.48
7	1.59	21.26	21.83	48.53
8	1.59	21.26	21.83	48.48
9	1.90	21.19	21.69	48.48
10	1.90	21.19	21.69	48.40
11	2.18	21.13	21.59	48.48
12	2.18	21.13	21.59	48.41
13	2.45	21.09	21.50	48.45
14	2.45	21.09	21.50	48.47
15	2.79	21.05	21.42	48.43
16	2.79	21.05	21.42	48.49
17	0.74	21.80	22.80	48.44
18	0.74	21.81	22.80	48.48

File Name: FB80R39
 Pressure Condition: Atmospheric
 Vapor Velocity: 0.9 (m/s)

Data #	Vw (m/s)	Tin (C)	Tout (C)	Ts (C)
1	0.74	21.79	22.77	48.45
2	0.74	21.78	22.77	48.41
3	0.94	21.57	22.40	48.53
4	0.94	21.56	22.39	48.53
5	1.25	21.38	22.06	48.57
6	1.25	21.38	22.06	48.52
7	1.59	21.25	21.82	48.47
8	1.59	21.25	21.82	48.54
9	1.90	21.17	21.67	48.47
10	1.90	21.17	21.67	48.37
11	2.18	21.11	21.57	48.40
12	2.18	21.11	21.57	48.34
13	2.45	21.07	21.48	48.44
14	2.45	21.07	21.48	48.39
15	2.79	21.02	21.39	48.53
16	2.79	21.02	21.39	48.50
17	0.74	21.76	22.75	48.49
18	0.74	21.76	22.75	48.37

File Name: FB70R37
 Pressure Condition: Atmospheric
 Vapor Velocity: 0.7 (m/s)

Data #	Vw (m/s)	Tin (C)	Tout (C)	Ts (C)
1	0.74	21.69	22.68	48.48
2	0.74	21.69	22.68	48.50
3	0.94	21.48	22.32	48.48
4	0.94	21.48	22.31	48.44
5	1.25	21.29	21.97	48.40
6	1.25	21.29	21.97	48.39
7	1.59	21.17	21.73	48.42
8	1.59	21.17	21.73	48.47
9	1.90	21.09	21.59	48.38
10	1.90	21.09	21.59	48.47
11	2.18	21.04	21.49	48.40
12	2.18	21.04	21.49	48.44
13	2.45	21.00	21.40	48.39
14	2.45	20.99	21.40	48.36
15	2.79	20.95	21.32	48.39
16	2.79	20.95	21.32	48.37
17	0.74	21.71	22.69	48.40
18	0.74	21.71	22.69	48.37

File Name: FB60R36
 Pressure Condition: Atmospheric
 Vapor Velocity: 0.5 (m/s)

Data #	Vw (m/s)	Tin (C)	Tout (C)	Ts (C)
1	0.74	21.67	22.65	48.46
2	0.74	21.67	22.65	48.42
3	0.94	21.46	22.28	48.44
4	0.94	21.46	22.28	48.50
5	1.25	21.28	21.95	48.38
6	1.25	21.28	21.95	48.34
7	1.59	21.15	21.71	48.41
8	1.59	21.15	21.71	48.37
9	1.90	21.07	21.56	48.47
10	1.90	21.07	21.56	48.43
11	2.18	21.02	21.46	48.44
12	2.18	21.02	21.47	48.50
13	2.45	20.98	21.38	48.44
14	2.45	20.98	21.38	48.43
15	2.79	20.93	21.30	48.40
16	2.79	20.93	21.30	48.40
17	0.74	21.68	22.66	48.33
18	0.74	21.68	22.66	48.39

File Name: FC112R23
 Pressure Condition: Atmospheric
 Vapor Velocity: 1.9 (m/s)

Data #	Vw (m/s)	Tin (C)	Tout (C)	Ts (C)
1	0.74	21.59	22.39	48.42
2	0.74	21.59	22.38	48.46
3	0.94	21.39	22.05	48.42
4	0.94	21.39	22.05	48.44
5	1.25	21.20	21.74	48.39
6	1.25	21.21	21.74	48.42
7	1.59	21.08	21.52	48.46
8	1.59	21.08	21.52	48.42
9	1.90	21.00	21.39	48.42
10	1.90	21.00	21.39	48.43
11	2.18	20.95	21.30	48.53
12	2.18	20.95	21.30	48.45
13	2.45	20.91	21.22	48.45
14	2.45	20.91	21.22	48.45
15	2.79	20.87	21.15	48.49
16	2.79	20.87	21.15	48.47
17	0.74	21.64	22.43	48.42
18	0.74	21.64	22.43	48.42

File Name: FC100R25
 Pressure Condition: Atmospheric
 Vapor Velocity: 1.4 (m/s)

Data #	Vw (m/s)	Tin (C)	Tout (C)	Ts (C)
1	0.74	21.69	22.47	48.47
2	0.74	21.69	22.47	48.42
3	0.94	21.47	22.12	48.49
4	0.94	21.47	22.12	48.47
5	1.25	21.29	21.81	48.46
6	1.25	21.29	21.81	48.45
7	1.59	21.16	21.59	48.43
8	1.59	21.16	21.59	48.47
9	1.90	21.08	21.46	48.38
10	1.90	21.08	21.46	48.40
11	2.18	21.03	21.36	48.41
12	2.18	21.03	21.37	48.47
13	2.45	20.99	21.29	48.47
14	2.45	20.99	21.29	48.39
15	2.79	20.95	21.22	48.39
16	2.79	20.95	21.22	48.36
17	0.74	21.70	22.49	48.42
18	0.74	21.70	22.49	48.42

File Name: FC90R28
 Pressure Condition: Atmospheric
 Vapor Velocity: 1.2 (m/s)

Data #	Vw (m/s)	Tin (C)	Tout (C)	Ts (C)
1	0.74	21.70	22.47	48.47
2	0.74	21.70	22.47	48.43
3	0.94	21.48	22.12	48.41
4	0.94	21.48	22.12	48.49
5	1.25	21.29	21.80	48.49
6	1.25	21.29	21.80	48.43
7	1.59	21.16	21.58	48.45
8	1.59	21.16	21.58	48.51
9	1.90	21.08	21.45	48.48
10	1.90	21.08	21.45	48.45
11	2.18	21.03	21.36	48.46
12	2.18	21.03	21.36	48.48
13	2.45	20.98	21.28	48.44
14	2.45	20.98	21.28	48.43
15	2.79	20.94	21.20	48.47
16	2.79	20.94	21.20	48.44
17	0.74	21.69	22.46	48.40
18	0.74	21.69	22.47	48.41

File Name: FC80R30
 Pressure Condition: Atmospheric
 Vapor Velocity: 0.9 (m/s)

Data #	Vw (m/s)	Tin (C)	Tout (C)	Ts (C)
1	0.74	21.72	22.48	48.44
2	0.74	21.72	22.48	48.37
3	0.94	21.51	22.14	48.48
4	0.94	21.51	22.14	48.47
5	1.25	21.32	21.83	48.46
6	1.25	21.32	21.82	48.52
7	1.59	21.19	21.61	48.37
8	1.59	21.19	21.61	48.39
9	1.90	21.12	21.48	48.48
10	1.90	21.12	21.48	48.49
11	2.18	21.07	21.39	48.40
12	2.18	21.07	21.39	48.43
13	2.45	21.02	21.32	48.41
14	2.45	21.02	21.32	48.43
15	2.79	20.99	21.25	48.47
16	2.79	20.99	21.25	48.44
17	0.74	21.75	22.51	48.50
18	0.74	21.75	22.51	48.42

File Name: FC70R32
 Pressure Condition: Atmospheric
 Vapor Velocity: 0.6 (m/s)

Data #	Vw (m/s)	Tin (C)	Tout (C)	Ts (C)
1	0.74	21.71	22.47	48.50
2	0.74	21.71	22.47	48.47
3	0.94	21.50	22.12	48.40
4	0.94	21.50	22.12	48.42
5	1.25	21.31	21.81	48.50
6	1.25	21.31	21.81	48.50
7	1.59	21.18	21.59	48.44
8	1.59	21.18	21.59	48.47
9	1.90	21.10	21.46	48.44
10	1.90	21.10	21.46	48.48
11	2.18	21.05	21.37	48.43
12	2.18	21.05	21.37	48.45
13	2.45	21.00	21.29	48.51
14	2.45	21.00	21.29	48.52
15	2.79	20.96	21.22	48.44
16	2.79	20.96	21.22	48.45
17	0.74	21.71	22.46	48.49
18	0.74	21.71	22.46	48.48

File Name: FC60R33
 Pressure Condition: Atmospheric
 Vapor Velocity: 0.4 (m/s)

Data #	Vw (m/s)	Tin (C)	Tout (C)	Ts (C)
1	0.74	21.70	22.46	48.42
2	0.74	21.70	22.45	48.44
3	0.94	21.49	22.10	48.47
4	0.94	21.49	22.10	48.41
5	1.25	21.30	21.79	48.43
6	1.25	21.30	21.79	48.44
7	1.59	21.17	21.57	48.44
8	1.59	21.17	21.57	48.42
9	1.94	21.08	21.43	48.49
10	1.94	21.08	21.43	48.40
11	2.18	21.03	21.35	48.38
12	2.18	21.03	21.35	48.44
13	2.45	20.99	21.27	48.49
14	2.45	20.99	21.27	48.51
15	2.79	20.94	21.20	48.45
16	2.79	20.94	21.20	48.50
17	0.74	21.70	22.45	48.41
18	0.74	21.70	22.45	48.40

Steam Data

File Name: S185S01
Pressure Condition: Low Pressure
Vapor Velocity: 31.5 (m/s)

Data #	Vw (m/s)	Tin (C)	Tout (C)	Ts (C)
1	1.16	22.46	24.92	48.44
2	1.16	22.46	24.93	48.44
3	1.48	22.27	24.42	48.50
4	1.48	22.27	24.42	48.48
5	1.97	22.10	23.97	48.50
6	1.97	22.10	23.97	48.50
7	2.51	21.97	23.59	48.40
8	2.51	21.97	23.59	48.37
9	3.00	21.90	23.36	48.51
10	3.00	21.90	23.35	48.51
11	3.43	21.82	23.17	48.51
12	3.43	21.82	23.17	48.48
13	3.86	21.71	22.96	48.46
14	3.86	21.67	22.92	48.47
15	4.40	21.33	22.50	48.39
16	4.40	21.31	22.47	48.40
17	1.16	22.05	24.53	48.45
18	1.16	22.06	24.53	48.48

File Name: S180S02
Pressure Condition: Low Pressure
Vapor Velocity: 23.6 (m/s)

Data #	Vw (m/s)	Tin (C)	Tout (C)	Ts (C)
1	1.16	22.43	24.83	48.44
2	1.16	22.43	24.83	48.44
3	1.48	22.23	24.33	48.51
4	1.48	22.23	24.32	48.51
5	1.97	22.04	23.85	48.41
6	1.97	22.04	23.85	48.40
7	2.51	21.91	23.48	48.58
8	2.51	21.91	23.47	48.59
9	3.00	21.83	23.25	48.40
10	3.00	21.83	23.26	48.42
11	3.43	21.78	23.09	48.44
12	3.43	21.78	23.09	48.42
13	3.86	21.74	22.96	48.42
14	3.86	21.73	22.95	48.43
15	4.40	21.70	22.82	48.48
16	4.40	21.69	22.82	48.50
17	1.16	22.46	24.85	48.40
18	1.16	22.46	24.85	48.40

File Name: S120S17
 Pressure Condition: Low Pressure
 Vapor Velocity: 12.9 (m/s)

Data #	Vw (m/s)	Tin (C)	Tout (C)	Ts (C)
1	1.16	21.81	24.10	48.35
2	1.16	21.81	24.10	48.34
3	1.49	21.60	23.60	48.43
4	1.49	21.60	23.60	48.44
5	1.97	21.41	23.11	48.42
6	1.97	21.41	23.12	48.45
7	2.51	21.28	22.77	48.37
8	2.51	21.28	22.77	48.38
9	3.00	21.20	22.53	48.43
10	3.00	21.20	22.53	48.45
11	3.43	21.15	22.37	48.51
12	3.43	21.15	22.37	48.56
13	3.86	21.10	22.24	48.50
14	3.86	21.10	22.24	48.47
15	4.40	21.06	22.10	48.38
16	4.40	21.06	22.09	48.37
17	1.16	21.84	24.14	48.40
18	1.16	21.84	24.14	48.28

File Name: S80S18
 Pressure Condition: Low Pressure
 Vapor Velocity: 4.8 (m/s)

Data #	Vw (m/s)	Tin (C)	Tout (C)	Ts (C)
1	1.16	21.85	23.97	48.41
2	1.16	21.85	23.98	48.40
3	1.49	21.64	23.47	48.47
4	1.49	21.64	23.47	48.49
5	1.97	21.44	22.98	48.38
6	1.97	21.44	22.98	48.38
7	2.51	21.30	22.60	48.38
8	2.51	21.30	22.60	48.39
9	3.00	21.22	22.38	48.44
10	3.00	21.22	22.38	48.44
11	3.43	21.16	22.22	48.40
12	3.43	21.16	22.22	48.38
13	3.86	21.11	22.07	48.41
14	3.86	21.12	22.08	48.43
15	4.40	21.07	21.95	48.40
16	4.40	21.07	21.95	48.38
17	1.16	21.85	23.97	48.39
18	1.16	21.85	23.97	48.37

File Name: FA185S05
 Pressure Condition: Low Pressure
 Vapor Velocity: 31.4 (m/s)

Data #	Vw (m/s)	Tin (C)	Tout (C)	Ts (C)
1	1.16	22.40	25.15	48.42
2	1.16	22.38	25.14	48.46
3	1.48	22.13	24.58	48.40
4	1.48	22.13	24.58	48.40
5	1.97	21.93	24.04	48.39
6	1.97	21.93	24.05	48.37
7	2.51	21.79	23.66	48.48
8	2.51	21.79	23.66	48.49
9	3.00	21.70	23.39	48.47
10	3.00	21.70	23.39	48.49
11	3.43	21.64	23.18	48.35
12	3.43	21.64	23.18	48.39
13	3.86	21.59	23.02	48.48
14	3.86	21.59	23.02	48.51
15	4.40	21.54	22.85	48.46
16	4.40	21.54	22.85	48.47
17	1.16	22.27	25.05	48.40
18	1.16	22.27	25.05	48.42

File Name: FA160S13
 Pressure Condition: Low Pressure
 Vapor Velocity: 23.8 (m/s)

Data #	Vw (m/s)	Tin (C)	Tout (C)	Ts (C)
1	1.16	22.08	24.81	48.45
2	1.16	22.08	24.81	48.39
3	1.49	21.86	24.26	48.40
4	1.49	21.86	24.26	48.47
5	1.97	21.67	23.73	48.47
6	1.97	21.66	23.73	48.47
7	2.51	21.52	23.32	48.42
8	2.51	21.52	23.32	48.42
9	3.00	21.45	23.08	48.40
10	3.00	21.45	23.08	48.38
11	3.43	21.39	22.89	48.50
12	3.43	21.39	22.89	48.49
13	3.86	21.34	22.73	48.47
14	3.86	21.34	22.73	48.49
15	4.40	21.29	22.56	48.37
16	4.40	21.29	22.56	48.35
17	1.16	22.07	24.80	48.38
18	1.16	22.07	24.81	48.43

File Name: FA120521
 Pressure Condition: Low Pressure
 Vapor Velocity: 13.2 (m/s)

Data #	Vw (m/s)	Tin (C)	Tout (C)	Ts (C)
1	1.16	21.97	24.55	48.38
2	1.16	21.97	24.55	48.28
3	1.49	21.77	24.05	48.52
4	1.49	21.77	24.05	48.44
5	1.97	21.58	23.53	48.37
6	1.97	21.58	23.53	48.40
7	2.51	21.45	23.16	48.44
8	2.51	21.45	23.16	48.40
9	3.00	21.37	22.91	48.45
10	3.00	21.37	22.91	48.50
11	3.43	21.32	22.73	48.42
12	3.43	21.32	22.73	48.40
13	3.86	21.27	22.58	48.45
14	3.86	21.28	22.58	48.44
15	4.40	21.23	22.42	48.38
16	4.40	21.22	22.42	48.38
17	1.16	22.02	24.60	48.43
18	1.16	22.03	24.61	48.44

File Name: FA80522
 Pressure Condition: Low Pressure
 Vapor Velocity: 4.8 (m/s)

Data #	Vw (m/s)	Tin (C)	Tout (C)	Ts (C)
1	1.16	22.01	24.50	48.44
2	1.16	22.01	24.50	48.37
3	1.49	21.79	23.96	48.33
4	1.49	21.78	23.95	48.36
5	1.97	21.59	23.45	48.39
6	1.97	21.59	23.45	48.40
7	2.51	21.45	23.07	48.37
8	2.51	21.45	23.06	48.38
9	3.00	21.36	22.81	48.37
10	3.00	21.36	22.82	48.38
11	3.43	21.30	22.64	48.43
12	3.43	21.30	22.64	48.40
13	3.86	21.25	22.48	48.41
14	3.86	21.25	22.48	48.39
15	4.40	21.20	22.32	48.40
16	4.40	21.20	22.32	48.40
17	1.16	21.99	24.47	48.38
18	1.16	21.99	24.48	48.41

File Name: FB185S12
 Pressure Condition: Low Pressure
 Vapor Velocity: 31.0 (m/s)

Data #	Vw (m/s)	Tin (C)	Tout (C)	Ts (C)
1	1.16	22.59	25.33	48.41
2	1.16	22.59	25.33	48.43
3	1.48	22.37	24.81	48.47
4	1.48	22.37	24.82	48.62
5	1.97	22.18	24.31	48.48
6	1.97	22.18	24.31	48.49
7	2.51	22.06	23.93	48.37
8	2.51	22.06	23.93	48.38
9	3.00	21.98	23.69	48.46
10	3.00	21.98	23.69	48.46
11	3.43	21.92	23.51	48.41
12	3.43	21.92	23.51	48.40
13	3.86	21.88	23.38	48.48
14	3.86	21.88	23.37	48.47
15	4.40	21.83	23.21	48.45
16	4.40	21.83	23.21	48.43
17	1.16	22.64	25.37	48.39
18	1.16	22.64	25.38	48.36

File Name: FB160S11
 Pressure Condition: Low Pressure
 Vapor Velocity: 23.5 (m/s)

Data #	Vw (m/s)	Tin (C)	Tout (C)	Ts (C)
1	1.16	22.44	25.16	48.52
2	1.16	22.45	25.16	48.49
3	1.48	22.23	24.65	48.45
4	1.48	22.24	24.66	48.46
5	1.97	22.04	24.15	48.35
6	1.97	22.05	24.15	48.35
7	2.51	21.92	23.78	48.40
8	2.51	21.92	23.79	48.45
9	3.00	21.84	23.54	48.40
10	3.00	21.85	23.54	48.42
11	3.43	21.81	23.39	48.46
12	3.43	21.81	23.39	48.46
13	3.86	21.76	23.23	48.40
14	3.86	21.76	23.23	48.42
15	4.40	21.72	23.08	48.46
16	4.40	21.73	23.08	48.47
17	1.16	22.54	25.26	48.54
18	1.16	22.55	25.26	48.55

File Name: FB120S19
 Pressure Condition: Low Pressure
 Vapor Velocity: 13.3 (m/s)

Data #	Vw (m/s)	Tin (C)	Tout (C)	Ts (C)
1	1.16	21.89	24.55	48.54
2	1.16	21.89	24.54	48.55
3	1.49	21.67	24.01	48.62
4	1.49	21.67	24.01	48.68
5	1.97	21.47	23.48	48.40
6	1.97	21.47	23.47	48.41
7	2.51	21.34	23.14	48.56
8	2.51	21.34	23.15	48.56
9	3.00	21.26	22.91	48.39
10	3.00	21.26	22.91	48.36
11	3.48	21.21	22.73	48.35
12	3.48	21.20	22.73	48.35
13	3.86	21.16	22.59	48.45
14	3.86	21.16	22.59	48.44
15	4.40	21.11	22.44	48.41
16	4.40	21.11	22.44	48.39
17	1.16	21.90	24.55	48.43
18	1.16	21.90	24.55	48.38

File Name: FB80S20
 Pressure Condition: Low Pressure
 Vapor Velocity: 4.8 (m/s)

Data #	Vw (m/s)	Tin (C)	Tout (C)	Ts (C)
1	1.16	21.88	24.51	48.40
2	1.16	21.88	24.51	48.52
3	1.49	21.67	24.01	48.49
4	1.49	21.68	24.01	48.51
5	1.97	21.48	23.50	48.33
6	1.97	21.49	23.50	48.34
7	2.51	21.36	23.13	48.37
8	2.51	21.35	23.14	48.39
9	3.00	21.28	22.91	48.42
10	3.00	21.28	22.91	48.40
11	3.43	21.23	22.74	48.35
12	3.43	21.23	22.74	48.39
13	3.86	21.18	22.59	48.42
14	3.86	21.19	22.60	48.39
15	4.40	21.14	22.44	48.40
16	4.40	21.14	22.44	48.44
17	1.16	21.94	24.56	48.50
18	1.16	21.94	24.56	48.46

File Name: FC185S16
 Pressure Condition: Low Pressure
 Vapor Velocity: 31.3 (m/s)

Data #	Vw (m/s)	Tin (C)	Tout (C)	Ts (C)
1	1.16	21.98	24.67	48.38
2	1.16	21.98	24.67	48.45
3	1.49	21.77	24.15	48.39
4	1.49	21.77	24.14	48.38
5	1.97	21.57	23.62	48.43
6	1.97	21.58	23.63	48.48
7	2.51	21.43	23.22	48.45
8	2.51	21.43	23.22	48.45
9	3.00	21.35	22.97	48.39
10	3.00	21.35	22.97	48.40
11	3.43	21.30	22.80	48.36
12	3.43	21.30	22.80	48.35
13	3.66	21.25	22.66	48.53
14	3.86	21.26	22.66	48.53
15	4.40	21.20	22.50	48.46
16	4.40	21.20	22.49	48.45
17	1.16	21.98	24.66	48.48
18	1.16	21.97	24.66	48.47

File Name: FC160S15
 Pressure Condition: Low Pressure
 Vapor Velocity: 23.8 (m/s)

Data #	Vw (m/s)	Tin (C)	Tout (C)	Ts (C)
1	1.16	22.03	24.67	48.49
2	1.16	22.03	24.66	48.44
3	1.49	21.79	24.11	48.44
4	1.49	21.79	24.11	48.46
5	1.97	21.60	23.60	48.45
6	1.97	21.60	23.61	48.44
7	2.51	21.46	23.22	48.40
8	2.51	21.46	23.22	48.40
9	3.00	21.38	22.97	48.55
10	3.00	21.38	22.98	48.43
11	3.43	21.32	22.80	48.41
12	3.43	21.32	22.81	48.42
13	3.86	21.27	22.66	48.42
14	3.86	21.27	22.66	48.43
15	4.40	21.22	22.50	48.37
16	4.40	21.22	22.50	48.33
17	1.16	21.99	24.65	48.37

File Name: FC120S23
Pressure Condition: Low Pressure
Vapor Velocity: 13.0 (m/s)

Data #	Vw (m/s)	Tin (C)	Tout (C)	Ts (C)
1	1.16	21.88	24.53	48.41
2	1.49	21.66	24.00	48.44
3	1.49	21.66	24.00	48.46
4	1.97	21.46	23.47	48.37
5	1.97	21.45	23.47	48.38
6	1.97	21.45	23.46	48.43
7	2.51	21.30	23.07	48.44
8	2.51	21.30	23.06	48.43
9	3.00	21.21	22.82	48.50
10	3.00	21.21	22.82	48.53
11	3.43	21.15	22.63	48.46
12	3.43	21.15	22.63	48.44
13	3.86	21.09	22.47	48.45
14	3.86	21.09	22.47	48.37
15	4.40	21.04	22.31	48.38
16	4.40	21.04	22.31	48.34
17	1.16	21.82	24.47	48.42
18	1.16	21.82	24.47	48.41

File Name: FC80S24
Pressure Condition: Low Pressure
Vapor Velocity: 4.8 (m/s)

Data #	Vw (m/s)	Tin (C)	Tout (C)	Ts (C)
1	1.16	21.78	24.41	48.53
2	1.16	21.78	24.40	48.44
3	1.49	21.56	23.86	48.37
4	1.49	21.56	23.86	48.38
5	1.97	21.36	23.35	48.50
6	1.97	21.36	23.35	48.50
7	2.51	21.22	22.95	48.48
8	2.51	21.22	22.95	48.47
9	3.00	21.13	22.70	48.38
10	3.00	21.13	22.70	48.37
11	3.43	21.07	22.51	48.47
12	3.43	21.07	22.51	48.44
13	3.86	21.01	22.36	48.49
14	3.86	21.01	22.36	48.48
15	4.40	20.96	22.19	48.42
16	4.40	20.96	22.19	48.40
17	1.16	21.75	24.37	48.34
18	1.16	21.75	24.37	48.35

LIST OF REFERENCES

1. Joule, J., Trans. Royal Society, Vol. 151, 1861.
2. Marto, P.J., "Film Condensation Heat-transfer Measurements on Horizontal Tubes: Problems and Progress," Invited paper, First World Conference on Experimental Heat Transfer, Fluid Mechanics and Thermodynamics, Dubrovnik, Yugoslavia, September 4-9, 1988.
3. Search, H.T., A Feasibility Study of Heat Transfer Improvement in Marine Steam Condensers, Master's Thesis, Naval Postgraduate School, Monterey, California, December 1977.
4. Thomas, D.G., and Hayes, P.H., "High Performance Heat Transfer Surfaces," Industrial and Engineering Chemistry, Vol. 62, No. 2, February 1970, pp. 4-9.
5. Yau, K.K., Cooper, J.R., and Rose, J.W., "Effects of Drainage Strips and Fin Spacing on Heat Transfer and Condensate Retention for Horizontal Finned and Plain Tubes," Fundamentals of Phase Change: Boiling and Condensation, HTD Vol. 38, C.T. Avedisian and D.M. Rudy (Eds.), December 1984, pp. 151-156.
6. Webb, R.L., "The Use of Enhanced Surface Geometries in Condensers," Proceedings of the Workshop on Modern Developments in Marine Condensers, Naval Postgraduate School, Monterey, California, March 1980, pp. 283-321.
7. Marto, P.J., "Heat Transfer and Two Phase Flow During Shell-side Condensation," Heat Transfer Engineering, Vol. 5, Nos. 1-2, 1984, pp. 31-61.
8. Webb, R.L., "Shell-side Condensation in Refrigerant Condensers," ASHRAE Trans., Vol. 90, Part 1, 1984.
9. Renz, U., "Measures to Improve Heat Transfer in Condensation," German Chemical., Vol. 9, No. 1, pp. 30-41.
10. Wanniarachchi, A.S., Marto, P.J., and Rose, J.W., "Filmwise Condensation of Steam on Horizontal Finned Tubes: Effect of Fin Spacing, Thickness and Height," Multiphase Flow and Heat Transfer, HTD-Vol. 47, V.K. Dhir, J.C. Chen, and O.C. Jones (Eds.), 1985, pp. 93-99.

11. Wanniarachchi, A.S., Marto, P.J., and Rose, J.W., "Filmwise Condensation of Steam on Externally-Finned Horizontal Tubes," Fundamentals of Phase Change: Boiling and Condensation, HTD-Vol. 38, C.T. Avedisian and J.M. Rudy (Eds.), December 1984, pp. 133-141.
12. Rudy, T.M. and Webb, R.L., "Condensate Retention of Horizontal Integral-Fin Tubing," Advances in Heat Transfer, ASME Symp., Vol. HTD-18, 1981, pp. 35-41.
13. Honda, H., Nozu, S., and Mitsumori, K., "Augmentation of Condensation on Horizontal Finned Tubes by Attaching Porous Drainage Plates," Proceedings of the ASME-JSME Thermal Engineering Conference, Honolulu, 1983, pp. 289-296.
14. Rifert, V.G., "Steam Condensation on Profiled Surfaces, Heat and Mass-Transfer Processes in Porous Media with Phase Transformation," Academy of Sciences, BSSR, A.B. Lykov (Ed.), Minsk, 1982, pp. 373-378.
15. Owen, R.G., Sardesai, R.G., Smith, R.A., and Lee, W.C., "Gravity Controlled Condensation on Horizontal Low-fin Tube," Condensers: Theory and Practice, Inst. Chem. Engrs. Symp., Ser. 75, 1983, pp. 415-428.
16. Rudy, T.M., and Webb, R.L., "An Analytical Model to Predict Condensation Retention on Horizontal Integral-Finned Tubes," Journal of Heat Transfer, Vol. 107, May 1985, pp. 361-368.
17. Cakan, O., Filmwise Condensation of Steam on Low Integral-Finned Tubes with Drainage Strips, Master's Thesis, Naval Postgraduate School, Monterey, California, December 1986.
18. Van Petten, T., Filmwise Condensation on Low Integral-Fin Tubes of Different Diameters, Master's Thesis, Naval Postgraduate School, Monterey, California, June 1988.
19. Ishihara, K.I., and Palen, J.W., "Condensation of Pure Fluids on Horizontal Finned Tube Bundles," I. Chem. E. Symposium Series, No. 75, pp. 429-446.
20. di Marzo, M., and Casarella, M.J., "Film Condensation Over a Horizontal Cylinder for Combined Gravity and Forced Flow," ASME Journal of Heat Transfer, Vol. 107, 1985, pp. 687-695.

21. Nusselt, W., "The Condensation of Steam on Cooled Surfaces," Chemical Engineering Fundamentals, Vol. 1, No. 2, May 1915, pp. 6-19.
22. Shekriladze, I.G. and Gomelaury, V.I., "Theoretical Study of Laminar Film Condensation of Flowing Vapour," Int. Journal of Mass and Heat Transfer, Vol. 9, 1966, pp. 581-591.
23. Berman, L.D. and Tumanov, Yu. A., "Condensation Heat Transfer in a Vapour Flow Over a Horizontal Tube," Teploenergetika, 1962, No. 10, pp. 77-84.
24. Fujii, T., Vehara, H., and Kurata, C., "Laminar Filmwise Condensation of Flowing Vapour on a Horizontal Cylinder," Int. Journal of Mass Transfer, Vol. 15, 1972, pp. 235-246.
25. Fujii, T., Honda, H., and Oda, K., "Condensation of Steam on a Horizontal Tube--the Influence of Oncoming Velocity and Thermal Condition at the Tube Wall," Condensation Heat Transfer, the 18th National Heat Transfer Conference, San Diego, California, August 1979, pp. 35-43.
26. Lee, W.C. and Rose, J.W., "Film Condensation on a Horizontal Tube--Effect of Vapor Velocity," Proc. 7th Int. Heat Transfer Conference, Munich, Vol. 5, 1987, pp. 101-106.
27. Rose, J.W., "Effect of Pressure Gradient in Forced Convection Film Condensation on a Horizontal Tube," Int. J. of Heat Mass Transfer, Vol. 27, No. 1, 1984, pp. 39-47.
28. Rose, J.W., "Fundamentals of Condensation Heat Transfer: Laminar Film Condensation," JSME International Journal, Series II, Vol. 31, No. 3, 1988, pp. 357-375.
29. Gogonin, I.I., and Dorokhov, A.R., "Enhancement of Heat Transfer in Horizontal Shell-and-Tube Condensers," Heat Transfer--Soviet Research, Vol. 13, No. 3, May-June 1981, pp. 119-126.
30. Yau, K.K., Cooper, J.R. and Rose, J.W., "Horizontal Plain and Low-finned Condenser Tubes--Effect of Fin Spacing and Drainage Strips on Heat Transfer and Condensate Retention," Transactions of the ASME, Vol. 108, November 1986, pp. 946-950.

31. Flook, F.V., Filmwise Condensation of Steam on Low Integral-finned Tubes, Master's Thesis, Naval Postgraduate School, Monterey, California, March 1985.
32. Georgiadis, I.V., Filmwise Condensation of Steam on Low Integral-finned Tubes, Master's Thesis, Naval Postgraduate School, Monterey, California, September 1984.
33. Mitrou, E.S., Film Condensation of Steam on Externally Enhanced Horizontal Tubes, Master's Thesis, Naval Postgraduate School, Monterey, California, March 1986.
34. Lester, D.J., Indirect Measurement on Local Condensing Heat-transfer Coefficient Around Horizontal Finned Tubes, Master's Thesis, Naval Postgraduate School, Monterey, California, September 1987.
35. Masuada, H., and Rose, J.W., "Static Configuration of Liquid Films on Horizontal Tubes with Low Radial Fins: Implications for Condensation Heat Transfer," Paper to be published in Proceedings of the Royal Society, London.
36. Yau, K.K., Cooper, J.R. and Rose, J.W., "Horizontal Plain and Low-finned Condenser Tubes--Effect of Fin Spacing and Drainage Strips on Heat Transfer and Condensate Retention," Transactions of the ASME, Vol. 108, November 1986, pp. 946-950.
37. Kline, S.J. and McClintok, F.A., "Describing Uncertainties in Single-sample Experiments," Mechanical Engineering, Vol. 74, January 1953, pp. 3-8.

INITIAL DISTRIBUTION LIST

	No. Copies
1. Defense Technical Information Center Cameron Station Alexandria, Virginia 22304-6145	2
2. Library, Code 0142 Naval Postgraduate School Monterey, California 93943-5002	2
3. Department Chairman, Code 69He Department of Mechanical Engineering Naval Postgraduate School Monterey, California 93943-5000	1
4. Professor Paul J. Marto, Code 69Mx Department of Mechanical Engineering Naval Postgraduate School Monterey, California 93943-5000	5
5. Dr. A.S. Wanniarachchi ERC-CRSS University of California at Santa Barbara Santa Barbara, California 93106	2
6. Professor John W. Rose Department of Mechanical Engineering Queen Mary College London E1 4NS England	1
7. Acting Program Director Thermal Systems and Engineering Program National Science Foundation Washington, D.C. 20550	1
8. LCDR Charles L. Hopkins III 2073 Silver Lake Drive Virginia Beach, Virginia 23456	2
9. Mr. D. Brown, Code 2724 David W. Taylor Naval Ship Research and Development Center Annapolis, Maryland 21402	1

10. CDR H.M. Holland, USN
Naval Sea Systems Command
Code 56XN1
Department of the Navy
Washington, D.C. 20362-5101

1